Study of A Humidity-Swing Carbon Dioxide Sorbent

Xiaoyang Shi

Submitted in partial fulfillment of the

requirements for the degree of

Doctor of Philosophy

in the Graduate School of Arts and Sciences

COLUMBIA UNIVERSITY

2017

ABSTRACT

Study of A Humidty-Swing Carbon Dioxide Sorbent

Xiaoyang Shi

Hydration of neutral and ionic species at interfaces plays an important role in a wide range of natural and artificial, fundamental processes, including in energy systems as well as biological and environmental systems. Owing to the hydration water at the interface, the rate and extent of various types of chemical reactions may be significantly enhanced. The hydration of ions does not only affect the physical structure and dynamics of water molecules, but also chemical energy transfers through the formation of highly structured water complexes that form in the bulk water. Indeed, dehydration could promote the energy levels of aqueous compounds. These shifts in energy states may receive wide applications such as in energy storage with anhydrous salts, enhancement of the free energy of binding ligands to biological systems, and gas separation using a water-modified basicity of ionic sorbents. Of particular interest in this study is a novel technology for direct air capture of carbon dioxide, driven by the free energy difference between the hydrated and dehydrated states of an anionic exchange resin and its effect on the affinity of CO_2 to the resin.

In this dissertation, we first demonstrate an unconventional reverse chemical reaction in nano-confinement, where changes in the amount of hydration water drive the direction of an absorption/desorption reaction, and apply this novel mechanism of controlling the behavior of a sorbent to air capture of CO_2. The reduction of the number of water molecules present in the pore space promotes the hydrolysis of CO_3^{2-} to HCO_3^- and OH^-. This phenomenon has led to a nano-structured CO_2 sorbent that binds CO_2 spontaneously in ambient air when the surrounding is dry,

while releasing it when exposed to moisture. We name this phenomenon of loading and unloading a sorbent with water a hydration swing.

Wide application of hydration swings to absorb CO_2 requires a detailed understanding of the molecular mechanisms of the hydration induced energy change at the ion hydration/solid interface. Using atomistic simulations, the mechanism of CO_2 absorption with respect to water quantity was elucidated via the explorations of the reaction free energy of carbonate ion hydrolysis in a confined nano-environment. Next, based on the understanding of the underlying driving mechanism, a systematic study of the efficiency of effective hydration-driven CO_2 capture with respect to different pore sizes, hydrophobic/hydrophilic confined layers, temperatures, and distances of cations may further benefit the optimization of the CO_2 capture system, in terms of the energetically favorable states of hydration ions in dry and wet conditions. This part of the research may sheds some insights on future research of designing high efficiency CO_2 capture sorbent according to adjust the above described parameters.

This unconventional reverse chemical reaction is not restricted to carbonate ions in nano-confined space. This is an universal phenomenon where hydrated ions carrying several water molecules in nanoscopic pores and in the natural atmosphere under low relative humidity. Such formations of hydrated ions on interfaces with the high ratio of ions to water molecules (up to 1:1) are essential in determining the energetics of many physical and chemical systems. In this dissertation, we present a quantitative analysis of the energetics of ion hydration in nanopores based on computational molecular modeling of a series of basic salts with the different quantities of water molecules. The results show that the degree of hydrolysis of basic salts with several water molecules is significantly different from the conventional degree of hydrolysis of basic salts in bulk water. The reduction of water molecules induces divalent and trivalent basic ions

(S^{2-}, CO_3^{2-}, SO_3^{2-}, HPO_4^{2-}, SO_4^{2-}, PO_4^{3-}) to hydrolyze water into a larger amount of OH^- ions, conversely, it inhibits monovalent basic ions (CN^-, HS^-) from hydrolyzing water. This finding opens a vast scope of new chemistry in nanoconfined water.

Ion hydrations containing interfaces play an important role in a wide range of natural and fundamental processes, but are much less noticeable currently. This thesis sheds some lights on a vast number of chemical processes of hydrated ion pairs containing interfaces, and design possibility for more efficient energy-saving sorbents.

Table of Contents

List of Figures

Acknowledgements

I would like to begin by sincerely thanking my advisor Prof. Klaus S. Lackner and my co-advisor Prof. Xi Chen, for their constant guidance, strong support, valuable advices and continuous encouragements over the course of my research.

Prof. Lackner always gave me clear directions, but freedom to choose my own ways on my scientific researches. Instead of step-by-step guidance, he preferred to enlighten me to find a solution to the problems by myself. Whenever I was bereft of ideas, my discussions with him always shed light on my research, and his insights always helped me get back on the right track. His rigorous research attitude and great innovations are my most valuable gains in my doctor career. He is also like a benign father and helpful friend in my life. I am grateful.

Prof. Xi Chen is the greatest mentor in my life, his passions on research and professional working skills make me realize scientific research area is a wonderland. He has always encouraged me to explore a wide variety of opportunities. His critical questions always helped me to correct errors and enlighten new ideas. Prof. Chen always organized parties on holidays, I felt so warm that I was in a big family in a foreign country. I have truly learnt a lot from him over the past 5 years. I'm so lucky and truly honored to have such a great mentor in the pursuit of education and research.

I would also like to thank my thesis committee members – Prof. Paul F. Duby and Prof. Upmanu Lall, Prof. Gautam Dasgupta, Prof. Baoxing Xu, and Prof. Peter Schlosser for their generosity and willingness to be my proposal and defense committees, and for their valuable suggestions and advice on my thesis.

Past and present members of Prof. Lackner's group and Prof. Chen's group have been great sources of cheer and comfort during the past 5 years. I am grateful to them for their suggestions and sincere friendship throughout my research and life. They are Tao Wang, Josh Browne, Zara L'Heureux, Diego Villarreal, Yinghuang Ji, Menglian Zheng, Junfeng Xiao, Hang Xiao, Jun Xu, Yinlun Liu, Qibin Li.

On a personal note, I know I could not complete my work without the tremendous love and support of my parents. Zhaojian Shi and Xinying Wang. They have always sacrificed to ensure that I could obtain the best opportunities for my education and my career. They always encouraged me to pursue my dreams and support me unconditionally. I cannot put into words what this has meant to me in my life, and I dedicate this thesis to them.

Chapter 1 Introduction and Motivation

1.1 Motivation for Air Capture CO_2

1.1.1 Current and Future Global Warming Situation

Global climate change induced by emission of green house gases increasingly attracts people's attention[1]. **Figure 1.1** shows the global temperature rise which is strongly correlated to rising CO_2 levels. According to the Intergovernmental Panel on Climate Change (IPCC), by 2050, CO_2 emissions will rise from the current 36 Gt/yr to between 48 and 55 Gt/yr, with energy demands increasing 40% to 150% increasing over current demand. Atmospheric CO_2 will be ranging from 535 to 983 parts per million (ppm) by 2100, roughly double the current value of 402 ppm and far higher than the preindustrial level of 280 ppm. The increase in CO_2 concentration will lead to a global mean temperature change from 1990 to 2100 of between 1.4 and 6.1℃.

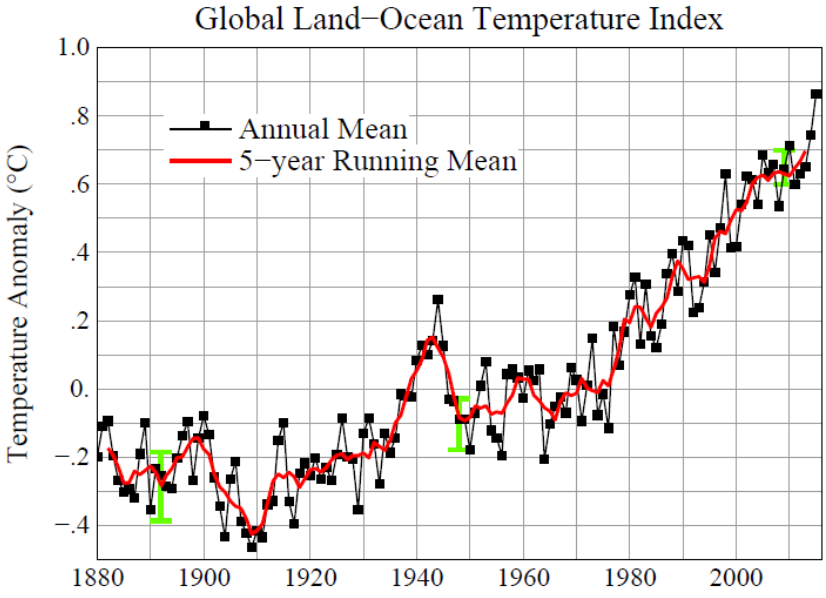

Figure 1.1: Plot of global instrumental temperature anomaly vs. time[1]

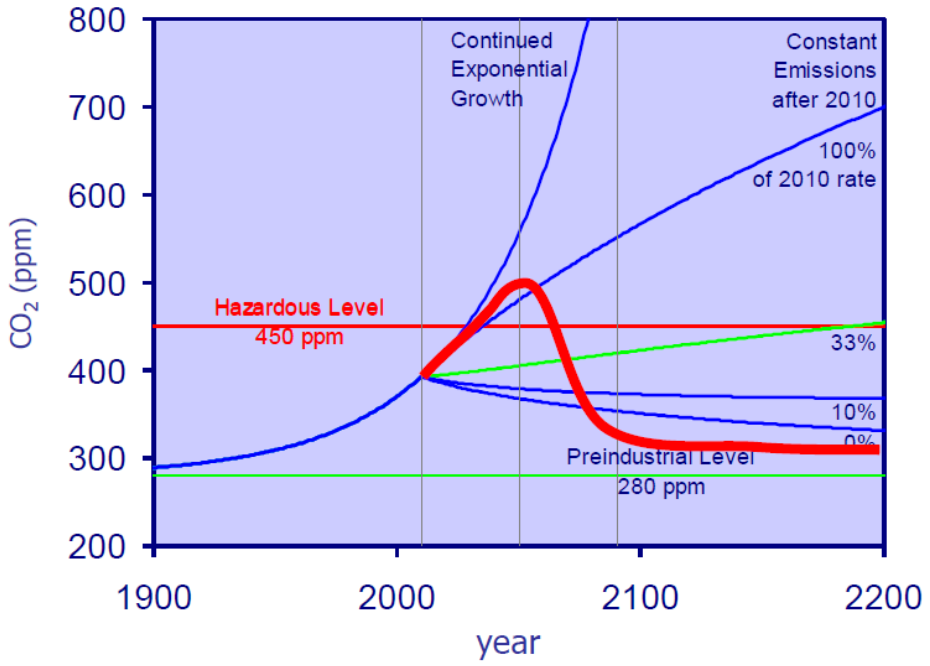

Figure 1.2: Plot of CO_2 concentration in atmosphere vs. time (image courtesy K. S. Lackner)

Figure 1.2 shows various projections of how CO_2 levels might increase in the future. From 1900 to 2010 the graph shows historical CO_2 concentration data. At the year 2010, there are several different scenarios. The first one shows CO_2 concentration as fossil fuel consumption keeps increasing exponentially as before. This scenario will hit 800 ppm quickly in this century. The second one holds the amount of CO_2 emission constant at the level of 2010. In this scenario CO_2 concentration will steadily rise hitting 450 ppm a few years later than in the first scenario. 450 ppm is deemed to be a threshold beyond which anthropogenic climate change poses a serious danger. Third, even if we emit CO_2 at 1/3 the rate of today, the CO_2 concentration in the atmosphere will still increase slowly, but sooner or later it will still pass 450 ppm. The red line indicates a scenario where human built systems recover CO_2 from the environment and lower the CO_2 concentration in the air. The IPCC named such scenarios “Negative Emission” which means

a permanent removal of the greenhouse gas CO_2 from the Earth's atmosphere. To prevent dangerous global warming, attention needs to focus on developing non-fossil energy sources, e.g. renewable energy source, CO_2 capture from power plants, and also CO_2 capture from ambient air.

1.1.2 Limitations of Renewable Energy on Solving Global Warming

A study from the Institute for Energy Research shows solar energy, nuclear energy, and fossil fuel are three main energy options for the future. Unfortunately, fossil fuel is behind 80% to 85% of total energy consumption today and will likely remain important in the foreseeable future. The percentage of different forms of energy consumption is shown as **Figure 1.3**. Moreover, total energy demand is growing. The global economy, especially in developing countries, is growing rapidly. It is extremely difficult to restrict the usage of fossil fuel by a substantial amount. Nevertheless, renewable energy can decrease the amount of CO_2 released from fossil fuel, thereby slowing the rate of global warming to some extent, but it cannot yet stop the trend of global warming.

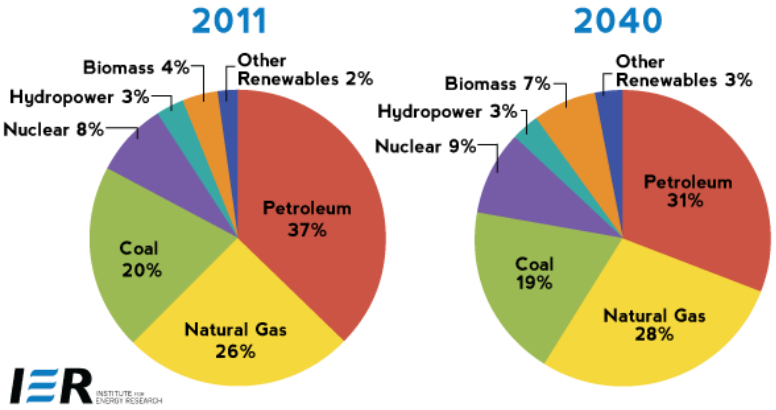

Figure 1.3: Compositions of Energy Consumption

1.1.3 The Roles of Air Capture CO_2

The Intergovernmental Panel on Climate Change (IPCC) claims CO_2 emissions must be reduced between 85% and 30% by 2050 to stabilize the atmospheric CO_2 concentration between 350 and 440 ppm[2]. Emission from coal and other fossil fuel would have to be essentially eliminated[3]. However, moving the energy infrastructure away from fossil fuels to renewable and nuclear energy resources is a challenging task. CO_2 capture and storage (CCS) from point-sources allows power plants and steel and cement production to continue to use fossil fuels, while largely reducing their CO_2 emission. Capturing CO_2 from ambient air could address mobile CO_2 emissions, like those from automobiles and airplanes. The objective of stabilizing atmospheric CO_2 at 450 ppm cannot be accomplished this century if point sources with CCS keep on emitting even as little as 10% of their current rates[4]. CCS needs to be complemented by Air Capture CO_2 to achieve the goal announced by IPCC. Air Capture CO_2 therefore could play five important roles in stabilizating atmospheric CO_2.

1) Compensating for mobile CO_2 Emissions. CO_2 emission from small sources and transport sector accounts for between 1/3 to 1/2 of total CO_2 emissions of about 36 Gt CO_2/yr. This part of CO_2 emissions could be addressed by capturing CO_2 directly from the air.

2) Moving CO_2 storage to remote sites. A major challenge to CCS is the need to construct an extensive CO_2 pipeline network for carrying CO_2 from the place where it is captured to the storage site. Building pipelines is costly; it is difficult to obtain legal permissions and pipeline systems face environmental issues. The need for transporting CO_2 limits the available storage space as storage has to be in proximity to the source of emission. By contrast, air capture can operate at the storage site and eliminate the expensive pipeline system for transporting CO_2 and give access to remote sites.

3) Air Capture as leakage insurance. CO_2 storage has a small probability of failure to retain CO_2. Air capture CO_2 could also recapture the leaked CO_2 from geologic storage sites of CCS. Air capture cannot prevent the damages associated with gas loss, but provides a means of recapturing leaked CO_2, thereby insuring against gradual leaks.

4) Air Capture Closes Carbon Cycle by Producing Synthetic Fuels. The use of carbon-based fuels in the transportation sector is not sustainable unless the CO_2 is eventually removed from the atmosphere. Therefore, air capture is also used to close the carbon cycle. In principle, the captured CO_2 from air together with H_2O can provide material feedstock for producing carbonaceous energy carriers such as methanol, synthetic diesel or gasoline, using electricity from renewable or nuclear energy sources.

5) Creating Negative Emissions. CO_2 in atmosphere has increased from 280 ppm in preindustrial period to 404 ppm today. The average global temperature on Earth has increased by about 0.8℃ since 1880 and will rise further, even if the CO_2 concentration in the atmosphere is held constant. As a result, atmospheric CO_2 concentration is probably already in an overshoot scenario. Air capture on a large scale could create net negative emissions, reducing excess CO_2 stored in the atmosphere, oceans and terrestrial biomass.

1.2 Current State of Air Capture CO_2 technology

Capture CO_2 from ambient air at small scales has been utilized for decades[5,6]. Air Capture CO_2 technology has been utilized to maintain safe levels of CO_2 concentration in submarines[7] and spaceships[8]. Approaches of capturing CO_2 from air include 1) terrestrial carbon sequestration[9] with formation of recalcitrant carbon[10], which are able to collect and store carbon dioxide by plants and soil. For example, the conversion of biomass to bio-char can hold 50% of

carbon residue comparing to 10% carbon remain of non bio-char material in agricultural soil. The bio-char application leads to considerably larger amounts of carbon remaining in soil than application of un-charred organic matter[10]. The terrestrial sequestration can reach 0.5-0.7 GtC/yr in this middle century wich are contributed from agricultural soils (0.2 GtC/yr), reforestation (0.31GtC/yr), and pasture (0.15 GtC/yr). The combined contribution of terrestrial sequestration over the next centry will ranges from 23 to 41 GtC totally. 2) biomass growth in the ocean via ocean fertilization[11], and 3) enhanced weathering involving land or ocean based techniques. An example of land based techniques is to carbonate ultramafic rock, producing a host of newly formed magnesium carbonate minerals[12]. This is also known as accelerated weathering. Ocean based techniques involve alkalinity enhancement such as grinding, dispersing and dissolving olivine, limestone and silicates[13] into ocean water.

Theses methods mentioned above are different from Direct Air Capture methods. Direct Air Capture uses absorption or adsorption on collector surfaces. Some of the air capture sorbents are liquid[14-17], others are solid[18-20]. Eisaman[20] uses a weak base amine membrane, and electric currents to maintain a high concentration of base on the airside contact area. Rau[21] proposes to operate electrolytic water-splitting systems that absorb CO_2 via a base near one electrode and also create acid on the other.

There are a wide range of options for choosing sorbent materials for air capture. Early technologies used sodium or calcium hydroxide[5,14,22]. For example, in 1999, K.S. Lackner proposed to utilize sodium hydroxide to absorb CO_2 from the atmosphere, forming sodium carbonate. Calcium hydroxide is then added to the sodium carbonate solution to cause calcium carbonate to precipitate out of solution leaving behind sodium hydroxide. Finally, the calcium

carbonate is heated at high temperatures to form calcium oxide and CO_2 which is then compressed for storage[14]. The reaction process has been shown as **Equation 1.1-1.4**.

$$2NaOH(solution) + CO_2 = Na_2CO_3 + H_2O, \Delta H = -105kJ/mol \quad 1.1$$

$$Na_2CO_3(solution) + Ca(OH)_2(slurry) \quad 1.2$$

$$= CaCO_3(wet\ solid) + 2NaOH(solution), \Delta H = -8kJ/mol$$

$$CaCO_3(solid) = CaO(solid) + CO_2(gas), \Delta H = 179kJ/mol \quad 1.3$$

$$CaO(solid) + H_2O = Ca(OH)_2(slurry), \Delta H = -65kJ/mol \quad 1.4$$

In terms of cost, K.S. Lackner also made an argument that the CO_2 in the air by some measure is much more concentrated than wind energy. At a wind speed of 10 m/s, the kinetic energy of air equals an energy flux of 600 W/m^2. The equivalent CO_2 flux through the same area represents an energy flux of 100,000 W/m^2. This energy flux is not energy embedded in the CO_2, but the energy that can be released by producing this much CO_2 from gasoline. If CO_2 is removed from the air, it becomes feasible to add new CO_2 to the air with a concurrent release of energy. Hence the cost of processing air for CO_2 should involve much less volume of air and be less expensive than processing the air for its kinetic energy content. Even though the cost of contacting the air could be quite small, this analysis does not consider the second stage of retrieving the CO_2 from the sorbent. This cost is slightly higher than the sorbent regeneration cost in the flue gas scrubber, because the binding energy needs to scale like the logarithm of the dilution[23].

Baciocchi et al.[22] proposed two process designs based on this technique. The total fuel energy reported in the paper are 17 and 12 GJ/t CO_2 (748 and 528 kJ/mol) captured, respectively for the two options, meaning that twice as much as energy is required to remove CO_2 emitted from a given amount of coal compared to the energy content of coal, 9 GJ/t of CO_2. The reason

is that the energy consumption of the calcination step is too large, due to the inefficiency of the process. **Figure 1.4** shows the scheme of a plant for CO_2 capture from air[24].

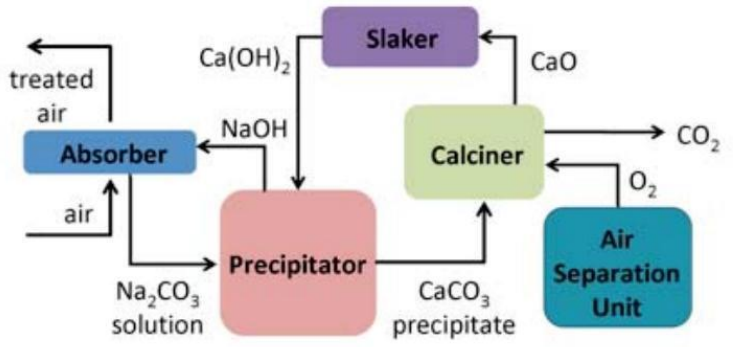

Figure 1.4: Scheme of a plant for CO2 capture from air

Keith and his group follow this approach[25]. He used a 3-6M NaOH solvent and an absorber with 110m diameter, 120m height. The paper concludes the energy requirement of calcination in lime production is 679 kJ/mol of CO_2, which is close as the value calculated by Baciocchi et al.

The high energy demand of the calcination process suggests that other options for CO_2 sorbents need to be investigated. Eisenberger and Jones use a solid tertiary amine, a weak base analogous to an ammonia solutions[20].

A new technique that also avoids sodium hydroxide was proposed by Lackner[18]. Lackner presented a novel solid sorbent technology: amine-based exchange resin dispersed in a flat sheet of polypropylene. This sorbent absorbs CO_2 when the surrounding is dry and releases CO_2 when the surrounding is wet. The resin acts like a strong base, analogous to NH_4^+, where each hydrogen has been replaced by an organic carbon chain attached to a polymer matrix. The chemical structure and a sample of the material are shown in **Figure 1.5**. The current solid

sorbent can be made to work in cool climates regardless of the average relative humidity. However, the the choice is best for a desert climate. The following **Figure 1.6** shows the working process of moisture swing sorbent for capturing CO_2. This method total energy consumption is estimated at 50 kJ/mol of CO_2. This value is about 1/10 of those calculated by Keith and Baciocchi.

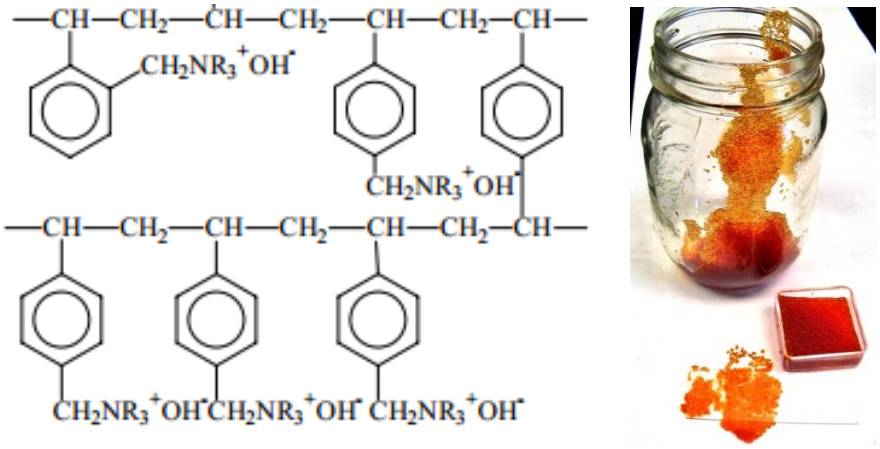

Figure 1.5: Chemical Structure and Exterior of Quaternary Amine Ligands Ion Exchange Resin

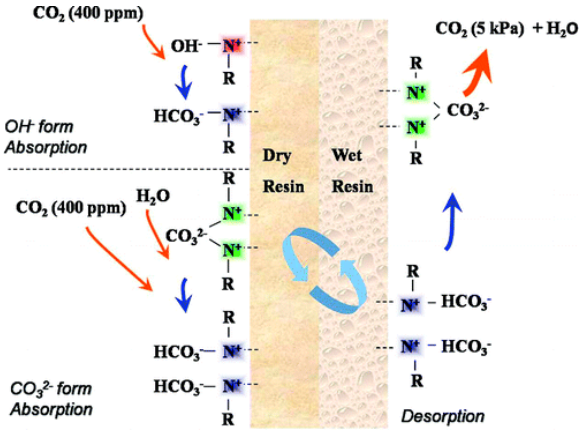

Figure 1.6: Moisture Swing Sorbent for Carbon Dioxide Capture from Ambient Air[26]

1.3 Novel Sorbent for CO_2 Capture from Air

1.3.1 Performance of A Moisture Swing Sorbent

It has been reported that conventional technologies for capturing CO_2 from air are most likely too expensive[24,27]. These reports are based on extrapolating known technologies to capture at the extreme dilution of CO_2 in the air. While we agree with these observations, our conclusion is not that CO_2 capture from air is impossible but that it will likely dramatically depart from conventional technologies and overcome difficulties by using innovative methods.

Of particular interest in this doctoral research is the study of a novel moisture-swing technology for direct air capture of CO_2 that is mentioned in the last paragraph of **Chapter 1.2**. The moisture swing replaces a thermal swing or pressure swing. The sorbent, an anionic exchange resin, readily absorbs CO_2 when dry and releases it again when exposed to moisture. The reaction pathway of CO_2 absorption/desorption on this novel absorbent is explained in detail in **Figure 1.7** and **Equation 1.5-1.8**.

$$H_2O \Leftrightarrow H^+ + OH^- \quad (1.5)$$

$$CO_3^{2-} + H^+ \Leftrightarrow HCO_3^- \quad (1.6)$$

$$OH^- + CO_2 \Leftrightarrow HCO_3^- \quad (1.7)$$

$$HCO_3^- + HCO_3^- \Leftrightarrow CO_3^{2-} + CO_2 + H_2O \quad (1.8)$$

For the wet resin without CO_2 loading, which we label **Empty-Wet,** the counter ions to the positive quaternary ammonium ions are carbonate ions. The carbonate ion is stabilized by the presence of ample water. The interaction of the ion with the water molecules reduces the energetic state of the carbonate ion. A similar effect occurs for the bicarbonate and hydroxide ion, but the energetics is such that the bicarbonate and carbonate do not co-exists in significant

quantities. As the water content of the resin is reduced during drying, the carbonate ion becomes less stable and the destabilization is relatively larger than that of the singly charged ions. This eventually results in the splitting of one of the remaining water molecules to form a HCO_3^- ion and a OH^- ion which both bind tightly to their respective cations. This state, labeled **Empty-Dry,** has a strong affinity to CO_2 due to the presence of OH^- ions in the solid. Even at low partial pressure of CO_2, the resin absorbs CO_2. This results in a CO_2-loaded state which is entirely bicarbonate; this state we refer to as **Full-Dry**. These three states are described by **Equation 1.5-1.7** Wetting the resin leads to the full hydration of the bicarbonate ions **Full-Wet.** In the wet state, the bicarbonate ions are now overrepresented relative to the carbonate ions and carbonic acid. As a result, the bicarbonate disassociates according to **Equation 1.8**. This results in the escape of CO_2 in the wet condition (desorption) resulting in the **Empty-Wet** state and the cycle is completed.

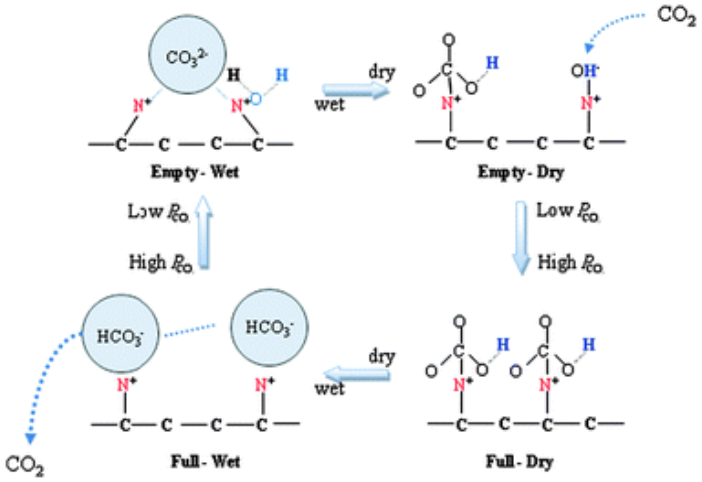

Figure 1.7: Reaction path way of CO_2 absorption/desorption on Ion Exchange Resin (image courtesy, K.S. Lackner)[28]

Lackner et al. have shown that the CO_2 loading of the resin is as function of the equilibrium CO_2 partial pressure over the sorbent. As a result, a resin that has been loaded to 400 ppm of CO_2 in the open air can release this CO_2 at a CO_2 partial pressure of about 8 kPa[26]. Lackner has shown that this technology has the potential to greatly reduce energy consumption in the collection of CO_2[29]. This innovation, passive collection and a novel regeneration method may advance air capture technology to a practical level.

1.3.2 The Advantages of Moisture Swing Sorbent

The moisture swing technology has several advantages over conventional thermal swing or pressure swing absorption systems:

1. The conversion between absorption and desorption of this new efficient sorbent can be switched with low-cost water instead using costly energy to regenerate.
2. Since absorbed water and CO_2 on the sorbent move in opposite directions, energy penalties for absorption and desorption of water are completely eliminated. For most CO_2 sorbents, water binds even more strongly than CO_2. Since there is 10 to 50 times as much water vapor as CO_2 in the air, freeing water with CO_2 is a nearly intractable energy penalty for any absorption/desorption cycle.
3. The moisture swing can avoid heating and cooling the sorbent. Much of the sorbent mass and mass of the sorbent support structure simply gains and loses sensible heat in a swing. In a thermal swing, heating up and cooling the bulk material is inefficient because the heat recovery in a cycle is quite incomplete.
4. Moisture swings are flexible, they can be amplified by adding a thermal swing or a vacuum assist. For example, compressors used in producing liquid CO_2 will always

provide waste heat that could be used to augment the moisture swing with a low-level thermal swing.

1.3.3 Importance of Understanding Mechanisms of Moisture Swing Sorbent

Even though Lackner et al. had already demonstrated the existence and the utility of the humidity swing for certain anionic exchange resins, they did not fully understand the underlying mechanisms at work at the beginning, and therefore could not rationally design better sorbent systems. The main purpose of this Ph.D. research is to elucidate the underlying mechanisms and verify them by experiments. Advances would be greatly helped by a better understanding of the underlying molecular dynamic processes, for example, we are looking for ways to enhance the uptake speed of the sorbent, raise the CO_2 partial pressure at release and increase the contact area between air and sorbent. Each one of these advances would greatly reduce the cost of an operational system and improve the thermodynamic properties of the material.

In order to understand the underlying physical mechanisms that result in the moisture control of the affinity of the sorbent to CO_2, we need to apply numerical tools of classical molecular dynamics and quantum mechanics to understanding the interaction of polymer, water and ions. A successful exploration of the novel phenomena at the root of the moisture swing will greatly enhance our ability for rational design, while at the same time elucidating unexplored phenomena of surface chemistry involving ions and water.

1.4 Methodology

Hydrated ions carry from several to several tens of water molecules in the natural atmosphere and on solid porous surface[30]. These ion hydrations containing interfaces play an important role in a wide range of natural and fundamental processes[31-34]. The existing interface of ion hydration serves to significantly enhance the rate and extent of chemical reaction probabilities[35-37]. Experiments are very costly and difficult to implement. Numerical simulation provides an alternative method to study the microscopic ion hydration energy changes at interfaces of solid surfaces. Combining Molecular Dynamics (MD) and Quantum Mechanics (QM) tools is the most effective method for the study. MD has relative high accuracy, low computational cost, and an ability to model the behavior of a large number of atoms, but is not able to simulate breakage and formation of chemical bonds[38-41]. QM is time consuming and has limited in the number of atoms. It is computational difficult to keep track of 100 atoms, but it is possible calculate the energy change of chemical bonds' breakage and formation. In this section, MD and QM theory and application will be reviewed in brief.

1.4.1 MD theory

The MD is a computational modeling approach to studying the physical movements of atoms and molecules, which is applied today in various scientific research fields, like chemical physics, materials science and the study of the dynamics of biomolecules. MD was demonstrated by Alder and Wainwright[39] in the late 1950s and rapidly developed with the advent of fast computer technology[40,41]. The trajectories and other characteristics of atoms and molecules over a period of time are determined by solving Newton's force principles, the Newton's equation of motion is shown as **Equation 1.9** and **Equation 1.10**:

$$m_i \frac{d^2 r_i}{dt^2} = -\frac{\partial U}{\partial r_i} \quad 1.9$$

$$v_i = \frac{dr_i}{dt} \quad 1.10$$

Where m_i is the mass of atom *i*, *i* equals 1,2,3, …, N, r_i is its position, v_i is its velocity, U is the total potential energy of all atoms. MD ignores electron movements assuming system energy is the function of the position of the atom's nucleus. The force between atoms and the potential energies of atoms are calculated using interatomic potentials or molecular mechanics force fields. Conceptually, the interatomic potential is divided into intramolecular and intermolecular atomic contributions[42]. The **intramolecular potential** reflects interactions among bonded atoms including three terms as **Equation 1.11**:

$$U_{intramolecular} = U_{stretch} + U_{angle} + U_{dihedral} \quad 1.11$$

Where $U_{stretch}$ represents the required potential energy to stretch or compress each covalent bond in the system, and depends on the bond length and bond strength. U_{angle} denotes the potential energy associated with the change of bond angle. $U_{dihedral}$ describes the potential energy that deforms a planar group of atoms held together by covalent bonds. The **intermolecular potential** describes attraction or repulsion interactions between pairwise additive potentials among atoms. In MD simulation, intermolecular potential energy includes van der Waals and electrostatic terms. The van der Waals term usually uses the Lennard-Jones (L-J) potential, as **Equation 1.12**, for simplicity[43].

$$U_{vdw}(r_{ij}) = 4\varepsilon_{ij}[\left(\frac{\sigma_{ij}}{r_{ij}}\right)^{12} - \left(\frac{\sigma_{ij}}{r_{ij}}\right)^{6}] \quad 1.12$$

where ε_{ij} is the depth of the potential well, σ_{ij} is the distance where the potential is zero, *i* and *j* are *i*-th and *j*-th atomic species. Parameters ε_{ij} and σ_{ij} are usually obtained from fitting

experimental data or from theoretical calculations. For an unknown pair of atom species, the Lorentz-Berthelot mixing rules are widely applied to obtain the interaction parameters from the interaction parameters of the individual atom species[44].

$$\varepsilon_{ij} = \sqrt{\varepsilon_i \varepsilon_j}, \sigma_{ij} = \frac{1}{2}(\sigma_i + \sigma_j) \qquad 1.13$$

The L-J potential curve is **Figure 1.8**

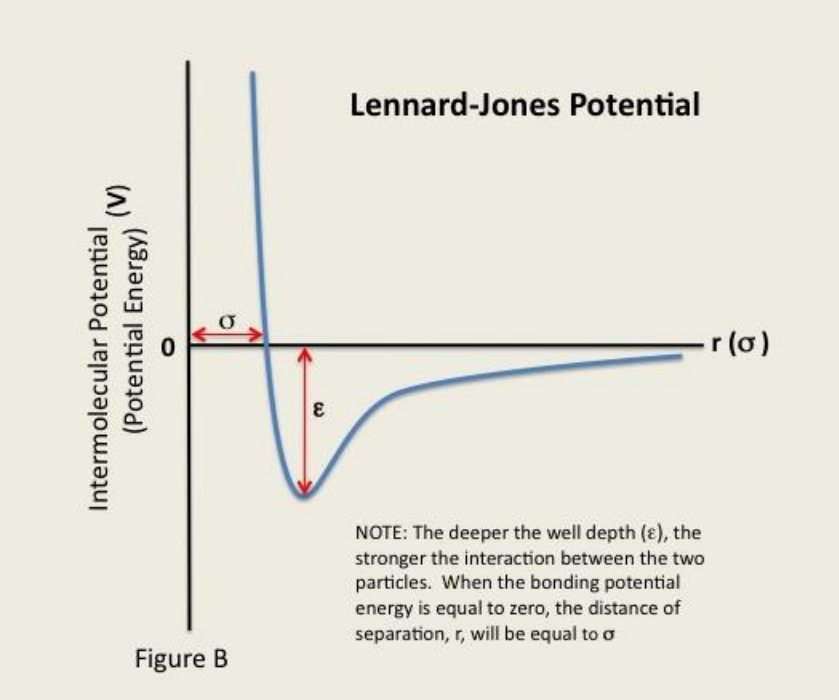

Figure 1.8: Lennard-Jones Potential Curve. Each distance corresponds to a potential energy between two atoms, and the potential energy is shown as Y axis.

The electrostatic term uses Coulomb law:

$$U_{coulomb}(r_{ij}) = \frac{q_i q_j}{4\pi\varepsilon_0 r_{ij}} \qquad 1.14$$

where q_i and q_j are the electrostatic charges of atom i and j, r_{ij} is the distance between these two atoms, ε_0 is the dielectric constant of vacuum.

Briefly, MD simulation typically consist of the following five steps:**1) Energy Minimization**, using a forcefield that has been assigned to the atoms in the system to find a stable point or a minimum on the potential energy surface in order to begin dynamics. **2) Initialization,** applying to thermodynamic distribution like Maxwell-Boltzmann distribution to endow atoms with initial velocities. **3) Equilibration,** solving Newton's equations of motion to discover the equilibrium state of all atoms. **4) Average,** accumulating thermodynamic averages of interest based on temporal averaging, which under the hypothesis of ergodicity is equal to the ensemble-average over the phase space. More on MD simulation techniques can be found elsewhere[44-47].

1.4.2 QM theory

QM theory is a fundamental branch of physics that gradually arose from Max Planck's solution in 1900 to the black-body radiation problem, and Albert Einstein's quantum-based theory in 1905 paper to explain the photoelectric effect. Early quantum theory was greatly reconceived in mid-1920s. One mathematical formalism is the famous wave function which offers information about the probability amplitude of physical properties of a particle. The QM development was slow because of the difficulty in solving Schrödinger equations for more than one atom. After 1960, scientists apply to QM computation rationally explain experimental results and design experiment because QM computation developed fast with the development of computer technology. Density Functional Theory (DFT) is the most popular method in Quantum mechanical computations of many-body system, which begins with a theorem by Hohenberg and

Kohn[48,49], and later generalized by Levy. Levy states that all ground-state properties are a functional of the square of the amplitude of the wave function, the density ρ. Specifically, the total energy E_t may be written as:

$$E_t[\rho] = T[\rho] + U[\rho] + E_{xc}[\rho] \quad 1.15$$

where $T[\rho]$ is the kinetic energy of a system of non-interacting particles of density ρ, $U[\rho]$ is the classical electrostatic energy due to coulombic interactions, $E_{xc}[\rho]$ includes all many-body contributions to the total energy, in particular, the exchange and correlation energies.

$$\rho(r) = \sum_i |\phi_i(r)|^2 \quad 1.16$$

where ϕ is the wave function, r is the location in space.

$$\phi_i = \sum_\mu C_{i\mu} X_\mu \quad 1.17$$

Where X_μ is called the atomic basis function which create atomic orbitals. These functions are typically atomic orbitals centered on atoms, but also can theoretically be any function. $C_{i\mu}$ is the expansion coefficient

$$\mathrm{T} = \langle \sum_i^n \phi_i \left| \frac{-\nabla^2}{2} \right| \phi_i \rangle \quad 1.18$$

where < > bracket represents expectation value. ∇^2 is the Laplacian operator.

$$\mathrm{U} = \langle \int V_N(r)\rho(r)dr + \frac{1}{2}\int \frac{\rho(r_1)\rho(r_2)}{|r_1 - r_2|} dr_1 dr_2 + V_{NN} \rangle \quad 1.19$$

where first term, $\int V_N(r)\rho(r)dr$, represents the electron-nucleus attraction, the second term, $\frac{1}{2}\int \frac{\rho(r_1)\rho(r_2)}{|r_1-r_2|}dr_1dr_2$, represents the electron-electron repulsion, and the final term, V_{NN}, represents the nucleus-nucleus repulsion.

The final term mentioned in Equation 1.15 is the exchange-correlation energy.

The exchange-correlation energy requires some approximation for this method to be computationally tractable. A simple and good approximation is the local density approximation (LDA), which is based on the known exchange-correlation energy of the uniform electron gas[50-52]. The LDA assumes that the charge density varies slowly on an atomic scales (i.e. each region of a molecule actually looks like a uniform electron gas). The total exchange-correlation energy can be obtained by integrateing the uniform electron gas result:

$$E_{xc}[\rho] = \int \rho(r)\varepsilon_{xc}[\rho(r)]dr \qquad 1.20$$

where $\varepsilon_{xc}[\rho(r)]$ is the exchange-correlation energy per particle in a uniform electron gas, and . ρ is the number of particles.

1.4.3 Water Model

In computational chemistry, classical water models are used for the simulation of water clusters, liquid water and aqueous solutions in nature. Water molecules are also an important element in this study. Many different water models have been developed for MD simulation in the past few decades. These models can be classified by following three points: 1) number of interaction points. 3-site models like SPC[53], SPC/E[54], and TIP3P[55]; 4-site models like TIP4P[55], OPC[56]; 5-site models like TIP5P[57] 2) whether the model is rigid of flexible 3) whether model includes polarization effects. The flexible SPC water model is one of the most accurate three-

center water model which has been chosen for our MD simulation. The O-H bond in SPC is made anharmonic and thus the dynamical behavior is well described. The charges on the oxygen site and hydrogen sites were chosen -0.82e and +0.41e, respectively.

1.5 Outline of Dissertation

Ion hydration is ubiquitous in natural atmosphere and nanoscopic pores and is essential in determining the energetics of many physical and chemical systems. By understanding these underlying mechanisms of chemical phenomena, we can apply this knowledge to a vast number of applications. Through the present thesis, the fundamental mechanism of a moisture swing sorbent is discovered and the discovery is applied to the design of novel and efficient CO_2 absorbents.

In this chapter, an introduction of global warming, motivation of air capture CO_2 and advantages of capture CO_2 from ambient air are provided. A brief overview is given to the moisture swing sorbents from its working performance to its advantages than other thermal swing sorbents, and also the computational methods for its underlying mechanism study.

In Chapter 2, A methodology of computational modeling combined with MD and QM is developed. Through numerical simulations, the underlying mechanism of moisture swing sorbent was explained by ion hydration energy change, and this explanation was verified via experiments.

In Chapter 3, A design of a moisture swing sorbent for CO_2 capture is investigated using MD and QM simulations. Its working mechanism is revealed and the influences of parameters, like pore size, spacing of cations, characteristics of surface, on CO_2 capture efficiency are elucidated.

Inspired by they study of carbonate/bicarbonate hydration system, Chapter 4 presents a quantitative analysis of the energetics of ion hydrations in nanopores based on computational molecular modeling of a series of basic salts with different quantities of water molecules. Counterintuitive hydrolysis of ion hydration in natural atmosphere and nanopores is applied to design efficient absorbents to absorb acid gases.

Chapter 5 reports the results of MD simulations of IER with carbonate ion system and bicarbonate ion system under different humidity conditions. The transport abilities and structures of ions species are explored with different numbers of water molecules.

Chapter 6 introduces a new moisture swing CO_2 sorbent by using a new polymer material PVC as binder for IER. The preparation process, sorbent structure, kinetic model, absorption and desorption characteristics are analyzed.

Chapter 2 Molecular Mechanism Study of Air Capture CO_2

2.1 Background

This Chapter is related to our paper "Capture CO_2 from Ambient Air Using Nanoconfined Ion Hydration", which has been published in Angewandte Chemie, and it is also related to a second paper "On the Molecular Mechanism of Carbon Dioxide Capture from Ambient Air by Using Moisture Swing Sorbent" which is to be submitted.

Hydration of neutral and ionic species at interfaces plays an important role in a wide range of natural and fundamental processes, including in energy systems as well as in physical[58], chemical[59], biological[60], and environmental systems[33]. Owing to the hydration water at the interface, the rate and extent of various types of chemical reactions may be significantly enhanced[37,61,62]. The hydration of ions does not only affect the physical structure and dynamics of water molecules[33,63], but also the chemical energy transfer through the formation of highly structured water complexes[64,65]. Nevertheless, it remains unclear whether the water structure could be affected by varying the amount of water present[66]. Indeed, dehydration could promote the energy level of water structures, which may receive wide applications such as energy storage with anhydrous salts[67], enhancement of the free energy of binding ligands to biological systems[68], and gas separation using modified basicity of ionic sorbents[69,70]. Anothere example is a novel technology for direct air capture of carbon dioxide, which is driven by the free energy difference between the hydrated and dehydrated states of an anionic exchange resin[18].

Previous experimental observations, such as XPS to observe structure and bonding environments at calcite surface[71], PS-SFVS to study structure and charging of hydrophobic material/water interfaces[72] and electrospray mass spectrometry to investigate the mechanism of proton transfer across water-hydrophobic media boundaries[73], can shed some light on the detailed structure and bonding information of the hydrated interface at the molecular level in similar systems. Spectrographic studies suggested highly ordered structure or dissociation of hydration water at the gas/solid interface[74,75]. Molecular dynamics (MD) simulation provides an alternative way to study the microscopic hydration energy changes at interfaces of the material, and several reliable methods, like thermodynamic integration[76], umbrella sampling, and a method basd on the Bennett acceptance ratio[77], *etc.*, were developed to calculate the ion hydration free energy in recent decades. These methods have been widely applied to calculate the free energy of solvation[78-80]. Recently, a few MD studies were conducted to explore the hydration phenomena on ions, ion pairs, and solid-liquid interfaces[81-83]. These studies shed light on how the hydration structure and hydration energies change when the water activity is reduced[84,85]. Simulation shows a high degree of positional ordering parallel to the surface, reflecting the structure of the underlying substrate. The energetics of adsorption of water onto the surfaces of minerals has been investigated by MD simulation. The study on $CaCO_3$ (1014) surface indicates that the adsorption of water on all calcite surface planes is energetically favorable[86]. An *ab initio* surface phase diagram of the calcite surface suggests that nonstoichiometric surfaces play an important role in the chemistry of calcite at a high relative humidity[87]. The comparison between dissociative and associative adsorption of water on the calcite surface was studied by *ab initio* calculations[88-90], which argued that the water dissociation is strongly disfavored even on surface defects of steps and vacancies, except near a carbonate ion, where water molecules can be

disassociated into protons and hydroxides. The carbonate ion, CO_3^{2-}, is a divalent weak base anion which will undergo hydrolysis in water. Ion hydration at interface has resulted in a flurry of interest in materials chemistry and physics, and many more contemporary issues such as climate change and challenges in water and energy promote the pressing need to a better understanding of the structure and dynamics of water/solid interface[91].

Current MD simulations on hydrated surfaces are so far limited to minerals and metal oxides, whereas hydration on resin polymers with strong ionic activity is of great interest for air capture applications. In this chapter, we employ Molecular Dynamics (MD) and Quantum Mechanics (QM) methods, to study the ion hydration energy changes with the amount of water available. Calculating these energy changes allows us to deduce the energetically favorable states of hydration ions in dry and wet. To the best of our knowledge, this is the first theoretical explanation of the moisture swing sorption for carbon dioxide capture from ambient air. In this first step toward such an investigation, we only focus on the effect of hydrated ions and replace the NH_4^+ cation with Na^+ which has the same Coulomb effect, but a much simpler structure. The findings may set a basis for future research on IER moisture swing and other related areas.

2.2 Description of Moisture Swing Sorbent for Air Capture CO_2

Of particular interest in this study is a novel technology for direct air capture of carbon dioxide, driven by the free energy difference between the hydrated and dehydrated states of an anionic exchange resin[18].

The hydration-induced energy change and its application to carbon capture with ion exchange resins (IER) was first discovered by Lackner et al. in 2009[18]. Hydration swing gas adsorption is of practical interest because it uses inexpensive liquid water, whose evaporation process drives the IER to absorb CO_2 when dry, and whose hydration process releases CO_2 when wet[26]. It has been speculated that the hydration water plays two important roles: it provides a medium for reactions and it protonates reactants through water dissociation. However, the underlying molecular mechanism of the hydration induced energy change at gas/solid interfaces or on ions has not been elucidated in a comprehensive way.

CO_2 sorption on a hydrated ion exchange resin with CO_3^{2-} as the mobile anion at low humidity could be depicted as a series of reactions of water dissociation, formation of bicarbonate and hydroxide ions, as shown **Figure 2.1**. State 1 is the ion exchange resin in dry condition with a few water molecules in the surrounding. State 2 shows how a carbonate ion can be split into bicarbonate ion and hydroxide ion, which is ready to absorb carbon dioxide.

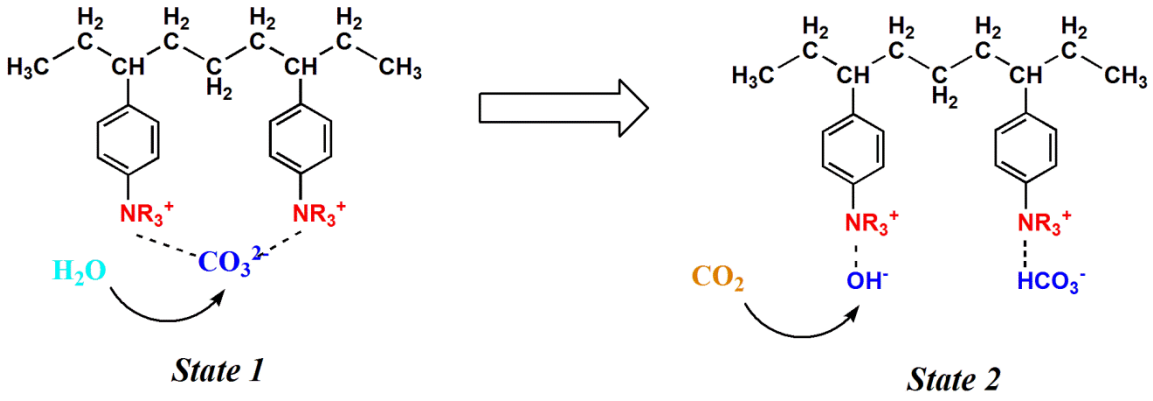

Figure 2.1: Reaction pathway of CO_2 absorption on IER

The process of CO_2 absorption/desorption can be depicted as a series of reactions of water dissociation, formation of bicarbonate and hydroxide ions, and CO_2 combination, as shown **Figure 2.2**. The ***Empty-Fresh*** state is the sorbent in dry condition with a few water molecules in the surrounding. In the ***Empty-Dry*** state the H_2O splits into H^+ ion and OH^- ion which is ready to absorb CO_2, while the H^+ ion is combined with CO_3^{2-} to form an HCO_3^- ion. The ***Full-Dry*** state rerpresents the fully loaded sorbent in the dry condition. The three states present the absorption process. The ***Empty-Wet*** state results as the sorbent regenerates and releases CO_2 in the wet condition (desorption).

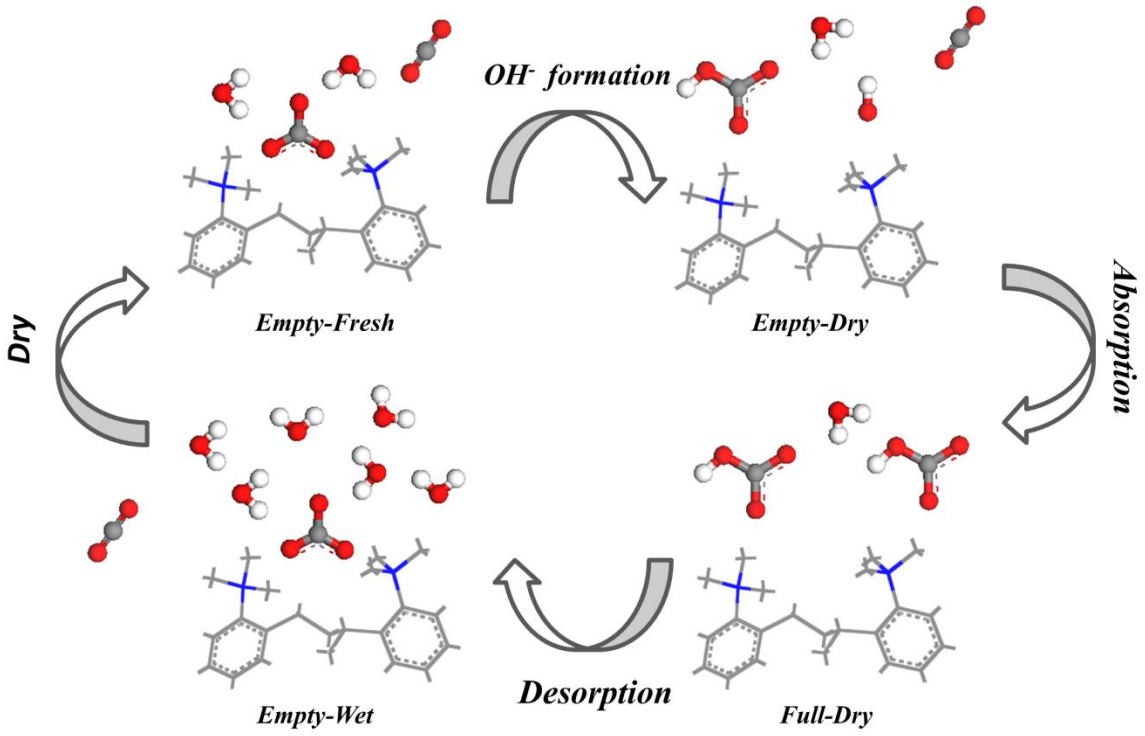

Figure 2.2: Reaction pathway of CO_2 absorption/desorption on IER.

2.3 Computational Model

The activity of water on the resin governs the interaction among all ions on the resin. This is very different from a hypothetical "dry" resin in which every carbonate ion is balanced by two singly charged cations without any water molecules present. In the presence of water, carbonate ions can react with water to form bicarbonate and hydroxide ions. This is well understood in aqueous solutions. It has been postulated that the reduction in water activity results in a loss of stability of the carbonate ion, which will be replaced by a hydroxide and a bicarbonate ion:

$$CO_3^{2-} + nH_2O \Leftrightarrow HCO_3^- + OH^- + (n-1)H_2O \qquad 2.1$$

Based on experimental results, the IER absorbs more CO_2 in relatively dry conditions (n is small) with the help of more OH^- ions, while it absorbs less CO_2 in relatively wet condition (n

is large) with less OH^- ions. In other words, as *n* increases, the equilibrium shifts to the left of **Equation 2.1**. This shift in equilibrium appears counter-intuitive, as it seems to go against the mass action law implicit in **Equation 2.1**. Usually, in the salt solution with the reduction of the number of water molecules, the concentration of the salt in the aqueous solution increases until saturation, and then ions start to precipitate. For example, the ratio of carbonate ion and water molecules is 1:20 in a saturated sodium carbonate solution whose solubility is 220g/l at 20 ℃. However, the ratio of carbonate ions and water molecules may be up to 1:1 in the surroundings of an ion exchange resin. Therefore, we hypothesize that the driving force for this change in equilibrium is the change in the size of the hydration clouds associated with the different ions in the material. The total equation taking into account hydration water is represented by **Equation 2.2**

$$CO_3^{2-} \cdot nH_2O \Leftrightarrow HCO_3^- \cdot m_1H_2O + OH^- \cdot m_2H_2O + (n - 1 - m_1 - m_2)H_2O \qquad 2.2$$

The observed direction of the reaction implies that $(n - 1 - m_1 - m_2)$ is larger than zero. The chemical reaction moves to the right hand side with small number of water molecules to produce more hydroxide ions, which is beneficial for carbon dioxide adsorption, and it swings to the left hand side with a large number of water molecules present. The partial pressure of CO_2 over a wet, fully-loaded bicarbonate state resin, is comparable to the equilibrium partial pressures over a one-molar sodium bicarbonate solution. This suggests that the unusual state is not the wet state, but the dry, absorption state in the CO_2 capture system. Note, that as *n* goes to zero, the state has to again shift back to the carbonate system, because there is simply no water available, and $(n - 1 - m_1 - m_2)$ cannot be positive anymore. However, this state is not reached in our experimental and computational system.

We postulate that the energetically favorable state of this system can be shifted with the different numbers of hydrated water molecules around ions, which will be verified using molecular simulations in this study. The classical molecular mechanical models can handle a large number of molecules, but they suffer from technical limitations for simulating bond breaking and forming. Quantum mechanical methods are powerful in simulating the chemical environment but are computationally expensive and therefore can handle only a few molecules in a simulation. A methodology combining MD and QM is outlined in **Figure 2.3**. It can overcome these limitations by calculating energy states in a hypothetical cycle connecting aqueous states to ionic states in the vacuum. In the corresponding thermodynamic cycle of the proposed process, a sequence of states is considered. Let ΔG_1 and ΔG_2 denote the hydration standard-state Gibbs free energy changes of system 1 (S1, a carbonate ion) and system 2 (S2, a hydroxide with a bicarbonate ion), respectively. ΔG_3 represents the standard-state Gibbs free energy change of the reaction $CO_3^{2-} + H_2O \Leftrightarrow HCO_3^- + OH^-$ in vacuum at room temperature. Using MD simulations of relevant systems, ΔG_1 and ΔG_2 can be determined by free energy Thermodynamic Integration (TI); Because the ions in a vacuum represents a system with few particles, ΔG_3 can be deduced from QM simulations using the density functional theory (DFT). Since energy is a state function and does not depend on the pathway used for its evaluation, the total free energy ΔG can be obtained as $\Delta G=\Delta G_1+\Delta G_2+\Delta G_3$. The objective is to quantify the total free energy ΔG as the number of surrounding water molecules (n) changes. Two mobile cations (Na^+) were put into the system, in order to balance the anionic charges.

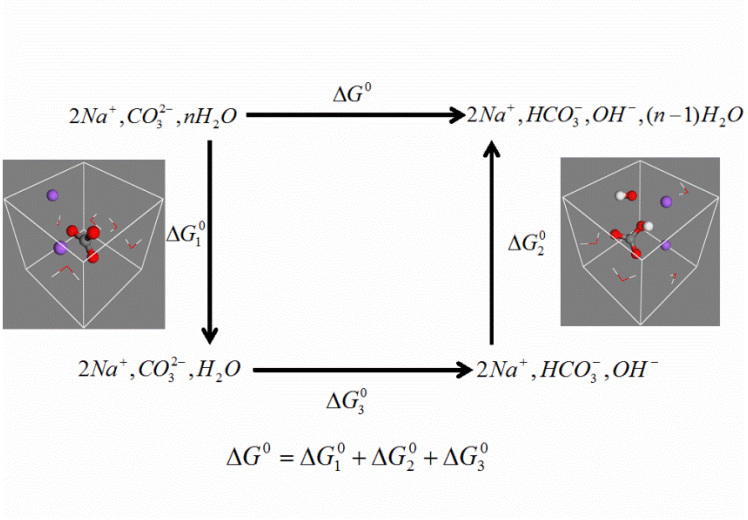

Figure 2.3: Thermodynamic cycle for calculating reaction energy change with water numbers.

2.4 Computational Method

All molecular dynamics simulations were carried out in Materials Studio[92], which is a modeling and simulation environment to study atomic and molecular structure in material science and chemistry. COMPASS Force Field was used for all geometry optimizations and MD simulations. COMPASS uses an *ab initio* force field optimized for condensed-phase applications. This force field was assigned to all atoms in the carbonate ion, bicarbonate ion, hydroxide ion, and water molecule.

Geometry and partial charges on all atoms of anions in gaseous and aqueous phases were calculated by density functional theory code DMol[3] [93], developed by Accelrys. Geometry optimizations and population analysis of the anions were obtained according to Generalized Gradient Approximations (GGA) DFT formulation which includes the effect of charge-density inhomogeneity, and the Perdew-Burke-Ernzerhof (PBE) gradient-corrected functional[94]. The "double numerical plus polarization" (DNP) basis set was utilized in the present work. DNP is

the most complete and most accurate basis set in the DMol[3] code. A p-type polarization function was employed for hydrogen bonding. Simple point charge (SPC) variable bond water model was used in our model.

Periodic boundary conditions (PBCs) were employed in three dimensions with a carbonated ion (S1), or a bicarbonate and a hydroxide ion (S2) solvated with different numbers of water molecules. Minimizations were carried out by the Quasi-Newton procedure, where the electrostatic and van der Waals energies were calculated by the Ewald summation method[95] (the Ewald accuracy was 0.001kcal/mol, and the repulsive cutoff for van der Waals interaction was 6 Angstrom). MD simulations for all configurations of solutions were performed first in an NPT ensemble (constant-pressure/constant-temperature) to obtain the relevant density values with different concentrations of solutions at standard state condition. Each solution with different concentration was calculated in an NVT-ensemble (constant-volume/constant-temperature) with different densities at 298 K. A time step of 1.0 fs was used in all simulations. In most cases, the equilibrium values of thermodynamic parameters were reached within the first 50 ps for NPT using Nose thermostat and Berendsen barostat, and 50 ps for NVT using Nose thermostat. All MD simulations were performed for 200 ps to achieve equilibrium followed by 300 ps simulation for parameter deduction.

The chemical reaction energy of $Na_2CO_3 + H_2O \Leftrightarrow NaHCO_3 + NaOH$ (S3) in a vacuum connecting ground states was simulated via first principle calculation. Na_2CO_3 and H_2O are the reactants; $NaHCO_3$ and NaOH are the products. The total energy at 0K was obtained via the Perdew-Burke-Ernzerhof generalized gradient approximation (GGA PBE), and a DNP basis set. The free energy change at finite temperatures was computed according to the various translational, rotational and vibrational components.

2.5 Free Energy Computation

The MD free energy calculation was performed by the Thermodynamic Integration method (TI)[96]. The free energy difference between two states, A and B, is determined from an interpolating Hamiltonian[97,98]. In this method, the system is extended with a mixing parameter λ, ranging from 0 to 1, which measures the degree of reaction between A (λ=0, reactant) and B (λ=1, product). The system potential energy can be described as

$$U(r,\lambda) = (1-\lambda)U_A(r) + \lambda U_B(r) \qquad 2.3$$

The free energy change can be calculated from

$$\Delta G = \int_0^1 d\lambda \frac{\partial G(\lambda)}{\partial \lambda} = \int_0^1 d\lambda \langle \frac{\partial U}{\partial \lambda} \rangle_\lambda \qquad 2.4$$

where $\langle \frac{\partial U}{\partial \lambda} \rangle_\lambda$ signifies an ensemble average over the distribution $e^{[\beta U(r,\lambda)]}$. Considering solvation system, U_A=$U_{water\text{-}water}$ and U_B=$U_{water\text{-}water}$ + $U_{ion\text{-}water}$, then

$$\frac{\partial U(r,\lambda)}{\partial \lambda} = U_{ion-water} \qquad 2.5$$

$U_{ion-water}$ can be determined from water-ion van der Waals and electrostatic interactions. In TI, $\langle U_{iw} \rangle_\lambda$ needs to be calculated for different λ values between 0 to 1. In our present work, we evaluated ΔG at ten equidistant value for λ (0.1 to 1) from which $\langle U_{iw} \rangle_\lambda$ was calculated[99], and then the free energy of solvation was determined by numerical integration.

To determine the free energy of reaction from QM calculations, the thermodynamic cycle shown in **Figure 2.4** was employed. If the heat capacities of the reactants and products between the two temperatures are known, the enthalpy of reaction at temperature T_1 can be calculated

from the enthalpy of reaction at T_0. ΔS is given by $\Delta S = \Delta S_{vib} + \Delta S_{trans} + \Delta S_{rot}$. The Gibb's free energy difference is given by $\Delta G = \Delta H - T\Delta S$.

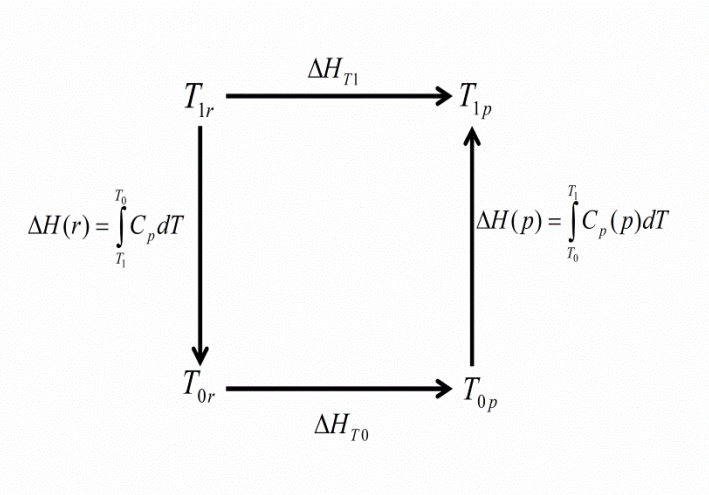

Figure 2.4: Chemical reaction thermodynamic cycle between different temperatures.

2.6 Free Energy of Ion Hydration

The system's free energy change for different numbers of water molecules present is calculated from MD and QM simulations. The hydration free energies of system 1 (S1, with two Na^+, one CO_3^{2-} and one H_2O), and system 2 (S2, with two Na^+, one HCO_3^- and with one OH^-) in the presence of water were plotted against the number of water molecules (*n*). The result is shown in Figure 2.5. In the carbonate ion system simulations (S1), the CO_3^{2-} : H_2O ratio is selected to be 1:2, 1:3, 1:4, 1:5, 1:6, 1:7, 1:8, 1:9, 1:10, 1:20, 1:40, 1:60 respectively, and for the bicarbonate ion system (S2), the HCO_3^- to water ratio is tested at 1:1, 1:2, 1:3, 1:4, 1:5, 1:6, 1:7, 1:8, 1:9, 1:19, 1:39, 1:59 respectively, from dense to dilute solution. These cases have one-to-one correspondence, since one water molecule reacts with one carbonate ion to form a bicarbonate and a hydroxide. The region around each ion dissolved in water can be divided into two parts: a hydration shell, in which the water is immobilized and electrostricted, and bulk water, which is

still attracted by the Coulomb electric field of the ion, but the water is mobile and not bound to the ion. Based on MD modeling results, typically the free energies of hydration in the Na^+- CO_3^{2-} - H_2O system and in the Na^+ - HCO_3^- - OH^- system decrease, when the number of water molecules increases from 0 to 40. These hydration free energies are stable in the range of 40 to 60 water molecules. In system S1, the free energy fluctuates rapidly with the number of water molecules available. We speculate that this reflects the filling of an inner hydration shell, where different number of water molecules would result in different geometries. If more water is available, the Coulomb potential of the ion likely causes a gradual decrease in the free energy until the system asymptotically reaches a state similar to that in free water. If the water molecules are more than 300, the hydration free energies of S1 and S2 stabilize around -80 kcal/mol and -50 kcal/mol, respectively, see **Figure 2.6**.

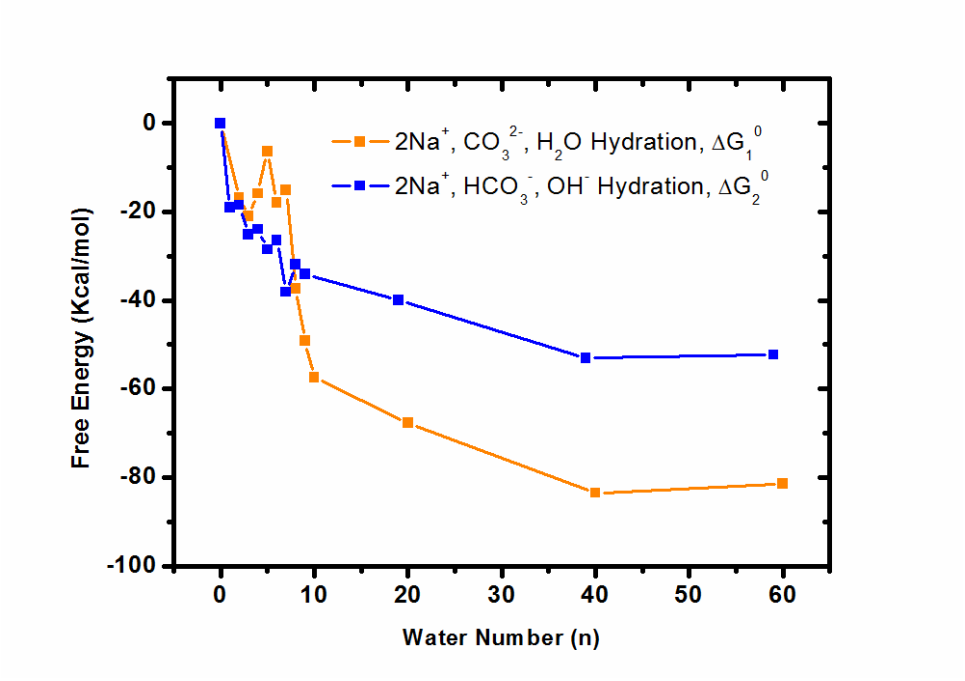

Figure 2.5: Free energy change with number of water molecules.

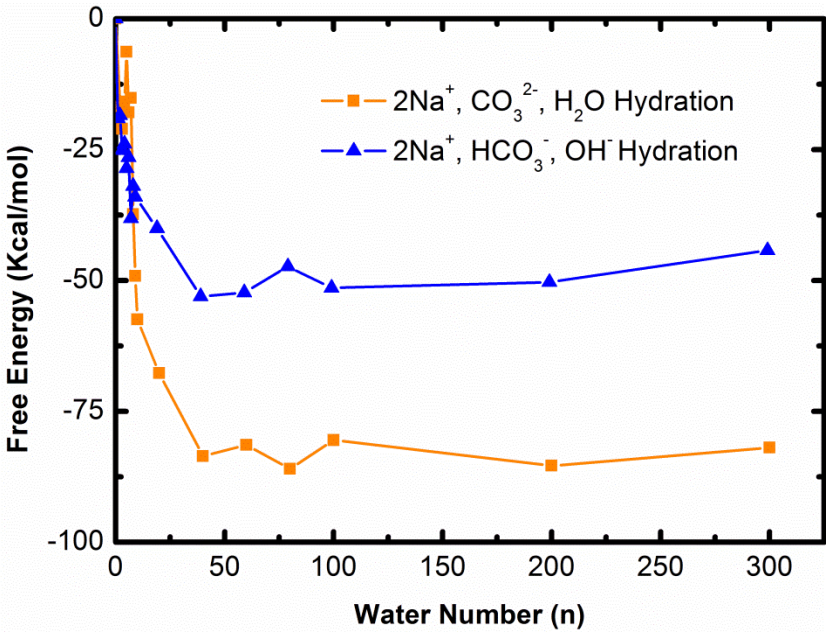

Figure 2.6: Free energy change with number of water molecules (300 water molecules).

2.7 Mechanism of Moisture Swing CO_2 Sorbent

In **Figure 2.7**, attention is restricted to the energy difference between the two competing scenarios. Here the free energy difference between the two systems is plotted as function of the number of water molecules. With less than 7 water molecules, the hydration free energy of S2 is smaller than S1. However, as the number of water molecules increases from 8 to 60, the hydration free energy of S2 is larger than S1, and the difference becomes stable in bulk water. The number of water molecules affects the systems' hydration free energies, which could further influence the chemical reaction pathway in **Equation 2.2**. For small numbers of water molecules present, the thermodynamically favored state is that of a bicarbonate ion and hydroxide ion over that of a carbonate ion and a water molecule.

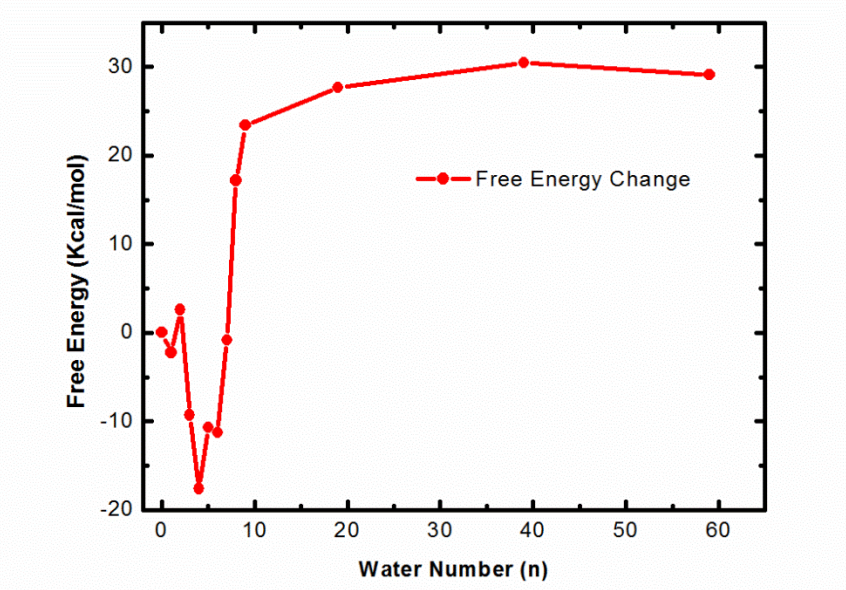

Figure 2.7: Free energy difference between two systems.

According to **Figure 2.3**, $\Delta G^0=\Delta G_1{}^0+\Delta G_2{}^0+\Delta G_3{}^0$, where $\Delta G_3{}^0$ is the reaction energy of$Na_2CO_3^{2-} + H_2O \Leftrightarrow NaHCO_3^- + NaOH^-$ in vacuum at room temperature. This includes the total energy difference at ground state ΔE_{total} and a finite temperature correction for the free energy difference ΔF_{total} between reactants and products, i.e. $\Delta G = \Delta E_{total} + \Delta F_{total}{}^{298.15K}$. The resulting free energy $\Delta G_3{}^0$ is deduced as -9.28 kcal/mol. The negative sign of the free energy indicates that this reaction can occur spontaneously at room temperature. Based on the above MD and QM free energy calculations, the total free energy change of reaction pathway **Equation 2.2**, can be plotted as a function of the number of water molecules in the cell, **Figure 2.8**. The free energy is negative when there are less than 7 water molecules, favoring the formation of hydroxide ions. With the increase in the number of water molecules, the free energy difference increases rapidly from negative to positive value, then becomes stable at a plateau of 15 kcal/mol in bulk water. The experimental value of the carbonate hydrolysis equilibrium constant K in bulk aqueous solution is 1.9×10^{-4},[100] using G=-RTlnK. Based on this result, the free energy of

hydrolysis can be calculated as 5.08 kcal/mol. Using tabulated thermodynamic properties, one can estimate the free energy of hydrolysis at 2.97 kcal/mol. ($\Delta G_{Na^+(aq)} = -62.66 kcal/mol$, $\Delta G_{CO_3^{2-}(aq)} = -126.27 kcal/mol$ $\Delta G_{HCO_3^-(aq)} = -140.37 kcal/mol$, $\Delta G_{OH^-(aq)} = -37.62\ kcal/mol$) Although on the same order of magnitude, the error of present molecular simulation of ion hydration free energy in aqueous solution may result from the force field of MD, or be due to the QM simulation of the free energy in vacuum. Despite the small offset, the present analysis showed, at least in terms of qualitative trend, that the hydrolysis degree of carbonate ion in aqueous solution is affected by the number of water molecules present in the resin. This alone enables the moisture swing of the sorption process. Put another way: in a system with little water present the nominal carbonate state disassociates into a mixture of bicarbonate and hydroxide. Where the latter has a high afficinity for CO_2. The CO_2 once bound, can be released again, even at a higher pressure, simply by profdicing moisture to the resin. Hence moisture drives an sorption/desorption cycle or swing.

The trend in **Figure 2.8** shows that with the reduction of the number of water molecules available, it becomes more energetically favorable to form bicarbonate ion and hydroxide ions hydration, whereas carbonate ion hydration occurs in relative wet condition. This discovery sheds some light on the molecular mechanism of the observed phenomenon of dry absorption of CO_2 on an ion exchange resin. In a relatively dry environment, the amount of water bound to the resin is small and a large amount of hydroxide ions exist, which promotes the absorption of carbon dioxide, since the hydrolysis equilibrium constant increases with the reduction of the number of water molecules.

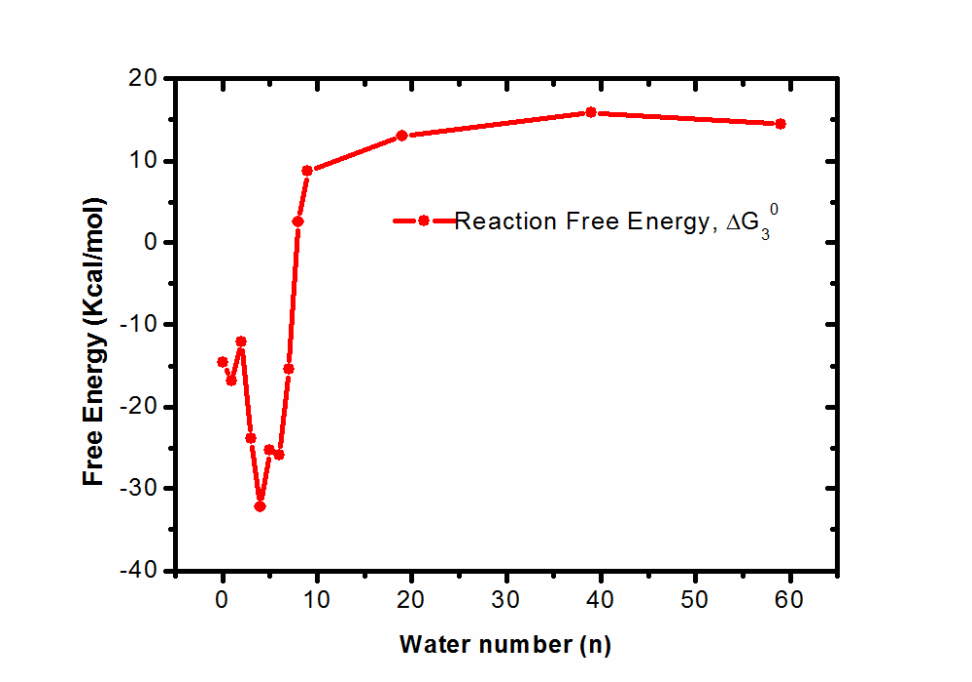

Figure 2.8: Equation 2.2 Chemical reaction free energy change with water numbers.

2.8 Mechanism of Moisture Swing CO_2 Sorbent with polystyrene backbone

The above studies of free energy is based on ions with different number of water molecules in vacuum surroundings. The computational model differs from the real IER system in two crucial aspects. First, ions and water molecules do not exist in vacuum surrounding but at the surface of polystyrene backbones, on which a series of chemical reactions occur; the second difference is that the cations are not sodium cations, but quaternary ammonium ions. The quaternary ammonium ions are composed of C, H and N atoms, which have a larger size and also have a different strength of van der Wall force on anions. Here, we calculated the energy/enthalpy change of in IER system with polystyrene backbones using the same method as

outlined in **Figure 2.3** as above. This more complete model can better capture the characteristics of the real system, but complicates the numerical analysis..

2.8.1 Models of Ion Exchange Resin

The IER is composed of polystyrene backbones and attached quaternary ammonium ions. These quaternary amine groups have one permanent positive charge, which can be shown as NR_4^+. R stands for organic carbon chains.nOne of these chains is also attached to the polystyrene matrix.

A model of an oligomer containing eight side chains with eight quaternary ammonium ions is established for MD simulation. The oligomer includes two quaternary ammonium ions is shown as an example in **Figure 2.9**. Four oligomers, each containing eight quaternary ammonium ions, were packed in an amorphous cell. The periodic boundary conditions is applied to eliminate surface effects. In this study, two IER systems containing different classes of anions were established in charge balance. System 1 has 4 oligomers[101] attaching 16 carbonate ions to balance the charge, and the other one, system 2, has 4 oligomers attaching 16 bicarbonate ions and 16 hydroxide ions to balance the charge. System 1 and system 2 represent the reactant and product of **Equation 2.2**, respectively, shown in **Figure 2.10**

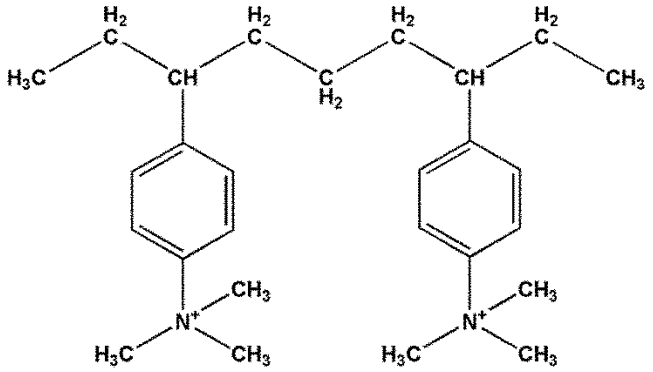

Figure 2.9: Chemical structure of IER containing two side chains

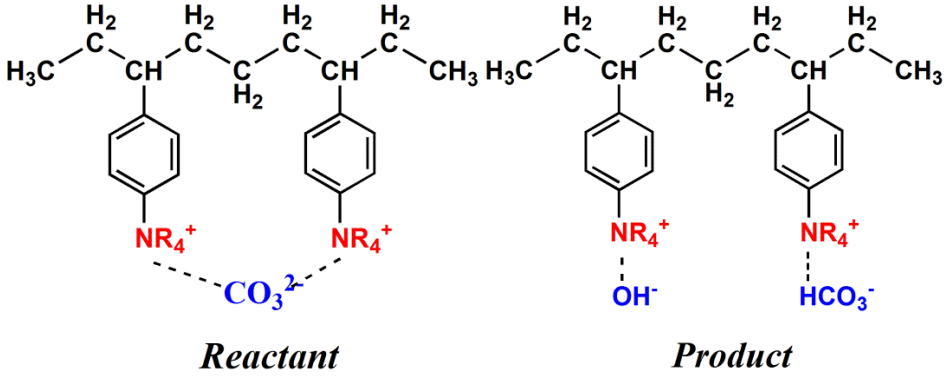

Figure 2.10: Chemical structures of reactant system 1 and product system 2

System 1 (S1) and system 2 (S2) are solvated with different numbers of water molecules. In the carbonate ion system (S1) simulations, the CO_3^{2-} : H_2O ratio is selected to be 1:1, 1:2, 1:3, 1:4, 1:5, 1:6, 1:7, 1:8, 1:10, 1:15, 1:20, 1:25, 1:30, 1:50, and 1:80 respectively, and for the bicarbonate and hydroxide ion system (S2), HCO_3^- : H_2O ratio or OH^-:H_2O ratio is tested at 1:0, 1:1, 1:2, 1:3, 1:4, 1:5, 1:6, 1:7, 1:9, 1:14, 1:19, 1:24, 1:29, 1:49, 1:79 respectively, from low to high humidity conditions. These two cases have one-to-one correspondence, since one water molecule reacts with one carbonate ion to form a bicarbonate and a hydroxide ion. The geometry configurations of S1 containing 80 water molecules (CO_3^{2-} : H_2O is 1:5) and S2 containing 64 water molecules (HCO_3^- : H_2O is 1:4) are shown in **Figure 2.11**

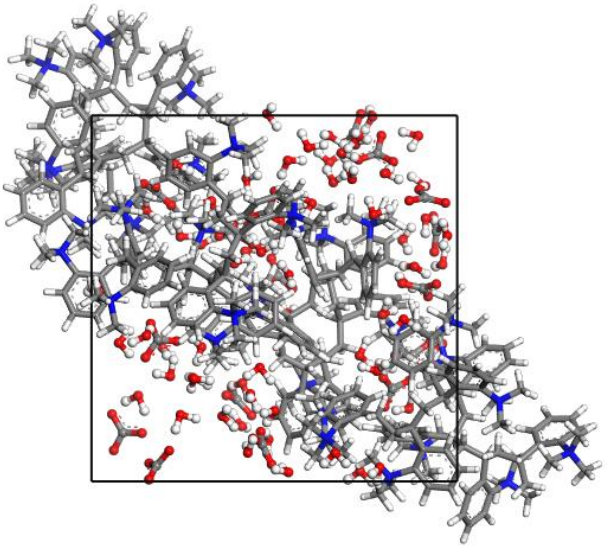

(a)

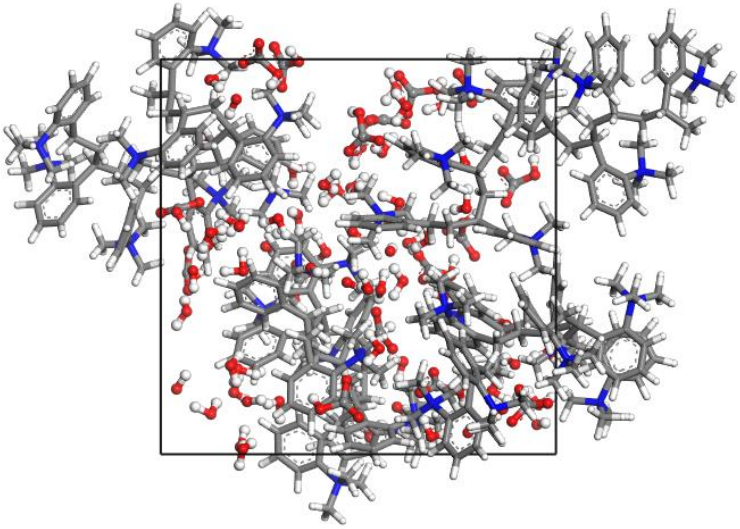

(b)

Figure 2.11: Geometry configurations of IER with ion species and water molecules. **(a)** S1 contains 4 oligomers, 32 quaternary ammonium ions, 16 carbonate ions, and 80 water molecules. **(b)** S2 contains 4 oligomers, 32 quaternary ammonium ions, 16 bicarbonate ions, 16 hydroxide ions and 64 water molecules.

2.8.2 Simulation Procedure

All molecular dynamics simulations were carried out in Materials Studio,[92] the COMPASS Force Field was used for all geometry optimizations and MD simulations. The Dmol3 module was applied for QM calculation. The charges of all atoms in the carbonate ion, bicarbonate ion, hydroxide ion, and water molecule were assigned by QM calculation.

The initial structures of S1 and S2 with different numbers of water molecules each were build in amorphous cells. Minimizations were carried out by the Quasi-Newton procedure, where the electrostatic and van der Waals energies were calculated by the Ewald summation method (the Ewald accuracy was 0.001kcal/mol, and the repulsive cutoff for van der Waals interaction was 6 Angstrom). In order to achieve a relaxed structure, the systems were further equilibrated by NVE ensemble simulation with 100 ps, and then an NPT ensemble was performed to obtain the relevant density values with different water numbers at standard state condition. Then run NVT ensemble for 200 ps to allow systems to achieve equilibrium. To estimate the energy/enthalpy difference of ΔG_1^0 and ΔG_2^0 in **Figure 2.3**. NVT ensembles for another 300 ps were run with different densities at 298 K. A time step of 1.0 fs was used in all simulations. NPT ensemble used Nose thermostat and Berendsen barostat, and NVT ensemble used Nose thermostat.

2.8.3 Energy Change of Chemical Reaction on Ion Exchange Resin

We explored the fundamental mechanism of moisture swing IER sorbent for CO_2 capture from air. Based on atomistic modeling, the system energy/enthalpy changes between two states with different number of water molecules were calculated. The energies/enthalpies of system 1 (S1, polystyrene backbone with 32 NR^+, 16 CO_3^{2-} and n H_2O), and system 2 (S2, polystyrene

backbone with 32 NR^+, 16 HCO_3^-, 16 OH^- and n-1 H_2O) were plotted against different number of water molecules in **Figure 2.12**(a) and (b) for energy and enthalpy respectively.

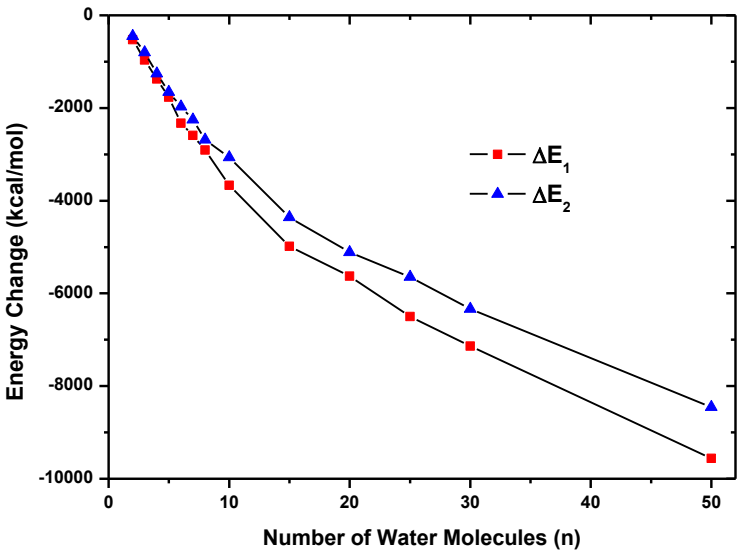

(a)

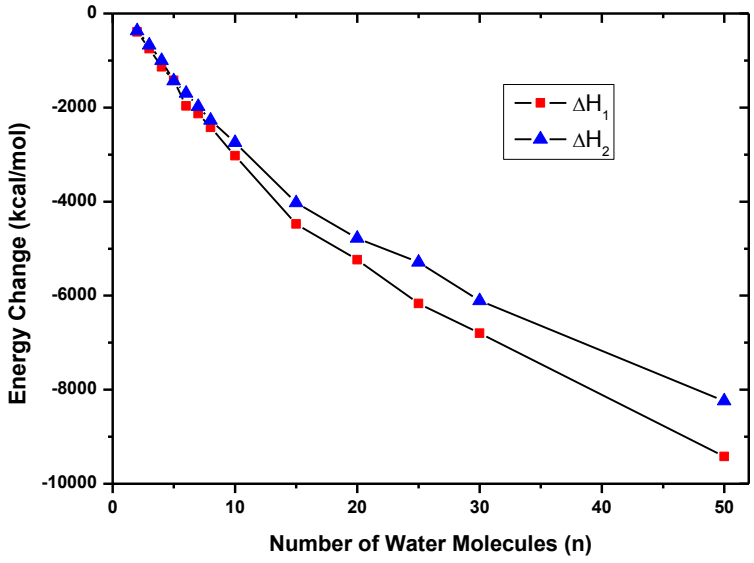

(b)

Figure 2.12: (a)/(b) Change of Energy/Enthalpy in system 1 and system 2 as a function of the water numbers. In the carbonate ion system (S1), the CO_3^{2-} to water ratio is selected to be 1:2,

1:3, 1:4, 1:5, 1:6, 1:7, 1:8, 1:10, 1:15, 1:20, 1:25, 1:30, 1:50 and 1:80 respectively, and for the bicarbonate ion system (S2), the HCO_3^- to water ratio is established at 1:1, 1:2, 1:3, 1:4, 1:5, 1:6, 1:7, 1:9, 1:14, 1:19, 1:24, 1:29, 1:49, 1:79 respectively, from low to high relative humidity. These cases have one-to-one correspondence because of the reaction between one carbonate ion and one water.

$\Delta E_1/\Delta H_1$ and $\Delta E_2/\Delta H_2$ lack physical meanings They are energy differences shown as **Figure 2.3**, but not hydration energy which is the amount of energy released when ions undergo hydration. According to **Figure 2.3**, The attention here is restricted to the vector sum of $\Delta E_3/\Delta H_3$ and the energy/enthalpy difference ($\Delta E_1/\Delta H_1$ and $\Delta E_2/\Delta H_2$) between S1 and S2, where $\Delta E_3/\Delta H_3$ is the reaction energy/enthalpy of $(NR_4)_2CO_3 + H_2O \Leftrightarrow NR_4HCO_3 + NR_4OH$, calculated by QM. Enthalpy includes the total energy difference at ground state ΔE_{total} and finite temperature correction enthalpy difference ΔH_{total} between reactants and products, i.e. $\Delta H = \Delta E_{total} + \Delta H_{total}^{298.15K}$. The QM calculated energy and enthalpy are -13.996 kcal/mol and -14.497 kcal/mol. Based on the developed atomistic modeling methodology, the total energy/enthalpy change of **Equation 2.2** is plotted with different number of water molecules, shown as **Figure 2.13**. The results also reveal that the system from an energy perspective favors forming HCO_3^- ion and OH^- ion hydration in relatively dry condition, while forming CO_3^{2-} ion hydration in relative wet condition. This discovery is consistent with the previous findings on free energy changes in **Equation 2.2** in a vacuum surrounding. The difference is the greater number of water molecules required for the system to stabilize in the bulk water limit. Reaction energy needs about 50 water molecules to reach this stable state in polystyrene system, which is far more than the about 30 water molecules required in a vacuum surrounding. The reason is that the polystyrene backbones also attracts some water molecules around its matrix due to the van der Waals force acting on

them. These part of water molecules may not contribute to the chemical reaction of **Equation 2.2**. Plus the columbic force and van der Waals force caused by quaternary ammonium cations to water molecules are different from those of Na^+ cations. Though the both models can explain the fundamental mechanisms of moisture swing CO_2 capture phenomenon, the model with backbone can better describe a real ion exchange resin CO_2 capture sorbent.

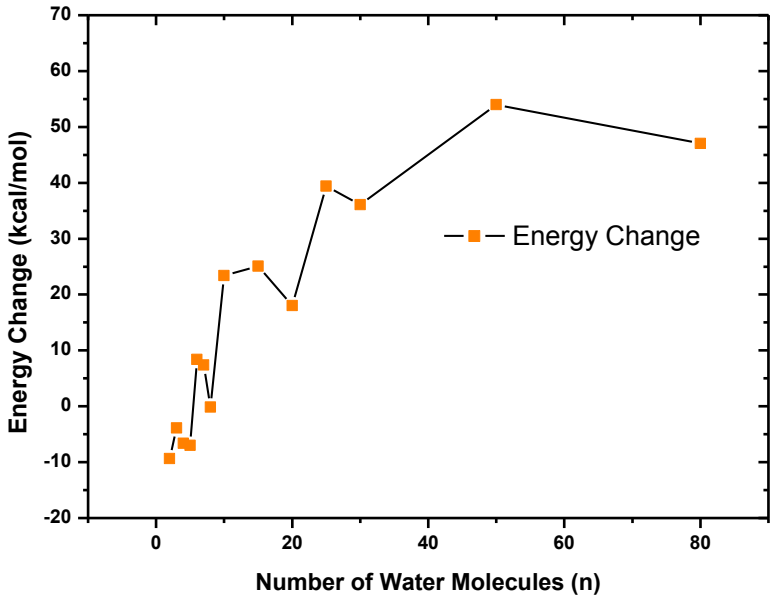

(a)

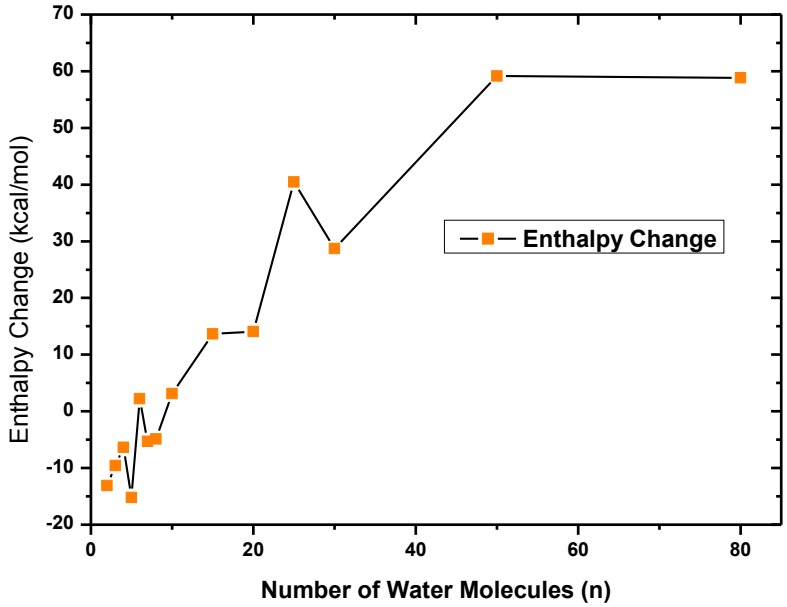

(b)

Figure 2.13: (a)/(b) energy/enthalpy change of chemical reaction **Equation 2.2** with different number of water molecules.

2.9 Experimental Verification

To confirm the effect of CO_2 capture sorbent driven by water quantity. The CO_2 equilibrium concentrations and CO_3^{2-}/H_2O ratios at different humidity conditions are shown in **Figure 2.14**. In this process, IER with CO_3^{2-} were exposed to different levels of moisture in the surrounding air. If the sorbent is exposed to a low level of moisture, relatively larger amounts of OH^- ions are produced which react with CO_2 in gas-phase without a free energy barrier[102]. By contrast, if the sorbent is exposed to a high level of moisture, the concentration of CO_2 equilibrated in the air is at a relative high level because of the low OH^- ion concentration on the sorbent. The CO_2 sorbent sample, with a mass of 0.1299g, was made by soaking the IER in a 1M solution of Na_2CO_3 for four hours. Next, it was dried in a sealed chamber with dry air free of CO_2 and then put into an experimental device comprising a sealed and closed chamber with

internal humidity control (See **Figure 2.15**). The CO_2 concentration in the device was continuously measured by an infrared gas analyzer (IRGA, LI-COR, LI-840). Outside the chamber, the weight of absorbent sample at each relative humidity was measured in its CO_2 free condition. The weight change of the sample indicates the amount of water bound to the IER under different humidity conditions. With the known resin's ion charge density 1.9mol/kg (1.9kg CO_3^{2-} per mole of resin), the ratio of H_2O to CO_3^{2-} ions can be calculated by the weight change. The ratio is taken relative to the nominal number of carbonate ions present, which assumes that all the anions are carbonate ions. The nominal ratio of H_2O to CO_3^{--} does not take into account the hydrolysis of some of the carbonate ions. The ratio considers the combination of a bicarbonate and hydroxide ion as equivalent to a carbonate. In effect, the ratio of water uptake per carbonate can also be viewed as twice the ratio of water molecules to cations (NR_4^+), which are also assumed to be not hydrolyzed. Lastly we note that in the closed system, where we measure the CO_2 concentration in the gas volume, the gas volume is sufficiently small that a change in the CO_2 concentration in the air, does not significantly affect the CO_2 content of the resin. The blue line shows how the H_2O to CO_3^{2-} ion ratio increases with relative humidity (RH) increases. Then, the CO_2 equilibrium concentration was recorded at each RH point. The equilibrium concentration of CO_2 increases as the ratio of H_2O to CO_3^{2-} ion increases. This is shown as the red line. The experiment validates the theoretical results in **Figure 2.8.** Under relatively dry conditions, the low ratios of H_2O/CO_3^{2-} are conducive to the production larger amounts of OH^- ions to absorb CO_2 from air. The CO_2 can again be released at higher pressures water vapor pressures by exposing the resin to higher levels of humidity. The efficient CO_2 absorption-desorption cycle is driven by inexpensive water instead of thermal energy or pressure changes. As noted above, the observed changes is essentially a change in the equilibrium

concentration over the resin, because the gas volume is too small to result in a large change of CO_2 loading on the resin.

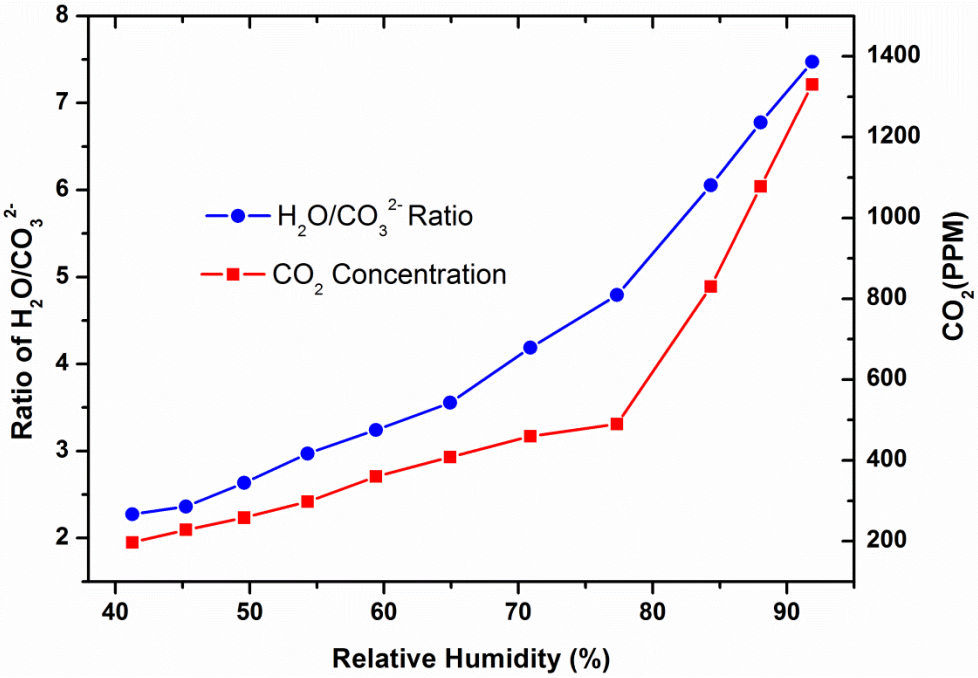

Figure 2.14: Experimental verification. CO_2 equilibrium concentration and water to carbonate ions ratio are corresponding to relative humidity. The blue line shows the H_2O to CO_3^{2-} ion ratio change with relative humidity change. Red line shows CO_2 equilibrium concentration change with relative humidity change.

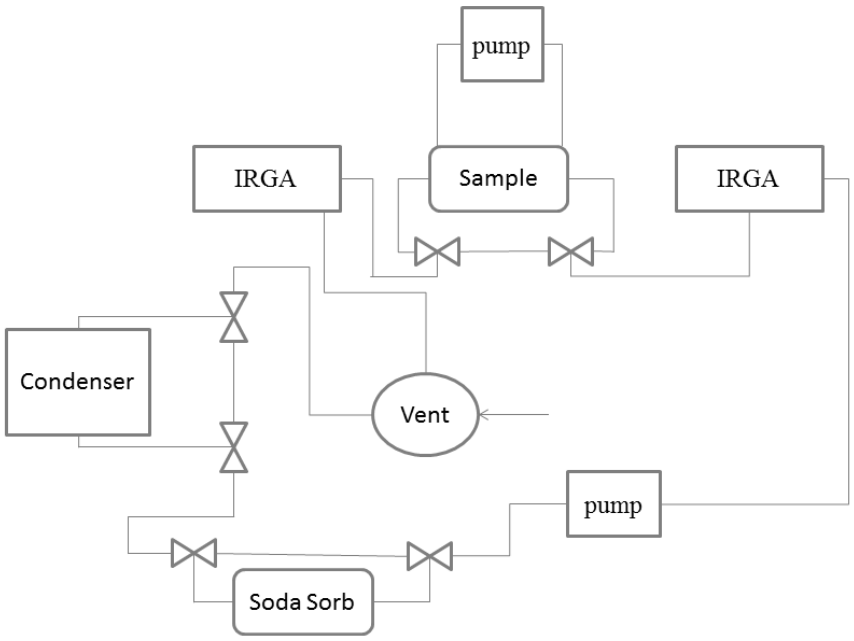

Figure 2.15: Schematic of Experimental Device. The total amount of carbon dioxide on the sample and in the gas volume is constant. We can track the absorption and desorption of carbon dioxide by measuring the carbon dioxide content of the gas. The device can control the water vapor level in the closed gas circulation system. We can determine and characterize the process of CO_2 absorption/desorption by sorbent in the test sample chamber. The experimental results validate the numerical simulations, underpinned by the molecular mechanism discovered in this paper.

2.10 Summary

In this chapter, the molecular mechanism of moisture driven sorbent for CO_2 capture from air is explained for the first time. The free energy of ion hydration has been simulated with different number of water molecules. The deduced free energy change of hydrated ions undergoing hydrolysis shows that the absorbent system energetically prefers a bicarbonate and hydroxide ion over a carbonate ion, when the environment is relatively dry, and the resulting high content of hydroxide ion is more attractive for absorbing carbon dioxide. The higher degree of hydrolysis of carbonate ions in a relative dry environment (with carbonate ion to water molecule ratio more than 1:10), cannot be observed in an aqueous environment (since the ratio is 1:20 when sodium carbonate is saturated in aqueous solution). This counterintuitive phenomenon, verified by both simulation and experiment, may be applicable to other basic and acidic ions, as well as shed some light on the fundamental interactions between ions and water in a confined space of solid materials. Based on this discovery, a nano-structured CO_2 capture absorbent is developed to absorb CO_2 spontaneously from ambient air when the surrounding is dry, while release CO_2 when wet. The conversion between absorption and desorption of this new efficient sorbent can be switched only by low-cost water quantities instead of consuming costly energy to regenerate the sorbent. The novel technology for direct air capture of CO_2 can help in dealing with the critical issue of global warming. A better characterization of the system will allow an improved design of sorbent material.

Chapter 3 Design A Moisture Swing CO_2 Sorbent

This chapter is related to the paper "A Carbon Dioxide Absorption System Driven by Water Quantity" which is ready to be submitted.

In **Chapter 2**, a moisture swing CO_2 sorbent working process is described. The sorbent captures CO_2 in a dry surrounding while releasing CO_2 in a wet surrounding. The underlying mechanism of moisture swing CO_2 sorbent is explored. The reason is that the capability of carbonate ion to hydrolyze water is significantly enhanced in the dry surrounding of air (the quantity ratio of carbonate ion to water is higher than 1:10). Large amount of hydroxide ion existing in the dry surrounding can absorb CO_2 from ambient air without energy barrier. The energy of chemical reactions on polystyrene backbones was also calculated. The moisture swing CO_2 sorbent is not restricted into IER, different materials can also be applied to capture CO_2 based on the mechanism, like activated carbon. . In this Chapter, a simpler model with two confined carbon layers is applied to study the efficiency of hydration driven CO_2 sorbent with respect to different pore sizes, hydrophobic/hydrophilic confined layers, temperatures, and distances of cations. Theses factors are also essential to the performance of the CO_2 sorbent. By understanding the working mechanism of the CO_2 sorbent and the role of each factor how to effect on the absorption performance, could help us to rationally design a higher efficiency moisture swing CO_2 sorbent.

The present study employs Molecular Dynamics (MD) and Quantum Mechanics (QM) simulations to reveal the ion hydration energy changes with water numbers under the condition of nano-confined layers, from which the mechanism of hydration driven absorption for CO_2 capture from ambient air is explained theoretically. Based on the principle of CO_2

absorption/desorption by water quantity, the CO_2 capture systems with other confined nanoporous structural materials or artificial nano-devices are investigated. The study may shed some insights on the future research of high-efficient CO_2 capture system driven by humidity, instead of consuming more extra energy to regenerate, like heating, and contribute to other related areas such as ion hydrations and water/solid chemical reactions.

In section 3.1, the new model with nanoconfined layer is introduced. In contrast to the calculations in **Chapter 2**, we introduce a confining layer of a hydrophobic material, here graphene to include the effects of the small pores that contain the water and the ions that interact to create a CO_2 sorbent that is subject to the humidity swing. With the confined layer, ions and water molecules have been restricted into a nanoconfined space without the ability to move freely. It captures aspects of the overall process that might have been overlooked in the previous calculation and introduces features and parameters to the reaction design that could be engineered for futre processes improvements. Nanoporous materials like activated carbon can provide uniform nano-pores structure, which can maintain higher ratio of CO_3^{2-} ions to H_2O molecules than the ratio of CO_3^{2-} ions to H_2O molecules in structure of IER material. Therefore, more CO_3^{2-} ions are functional in nanoporous material than in polystyrene material mentioned in **Chapter 2**.

A two-dimensional ion hydration shell is generated instead of a three-dimensional hydration shell, which determines different energy levels of constrained ion hydrations from unconstrained ion hydrations with the same number of water molecules. In section 3.2, the influences of different parameters on moisture swing CO_2 sorbent are investigated, as the distance of confinement layers, distance of cations, surface of treatment, and surrounding temperature. The motivation is to enhance the performance of original IER CO_2 sorbent

according to employ other substrates or design optimal parameters for this CO_2 sorbent. In section 3.3, results from several experiments are applied to prove the above computational theories, including design new functional nanomaterials for moisture swing CO_2 sorbents and the effect of the distance of confinement layers

3.1 Mechanism Study of Sorbent with Confined Layers

3.1.1 Computational Method

The computational method is similar as the one mentioned in Chapter 2. The free energy change in the reaction of **Equation 2.2**

$$CO_3^{2-} \cdot nH_2O \Leftrightarrow HCO_3^- \cdot m_1H_2O + OH^- \cdot m_2H_2O + (n - 1 - m_1 - m_2)H_2O$$

with different water amount is the key point to explain this phenomenon. Therefore, a methodology combined with MD and QM is outlined in **Figure 3.1** to overcome the limitations of MD on simulating bond breaking/forming, whereas full QM or *ab initio* MD would computationally expensive. A sequential molecular process may be established in the corresponding thermodynamic cycle. Let ΔE_1 and ΔE_2 represent the hydration standard-state energy changes of system 1 (S1, a carbonate ion) and system 2 (S2, a hydroxide with a bicarbonate ion), respectively. ΔE_3 represents the standard-state energy change of reaction $CO_3^{2-} + H_2O \Leftrightarrow HCO_3^- + OH^-$ in vacuum at room temperature. ΔE_1 and ΔE_2 can be determined by MD simulations; the state of ΔE_3 can be deduced from QM simulation. The total energy change $\Delta E=\Delta E_1+\Delta E_2+\Delta E_3$ of **equation 2.2** can be evaluated as the number of surrounding water molecules (*n*) changes. To balance the anionic charges, freely movable sodium cations (Na^+) are

included in the computational cell. Note that the entropy change is not calculated since its impact on the system is small.

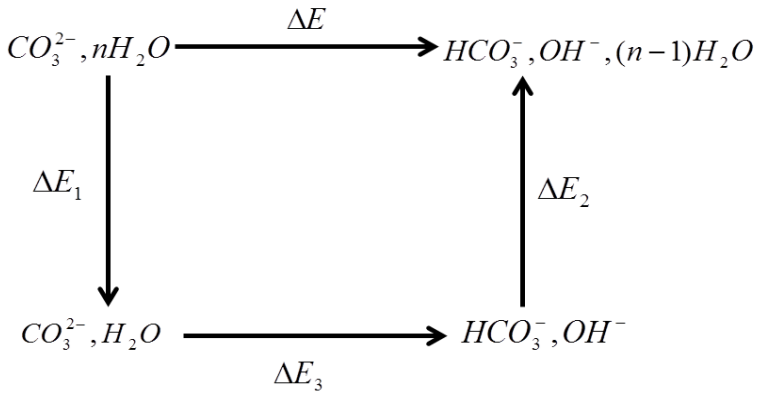

$$\Delta E = \Delta E_1 + \Delta E_2 + \Delta E_3$$

Figure 3.1: Thermodynamic cycle of reaction energy change

3.1.2 Computational Cell

The proof-of-concept computational cell consisted of a graphene layer attached 200 sodium cations, and 100 moveable carbonate ions (S1) as reactant, or 100 bicarbonate and 100 hydroxide ions (S2) as product with different number (100 to 1500) of water molecules. A repeated unit configuration is shown in **Figure 3.2** The graphene was treated as a rigid plate. Periodical boundary conditions (PBCs) were employed in three dimensions.

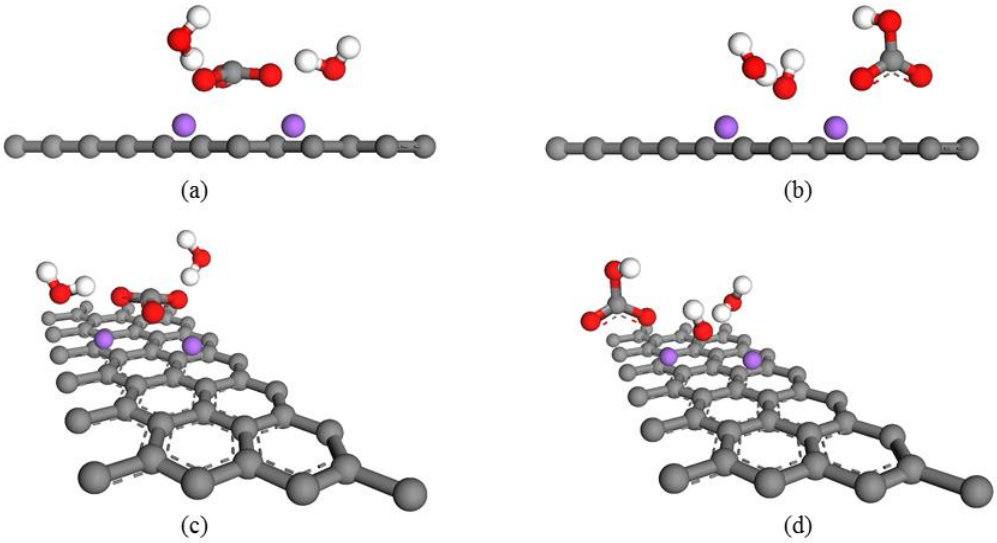

Figure 3.2: Computational Cell. (a) (b) The computational cell of the model S1 and S2 orthographic lateral view. (c) (d) Model S1 and S2 perspective plane view. The grey skeleton represents graphene, red balls represent oxygen, white balls represent hydrogen, and purple balls represent sodium. Graphene was treated as a rigid plate with fixed sodium cations attached. The ratio of carbonate ion to water molecules is 1:2 in the figure, which is only one example of various ratios of carbonate ion to water molecules. (1:1, 1:2, 1:3, 1:4, 1:5, 1:6, 1:7, 1:8, 1:9, and 1:15 studied in this paper) The initial distance between sodium cations was 3.5 Angstrom and 14 Angstrom, along x and y direction respectively.

The computational model represents a CO_2 capture system driven by humidity. Graphene layer characterizes the characteristics of hydrophobic surfaces. Na^+ ions represent a series of cations, such as K^+ ions and NH_4^+ ions, attached to the surface of the hydrophobic material, like ion exchange resin. In this system, the varied environmental factors include water quantities, pore size (space between the surface layers), which was not considered in **Chapter 2,** distance between the attached cations, which also was not considered in **Chapter 2**, hydrophobicity of the

surface layer, and surrounding temperature. The impact of these parameters will be analyzed in the following.

MD simulations were carried out using Materials Studio with the COMPASS forcefield,[103] which is an *ab initio* forcefield optimized for condensed-phase application, assigned to all atoms in graphene, carbonate ion, bicarbonate ion, hydroxide ion, and water. Geometry and partial charges on all atoms of anions in gaseous and aqueous phases were calculated by the DMol^3 program[93]. Geometry optimizations and population analysis of the anions were obtained according to Generalized Gradient Approximations (GGA) HCTH methods[104] and the The "driple numerical plus polarization" (DNP) basis set. A p-type polarization function was employed for hydrogen bonding. The Simple point charge (SPC) and variable bond water model was used in our model. Minimizations were carried out by Quasi-Newton procedure, where the electrostatic and van der Waals energies were calculated by the Ewald summation method[95] (the Ewald accuracy was 0.001kcal/mol, and the repulsive cutoff for van der Waals interaction was 6 Angstrom). MD simulations for all configurations of systems were performed in NVT-ensemble (constant-volume/constant-temperature) at 298 K. A time step of 1.0 fs was used in all simulations. In most cases, the equilibrium values of thermodynamic parameters were reached within the first 50 ps for NVT using a Nose/Hoover thermostat[105,106]. All MD simulations were performed for 200 ps to achieve equilibrium followed by a 300 ps simulation for parameter deduction.

The chemical reaction energy of $Na_2CO_3 + H_2O \Leftrightarrow NaHCO_3 + NaOH$ (S3) in vacuum at ground state was simulated via first principle calculation. Na_2CO_3 with H_2O, and $NaHCO_3$ with NaOH were treated as reactants and products respectively. The total energy at 0K was obtained via functional GGA HCTH and basis set DNP, the used functional is same as above.

Enthalpy correction at finite temperatures was computed according to Hessian evaluation of the translational, rotational and vibrational contributions.

3.1.3 Fundamental mechanisms of a CO_2 capture system driven by water quantity

We first explored the fundamental mechanism of CO_2 capture system driven by water quantity. From MD and QM simulations, the energy difference of the system between two states was calculated as the number of water molecules were varied. The energies of system 1 (S1, one layer graphene with two Na^+, one CO_3^{2-} and one H_2O), and system 2 (S2, one layer graphene with two Na^+, one HCO_3^- and with one OH^-) were plotted against the variation of the number of water molecules (*n*) in **Figure 3.3a** and **Figure 3.3b**, for energy and enthalpy respectively. In the carbonate ion system (S1), the CO_3^{2-} to water ratio is selected to be 1:1, 1:2, 1:3, 1:4, 1:5, 1:6, 1:7, 1:8, 1:9, and 1:15 respectively, and for the bicarbonate ion system (S2), the HCO_3^- to water ratio is established at 1:0, 1:1, 1:2, 1:3, 1:4, 1:5, 1:6, 1:7, 1:8, and 1:14 respectively, from low to high relative humidity. These cases have one-to-one correspondence because of the reaction between one carbonate ion and one water.

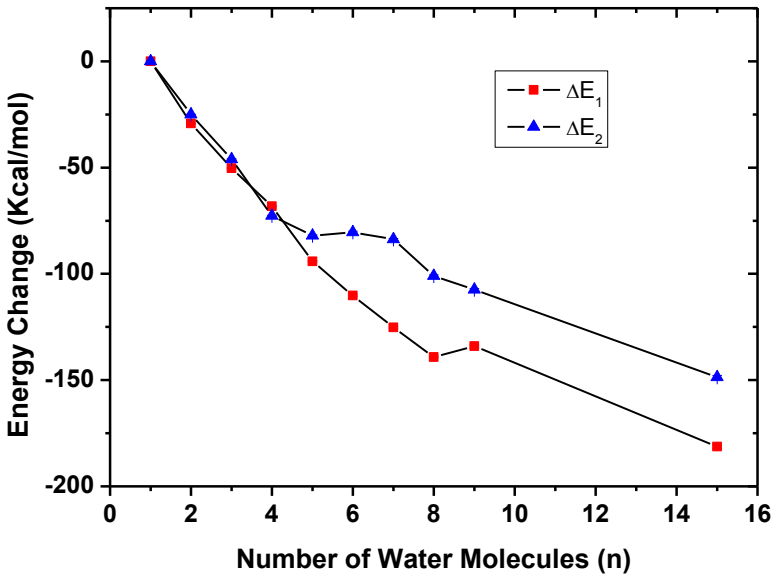

(a)

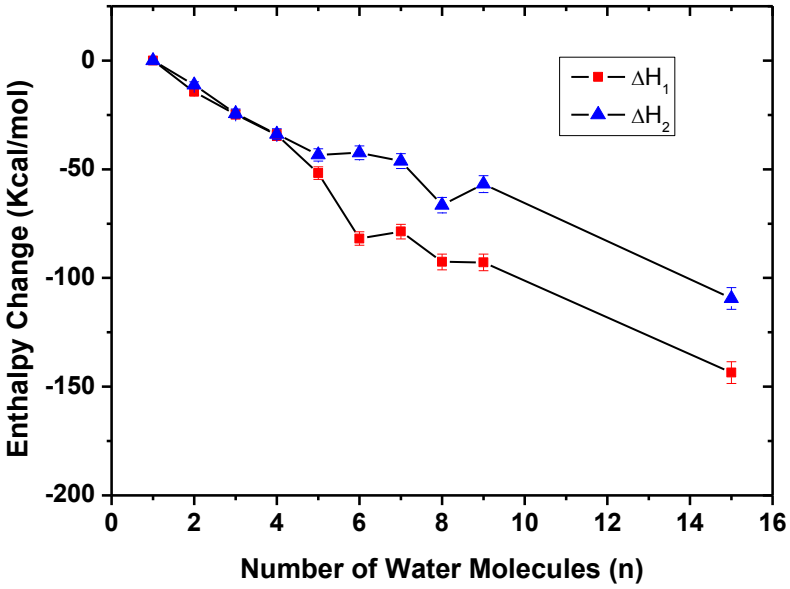

(b)

Figure 3.3: (a)/(b) Variation of Energy/Enthalpy in system 1 and system 2 as a function of the water numbers. The standard deviation of energy is smaller than symbols, and the standard deviation of enthalpy is less than 5.0.

The energy/enthalpy changes in isolated systems of type S1 and S2, shown in **Figure 2.3**, are not simple hydration energies which are the amount of energy released when ions undergo hydrations, thus, we restrict attention to the relative energy difference between the two competing scenarios, i.e., we focus on ΔE_3 and ΔH_3. According to **Figure 3.1**, $\Delta E=\Delta E_1+\Delta E_2+\Delta E_3$ or $\Delta H=\Delta H_1+\Delta H_2+\Delta H_3$ where ΔE_3 and ΔH_3 are the energy and enthalpy change, respectively, in the reaction of $Na_2CO_3 + H_2O \Leftrightarrow NaHCO_3 + NaOH$ in vacuum. Enthalpy includes the total energy difference at ground state ΔE_{total} and finite temperature correction enthalpy difference ΔH_{total} between reactants and products, i.e. $\Delta H = \Delta E_{total} + \Delta H_{total}^{298.15K}$. The resulting energy and enthalpy are deduced as -10.377 kcal/mol and -10.191 kcal/mol respectively. The negative sign of the energy change indicates that this reaction can occur spontaneously at room temperature. Based on the above MM and QM energy calculations, the total energy change of reaction pathway of equation $CO_3^{2-} \cdot n\mathrm{H_2O} \Leftrightarrow HCO_3^- \cdot m_1\mathrm{H_2O} + OH^- \cdot m_2\mathrm{H_2O} + (n-1-m_1-m_2)\mathrm{H_2O}$, can be plotted as a function of the number of water molecules in Fig. 5. With less than 5 surrounding water molecules, the energy value is negative favoring the reaction pathway, and the negative energy value fluctuates with the conformation variation of hydration shells. However, when the number of water increases from 5 to 15 molecules, the hydration energy difference increases rapidly from negative to positive, then approaches a steady plateau of about 23 kcal/mol. The reason is that the effect of ions on water molecules becomes gradually smaller with more water molecules present. This stands in contrast to the large impact on the average water molecule in the hydration shell when less water is available.

The variations and trend in **Figure 3.4** show that with the reduction of the number of water molecules, it becomes more energetically favorable to form HCO_3^- ion and OH^- ion

hydration in a relative dry condition, whereas forming CO_3^{2-} ion hydration in relative wet condition is favorable. The OH^- ions promote the absorption of CO_2, since OH^- ions react with CO_2 in gas-phase without a free energy barrier[102]. the hydrolysis effect on CO_3^{2-} ions increases with the reduction of the number of water molecules because ion hydration shells have a greater effect on the CO_3^{2-} hydrolysis equilibrium constant than bulk water, which results in this counterintuitive phenomenon. This discovery can explain the molecular mechanism of the observed phenomenon for absorbing CO_2 in a dry condition. In what follows, several environmental factors affecting the moisture swing absorption of carbon dioxide are analyzed, which could enhance its system efficiency.

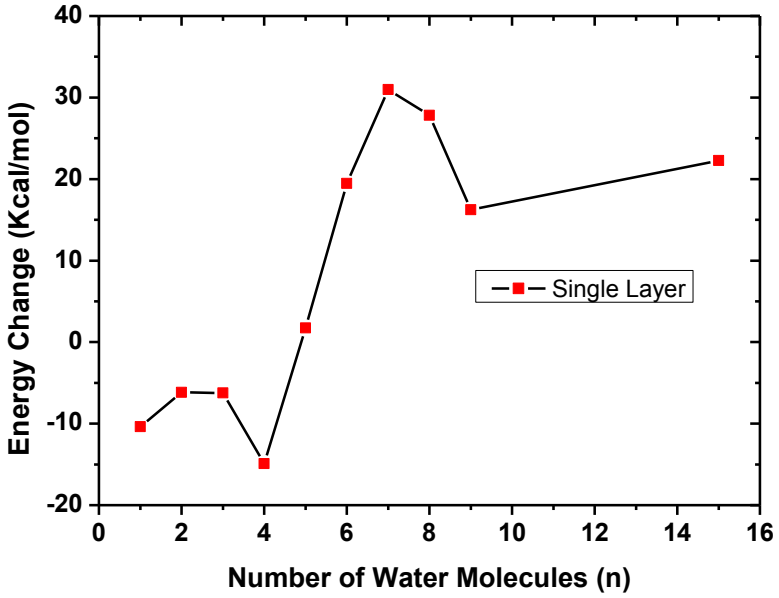

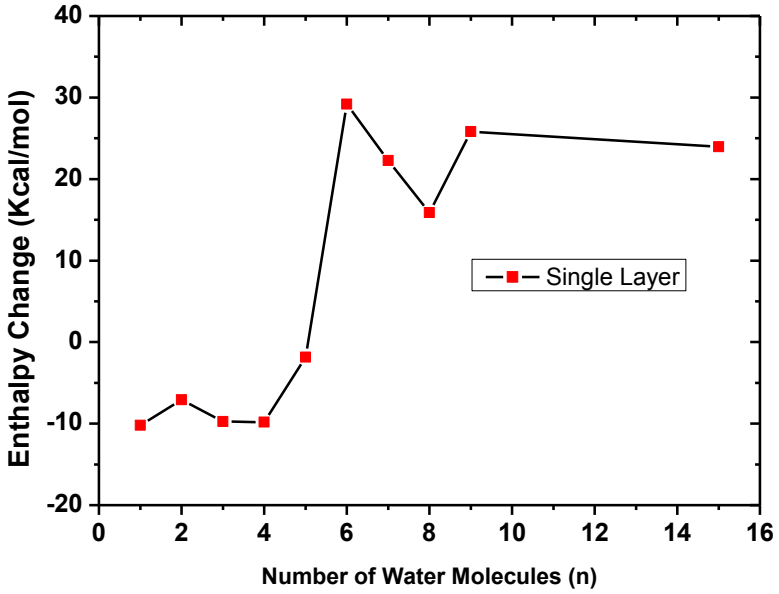

Figure 3.4: (a)/(b) Chemical reaction energy/enthalpy change of **equation 2.2** with different number of water molecules. $\Delta E_1/\Delta H_1$ and $\Delta E_2/\Delta H_2$ are the mean values shown in **Figure 3.3**.

3.2 Parametric study of CO_2 capture system

3.2.1 Effect of distance of confinement layers

The analyses above are based on the proof-of-concept model which consists of a mono surface of graphene layer. The surface effect is now examined by exploring two competing systems: one confined between two layers and one "bulk system" without a surface as a theoretical analysis. The former consists of ions and water molecules sandwiched between two parallel graphene layers with distance D = 5Å, 7Å, and 9Å (three models) between them, and the latter consists of only ions and water molecules in vacuum, shown in **Figure 3.5**. Note that the Na^+ cations are still fixed in their respective spatial locations (with the same pattern 3.5 Å × 14 Å as that in the proof-of-concept model).

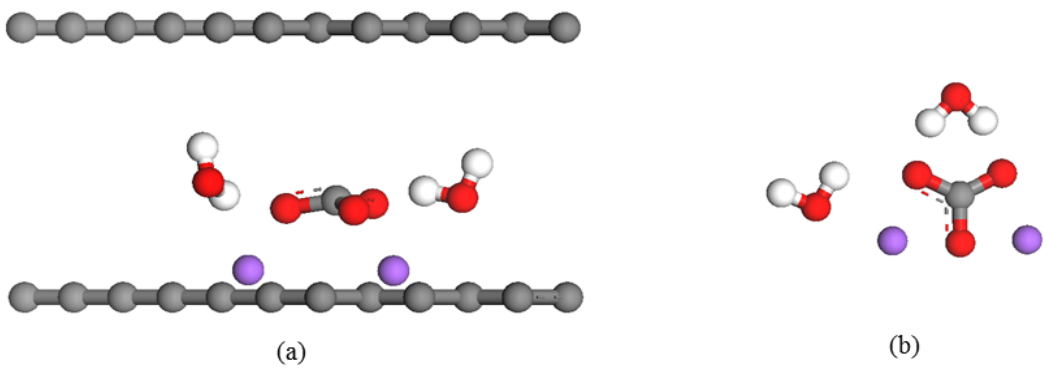

Figure 3.5: (a) system confined between two graphene layers (b) bulk system

Following the same MD/QM simulation procedure, **Figure 3.6** plots the variation of the total energy/enthalpy change of the reaction in **Equation 2.2** as a function of water molecules in the system. The energy/enthalpy change of the chemical reaction without confined layers is positive, shown as black line; whereas that in the 5Å confined system is negative, shown as blue line. The results notify that the smaller distance between two confined layers is more favorable to forming OH^- ion under the same humidity condition, which is more beneficial for absorbing CO_2 from the surrounding air. In essence, the confinement affects the geometry formation of ion hydrations and the hydrogen bonds: in the confined system, ion hydrations are physically enforced to become two-dimensional in form, whereas in the bulk system hydration shell formation is more complete. The smaller interlayer distance is more conducive to maintaining the two-dimensional shape of hydration layers. In this geometry configuration, the energy state of OH^- and HCO_3^- ion hydration is more stable than the hydrated carbonate ion. When the distance between the interlayer is larger than 9Å, the impact of nanoscale confinement on the chemical reaction **Equation 2.2** is same as the effect of one single surface layer. This indicates that the application of nanoporous materials may be attractive for absorbing CO_2, providing a feasible strategy of improving the efficiency of moisture-driven CO_2 capture system.

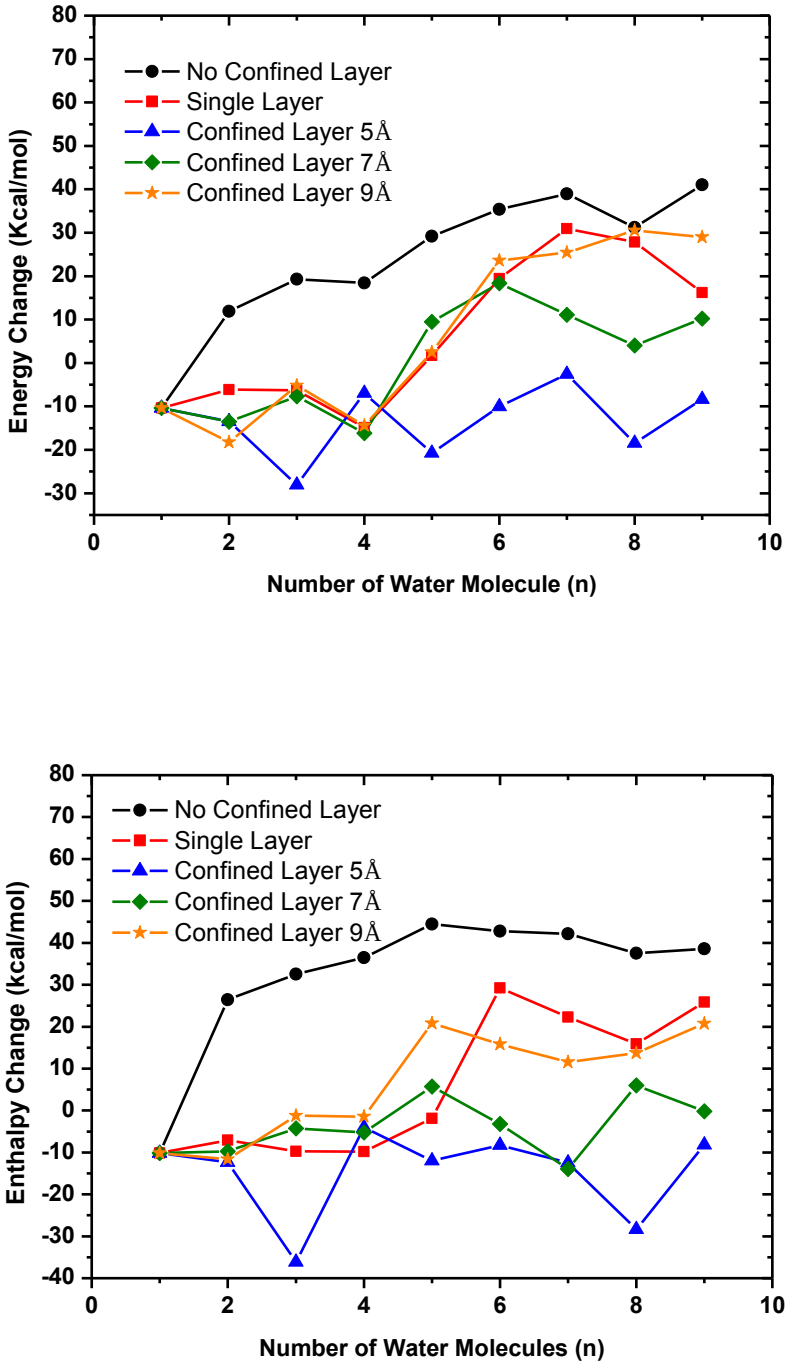

Figure 3.6: (a)/(b) Equation 2.2 Chemical reaction energy/enthalpy change with different water numbers under the condition of different distance of confined layers

3.2.2 Effect of distance of cations

The spacing between the cations on the solid surface is another key factor which has a pronounced effect on the absorption efficiency of moisture-driven CO_2 capture system. **Figure 3.7** shows the energy/enthalpy change of the reaction in **Equation 2.2**, under three rectangular patterns of sodium cations with different spacings: 14 Å × 3.5 Å, 14 Å × 7 Å, and 14 Å × 14 Å, respectively. All systems are confined between two graphene layers with separation of 7 Å. The 14 Å × 3.5 Å rectangular pattern renders an obvious increase in the degree of chemical reaction in **Equation 2.2**. In essence, the geometry configuration of the ion distribution has a decisive influence. When the distance of two Na^+ ions is relative close (3.5Å), a cross-shaped geometry configuration is formed by a HCO_3^- and a OH^- anion with the two Na^+ cations. The energy level of this geometry configuration is lower than the one of a CO_3^{2-} ion locates in the middle of two Na^+ ions under the condition of small number of water molecules, so that the reaction product tends to be HCO_3^- and OH^- ions. However, when the distance of two Na^+ ions is relative far (7.0Å), HCO_3^- and OH^- anions are located in the vicinity of each Na^+ cation, energy level of this geometry configuration is higher than the one of a CO_3^{2-} ion is in the middle of two Na^+ ions, which goes against the formation of HCO_3^- and OH^- ions.

In practice, the spacing or pattern of cations can be controlled by surface modification by attaching or self-assembling different groups of molecules on the surface, using nanoporous material with different pore size, or adjusting the ion charge density on an ion exchange resin.

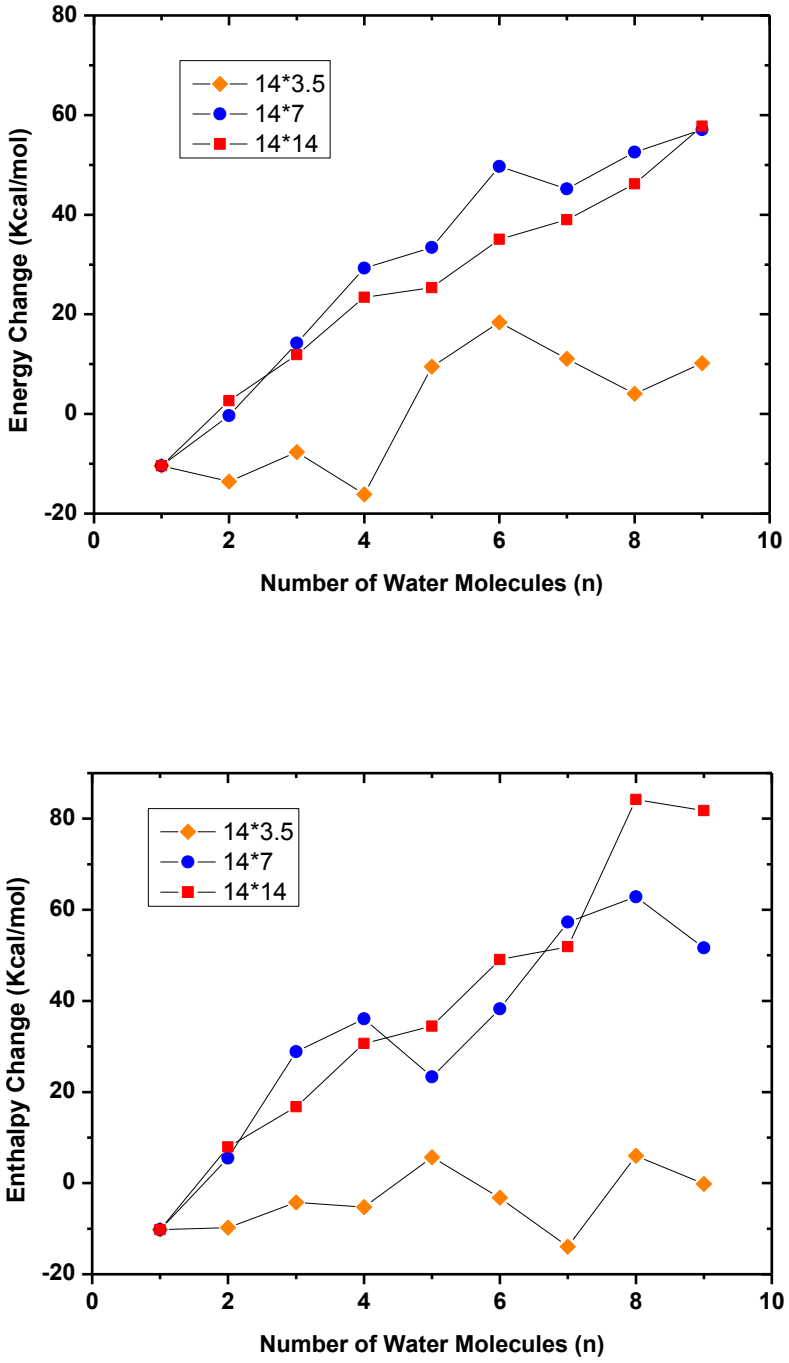

Figure 3.7: (a)/(b) Equation 2.2 Chemical reaction energy/enthalpy change with water numbers under the condition of different distance of cations

3.2.3 Effect of the surface treatment

Other factors can also affect the energy/enthalpy change of the reaction in **Equation 2.2**. Besides surface confinement and cation distance explored in Section 3.3.1 and 3.3.2, surface modification is another one. **Figure 3.8** compares two CO_2 capture systems confined by two hydrophilic hydroxyl graphene layers and that sandwiched between two hydrophobic graphene layers. The distance of confined layers and the patterns of attached cations are identical in both systems. **Figure 3.9** shows that with the electrostatic attraction of the hydrogen bonds between water molecules and hydroxyls on hydrophilic surface, the hydrophilic layer is less conducive to generate OH^- ions, and thus less welcoming the formation of OH^- ions. Intrinsically, the solvation layers arise between two hydrophilic layers is not only as a result of the water molecules are physically confined between two surfaces and the existing anions and cations, but also as the hydrogen bonding between the water molecules and the hydroxyl surface,[107] wherefore the hydrophilic layer undermines the original 2-D geometry configuration of ion hydration formed by ions and hydrophobic confined layers.

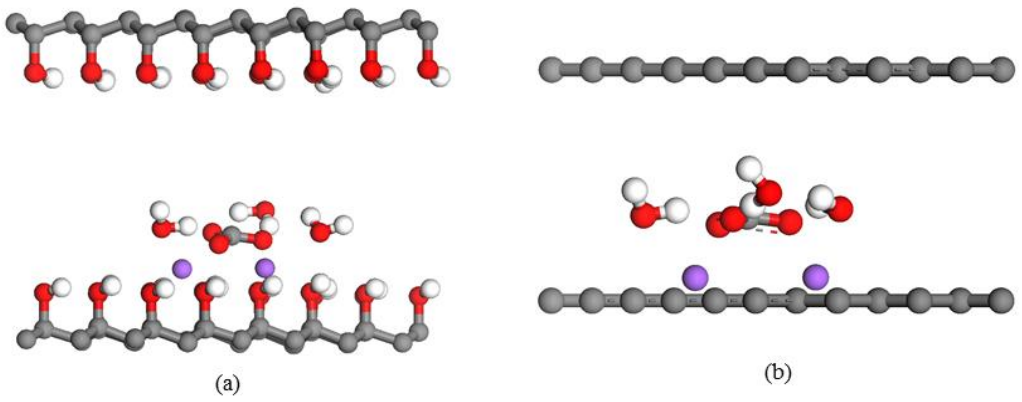

Figure 3.8: Water-driven CO_2 capture system (a) Hydrophilic layer, partial charges of 0.412e and -0.57e are imposed on each hydrogen and oxygen atom of hydroxyl (b) Hydrophobic layer

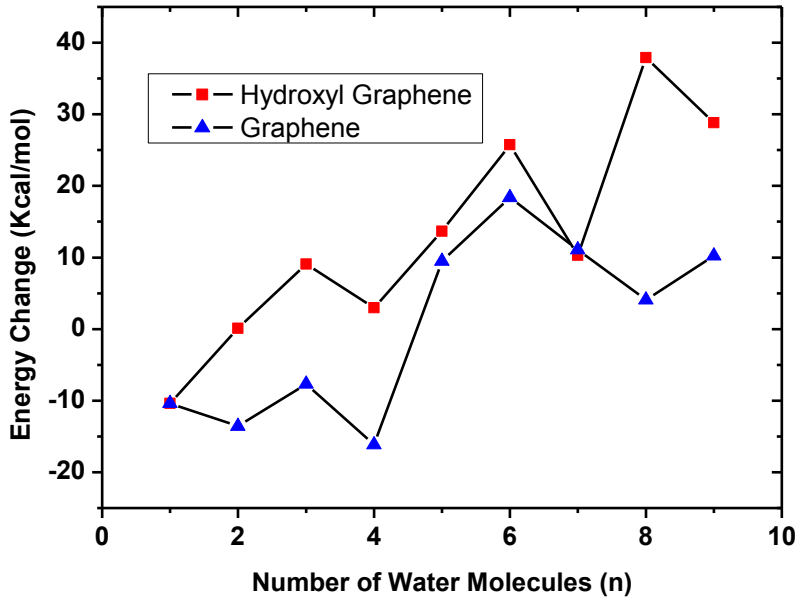

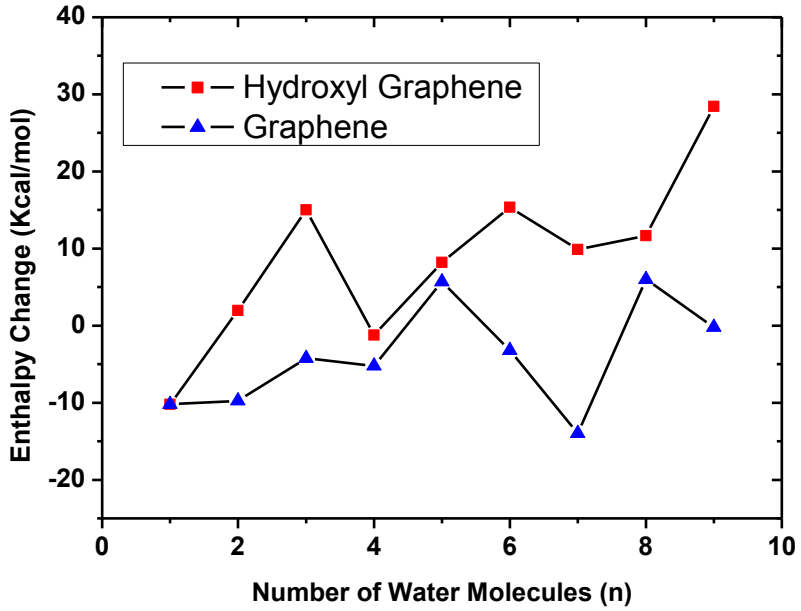

Figure 3.9: (a)/(b) Equation 2.2 Chemical reaction energy/enthalpy change with water numbers under the condition of different treatment of surface.

3.2.4 Effect of the temperature

Another factor governing system performance may be the ambient temperature. **Figure 3.10** shows that with the same amount of water bound to the sorbent, the higher temperature is conducive to produce a larger amount of OH^- ions, enhancing carbon dioxide absorption efficiency. The enthalpies of reactants and products both have increased because of the rise of temperature, the increased amounts are different leading to a slightly greater relative energy gap, which makes **Equation** 2.2 have more trends to react to the direction of product. The increased temperature may also help to increase the number of effective collisions between molecules to overcome energy barrier, and then produce more OH^- ions.

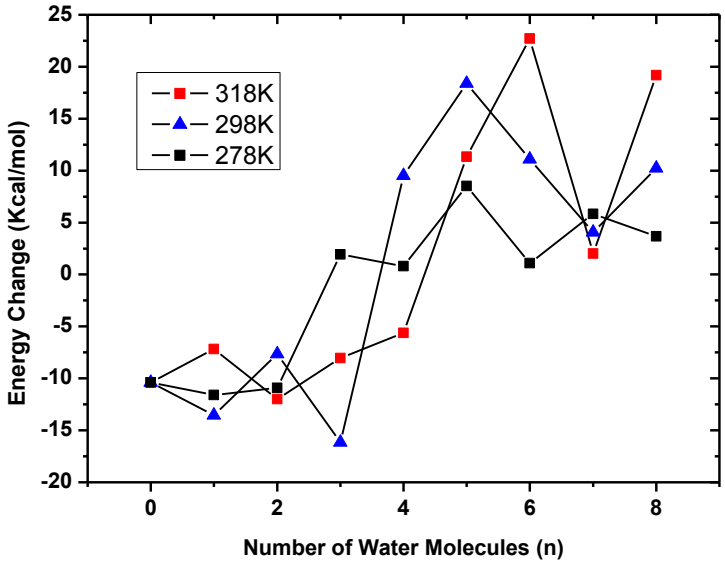

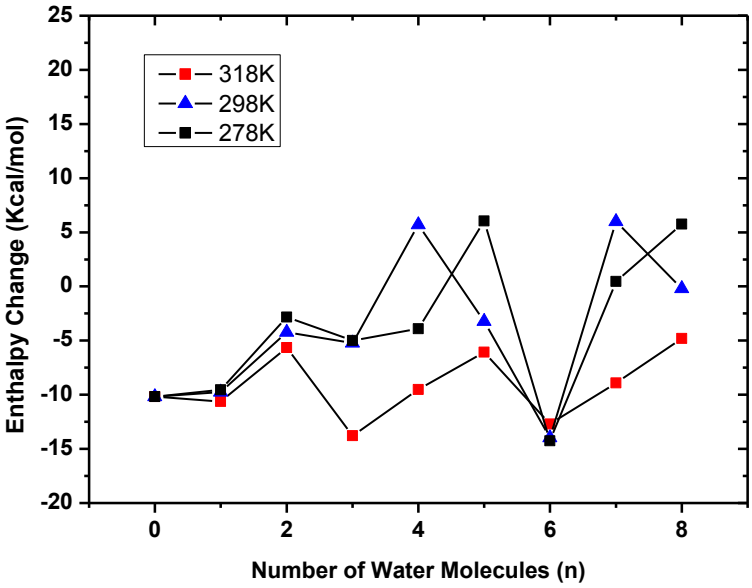

Figure 3.10: (a)/(b) Equation 2.2 Chemical reaction energy/enthalpy change with water numbers under the condition of different temperature.

A more systematic parametric investigation may be carried out in future to optimize the material and system parameters, such as the confined pore size, cation's distance or pattern on solid surface, hydrophobic surface treatment, and the temperature, *etc*.

3.3 Experimental verification

Based on the molecular mechanism of moisture-driven CO_2 capture system, various nanoporous materials may be tested for absorption and desorption of carbon dioxide. **Figure 3.11**, shows a number of examples of porous structures, whose performance may be modified using the aforementioned factors.

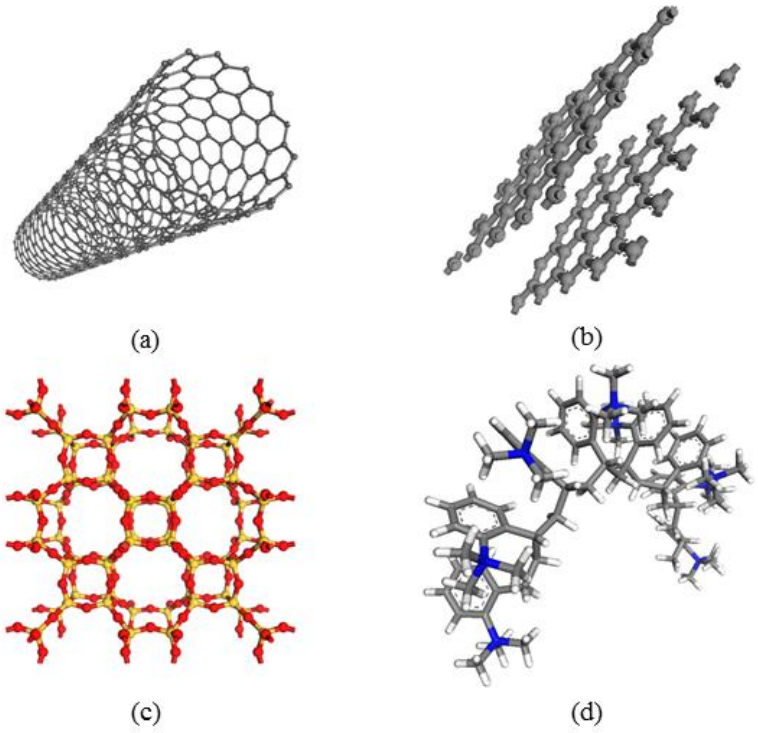

Figure 3.11: (a) Carbon nanotube (b) Activated carbon (c) Zeolite (d) Ion exchange resin. Grey ball is carbon, red is oxygen, yellow is silicon, blue is nitrogen, and white is hydrogen.

3.3.1 CO_2 capture system driven by water quantities

To validate the feasibility of the water-driven CO_2 capture system, we performed a humidity controlling test on CO_2 capture based on an activated carbon material. The sorbent sample was prepared by soaking 0.0395g activated carbon into a 1M sodium carbonate solution for 4 hours, then dried out with free CO_2 dry air. The prepared sample was put into a sealed chamber of an experimental device with temperature and humidity control. For the structure of experimental device, see **Figure 2.15.** The air humidity dew point in the experimental device was set first to 23.0°C fand then turned down to -2.0°C to detect the variation of CO_2 concentration which was measured by an infrared gas analyzer (IRGA, LI-840)

The CO_2 concentration in the sample chamber changes with relative humidity. This is shown in **Figure 3.12 (a)**. It shows that activated carbon impregnated with carbonate ions has a very clear moisture effect on CO_2 absorption. The CO_2 absorption process took place when the dew point was decreasing from 23.0°C to -2.0°C. In this process, relative larger amounts of OH^- ions were produced which could react with CO_2 in gas-phase without a free energy barrier.[102] Whereas, if the sorbent is exposed to higher level of moisture, the concentration of CO_2 equilibrated in the air is at a relative high level because of low hydroxide ion concentration on the sorbent. The 420 ppm lowest CO_2 concentration at around the time 800s is because the nanopores physically constrains relative small amount of CO_2, subsequently releases a part of CO_2 to achieve the equilibrium partial pressure of CO_2 over the sorbent. The effect on a sample of activated carbon without Na_2CO_3 on CO_2 absorption was also measured as a reference test. The dew point was also decreasing from 23.0°C to -2.0°C, and then increasing back to 23.0°C. The CO_2 concentration decreases from 655 ppm to 639 ppm then back to 655 ppm, only with 20 ppm amplitude variation. It proves that the factor of CO_3^{2-} ions with different number of water molecules plays a decisive role on CO_2 absorption.

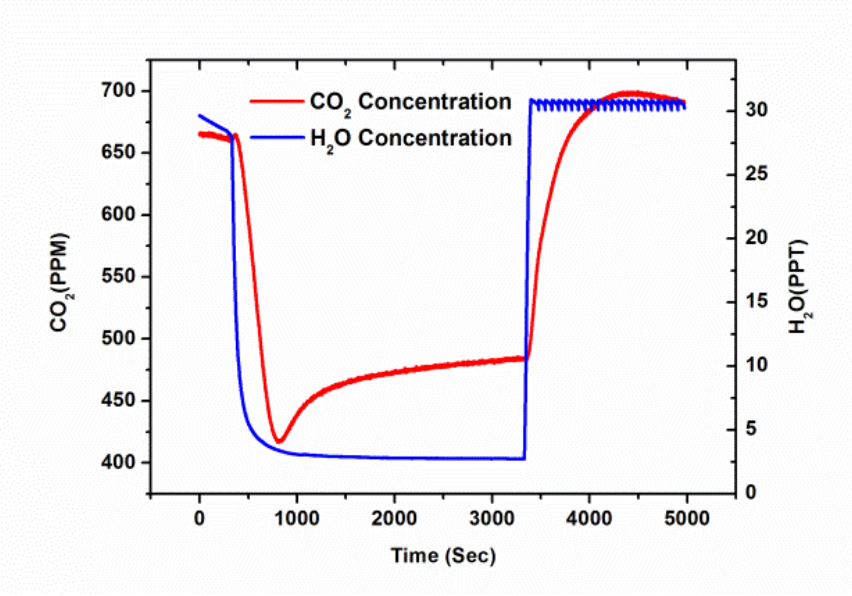

(**a**)

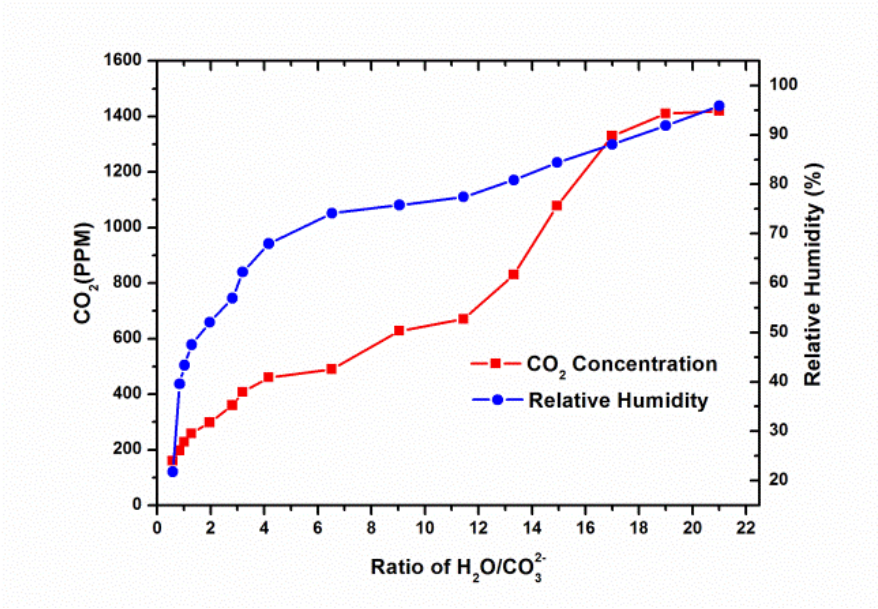

(**b**)

Figure 3.12: Experimental verification. (**a**) CO_2 concentration changes with relative humidity. Red line is the CO_2 concentration. Blue line is the Dew Point in experimental device. (**b**) CO_2 equilibrium concentration and relative humidity are corresponding to water to carbonate ions ratio. The blue line shows the H_2O to CO_3^{2-} ion ratio change with RH change. Red line shows CO_2 equilibrium concentration change with H_2O to CO_3^{2-} ion ratio change.

Another experiment was conducted by using the same sample as above. The same experimental device (**Figure 2.15**) was employed to determine the sample weights and CO_2 equilibrium concentrations at different humidity conditions, The experiment was conducted by using 0.204g activated carbon with 0.2 ml 1M Na_2CO_3 solution dripped on it, then the sample was dried in vacuum chamber 72 hours. Next, the sorbent were full-loaded CO_2 under the surrounding of dry (Dew Point is -10 ˚C) and 400ppm CO_2 atmosphere.

Figure 3.12 (b) First, the weight of absorbent sample at each dew point was measured in the CO_2 free condition. The weight change of the sample is due to the changing amount of water adsorbed on the surface of activated carbon under different humidity conditions. Then, the ratio of water molecules to CO_3^{2-} ions can be calculated by the weight change. Blue line shows the H_2O to CO_3^{2-} ion ratio increases with RH increases. Then, with the known ratio of water molecules to CO_3^{2-} ions at each RH point, the CO_2 equilibrium concentration was recorded under the each same RH point in the experimental device. The equilibrium concentration of CO_2 increases with the ratio of H_2O to CO_3^{2-} ion increases shown as red line. The experiment validates the theoretical results in **Figure 3.4.** In a drier condition, a lower ratio of H_2O to CO_3^{2-} ion ratio is conducive to produce larger amount of OH^- ions to absorb CO_2 from air.

3.3.2 Effect of distance of confinement layers

In order to prove the nanoporous materials with confine-layer structure are attractive for absorbing CO_2 by producing larger amount of OH^- ions than single-layer structure. Four candidate samples: 1st candidate nanostructured graphite containing nanopores 0.1610g and 2nd candidate single-layer graphene 0.1494g were prepared by dripping 1M Na_2CO_3 solution 0.2cc on each sample, and then dried in vacuum chamber. The weights of ready-to-test samples are 0.1820g and 0.1689g, respectively, both carrying around 0.02g Na_2CO_3 powder. The 3rd candidate 0.02g pure Na_2CO_3 powder and 4th candidate 0.1610g nanostructured graphite were also prepared as reference. Same experimental device (see **Figure 2.15**) was employed to determine the amount of CO_2 under different humidity conditions, shown as **Figure 3.13**. All four fresh samples were put into the experimental device at the same starting state: 655 ppm CO_2

concentration and 15℃ Dew Point water concentration. The equilibrium CO_2 concentrations of each sample at 15℃ Dew Point and 5℃ Dew Point were measured. The 1st sample nanomaterial with Na_2CO_3 shows a clear CO_2 concentration variation under different humidity condition, 655 ppm CO_2 concentration at 15℃ Dew Point and 450 ppm CO_2 concentration at 5℃ Dew Point. The 4th sample nanostructured graphite also has a minor variation of CO_2 concentration under different humidity conditions. This is a common phenomenon of physical adsorption. Sample adsorbs more water molecules when the water pressure above the sample increases while desorbs CO_2 leading CO_2 concentration increases. However, sample adsorbs less water molecules when the water pressure above the sample decreases while absorbs CO_2 leading to CO_2 concentration decreases. Note that single-layer graphene sample and pure Na_2CO_3 powder don't show the humidity swing which means these two absorbents cannot be regenerated by increasing water amount. This experiment verifies that the confined nanopores cause the moisture swing CO_2 sorbent to absorb CO_2 when surrounding is dry while release CO_2 when surrounding is wet.

Meanwhile, the CO_2 absorption capacity of the four candidates were measured under the same humidity condition at Dew Point 5°C, shown as **Figure 3.14**. The experiment results show that nanostructured graphite sample absorbed 2.80cc CO_2 which is more than 0.65cc, 0.50cc CO_2 and 0.45cc CO_2 absorbed by 2nd single-layer graphene sample, 3rd Na_2CO_3 powder and 4th nanostructured graphite sample, respectively. This experiment qualitatively verifies the theoretical results in **Figure 3.6** and provides a feasible strategy of improving the efficiency of moisture-driven CO_2 sorbent. Capacities of sorbents with various pore sizes will be proceeded in the next step. The objective is to find the optimal pore size to enhance the capacity of moisture swing CO_2 sorbent.

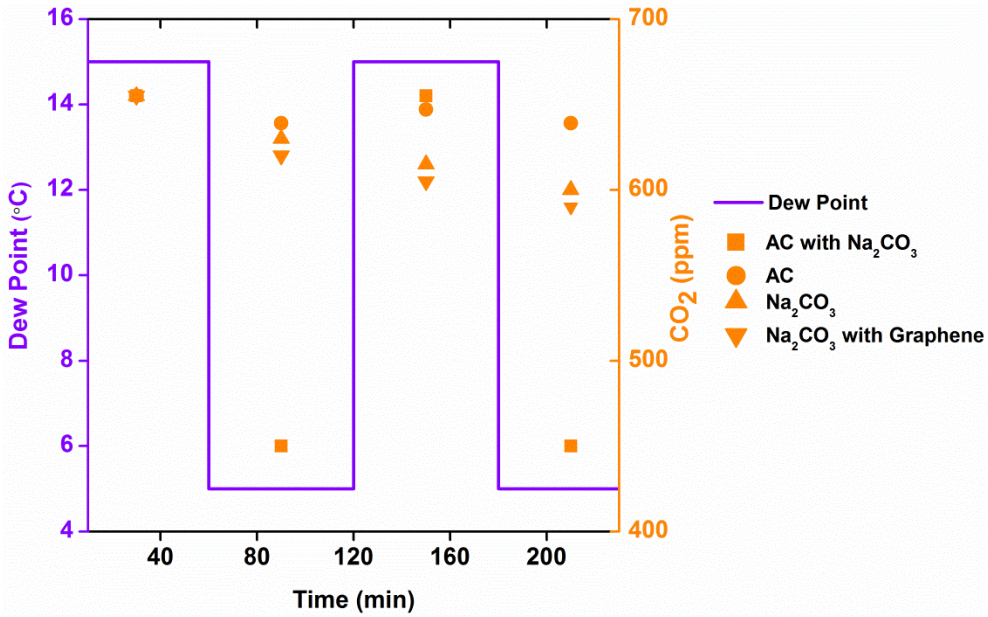

Figure 3.13: CO_2 concentration change with different water numbers under the condition of different distance of confined layers.

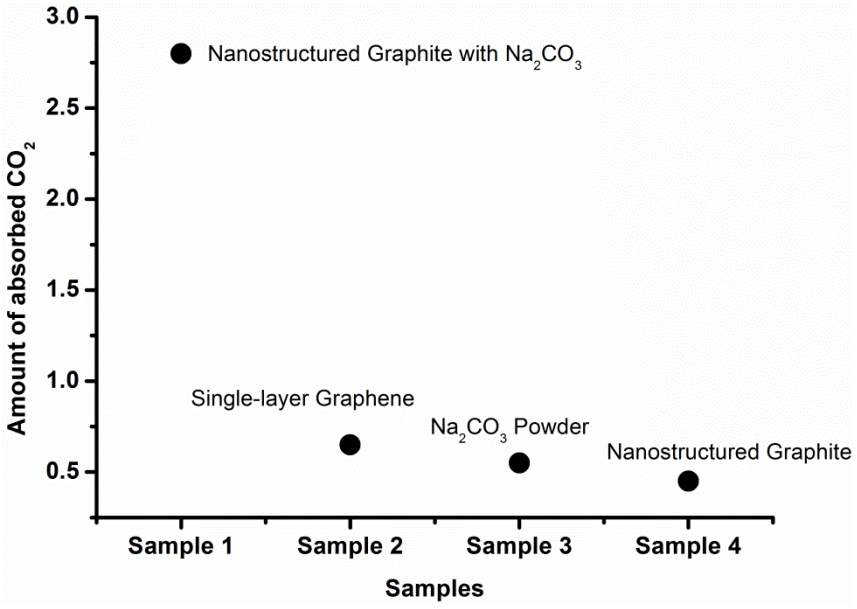

Figure 3.14: CO_2 absorption capacity of four different samples. Sample 1 is Nanostructured Graphite with Na_2CO_3, Sample 2 is Single-layer Graphene, Sample 3 is Na_2CO_3 Powder, Sample 4 is Nanostructured Graphite.

The experiment about effect of distance between cations will be performed by using Ion Exchange Resin with different ion charge densities, and the temperature effect will be fulfilled in incubator next step.

3.4 Summary

The change in energetically favorable states of different ion species with different water quantities underpins water-driven CO_2 capture system from ambient air. Using MD combined with QM simulations, the deduced hydration ion energy shows that CO_2 capture system energetically prefers bicarbonate and hydroxide ion over a carbonate ion and water when the environment is dry, and the resulting high content of hydroxide ion is more attractive for carbon dioxide absorption. Moreover, the effects of pore size, hydrophobic or hydrophilic confined layer, temperature, and distance of cations on the efficiency of CO_2 capture system are illustrated via the amount variation of hydroxide ions as the function of water quantity. A parallel CO_2 absorption experiment by ion exchange resin is carried out to verify the working principles and simulation findings.

The MD combined QM methodology developed in this paper provides a more efficient way to study similar problems which can be depicted by thermodynamic cycle as **Figure 3.1**. The higher degree of the hydrolysis reaction between carbonate ion and water molecules at solid/water interface in a relative dry environment, may be applicable to other weak base and weak acid ions. This counterintuitive phenomenon also sheds some light on the fundamental interactions of ion hydrations in a confined space of solid materials. Underlying mechanism comprehension and parametric studies will help a developed design of more efficient energy-

saving water-driven CO_2 capture absorbent. The parametric optimization investigation may be carried out in future.

Chapter 4 The Effect of Moisture on the Hydrolysis of Basic Salts

This Chapter is derived from the paper "The Effect of Moisture on the Hydrolysis of Basic Salts" which has been published on Chemistry-A European Journal.

In Chapter 3, besides exploring the the working mechanism of the moisture swing of a CO_2 sorbent by computational modeling and experiment, the parameters describing a sorbent material were also explored from the perspective of designing new sorbents with better performance. The boundary layers of a moisture swing CO_2 sorbent were modeled as graphene, which was treated as rigid plate standing in for a series of materials containing nanoconfined spaces. The results show that the degree of hydrolysis of carbonate ions in the presence of water is significantly enhanced in nanoconfined space. The reason is the high ratio of carbonate ions to water in nanopores. This ratio may be as large as 1:1 which is much higher than the 1:20 achievable in a bulk water surrounding. As a result of the hydrolysis, large numbers of hydroxide ions are produced. The hydroxide ions present can absorb CO_2 from ambient air.

This discovery inspired us to explore the hydrolysis of a series of basic salts in nanoconfined spaces and in small droplets in the open atmosphere, where high ratios of ions to water molecules have also been observed. The hydrolysis degrees of these basic salts in nanopores and in nano-droplets in the open atmosphere may differ from those in bulk water surroundings. These findings may shed light on vast chemical reactions in confined water surrounding, solid surface and atmosphere air. In this Chapter, we only rely on QM calculations and not MD calculation for more accurate calculation of energy. Based on the modeling of the

free energy of reactants and products, we found the free energy change in the hydrolysis reaction and how it changes with number of water molecules present.

First, we present a quantitative analysis of the energetics of ion hydration in nanopores with different number of water molecules present. This result is based on atomic modeling of a series of basic salts associated. The results show that the degree of hydrolysis of basic salts in the presence of a few water molecules is significantly different from that in bulk water. The reduced availability of water molecules promotes the hydrolysis of divalent and trivalent basic ions (S^{2-}, CO_3^{2-}, SO_3^{2-}, HPO_4^{2-}, SO_4^{2-}, PO_4^{3-}) which produces lower valent ions (HS^-, HCO_3^-, HSO_3^-, $H_2PO_4^-$, HSO_4^-, HPO_4^{2-}) and OH^- ions. However, reducing the availability of water inhibits the hydrolysis of monovalent basic ions (CN^-, HS^-). Next, we compared our modeling results with experimental results to access the reliability of our computational modeling work. Last, we separate the free energy into an enthalpic component and an entropic component to specify the dominant component in this chemical reaction. This finding sheds some light on a vast number of chemical processes in the atmosphere and on solid porous surfaces. The discovery has wide potential applications including designing efficient absorbents for acidic gases.

4.1 Background

A great deal of information exists concerning the hydration of ions in bulk water. Much less known, but equally ubiquitous is the hydration of ions holding on to several water molecules in nanoscopic pores or in small clusters in open air at low relative humidity. Such hydration of ions with a high ratio of ions to water molecules (up to 1:1) are essential in determining the energetics of many physical and chemical systems. Ions strongly interact with water and are usually hydrated carrying from several to several tens of water molecules when present in the

natural atmosphere or on solid porous surfaces[30]. Interfaces with hydrated ions play an important role in a wide range of natural and fundamental processes[31-34], such as environmental chemistry, electrochemistry, corrosion, and nanoparticle self-assembly. Hydration of ions on solid porous surface is of fundamental interest as it underpins numerous applications from desalination technologies[108-110], over fuel cells[111] to capacitors with enhanced capacitance[112]. Ion hydration clusters outside of bulk water significantly enhance the rate and extent of chemical reaction probabilities[35-37]. For example, Cl^- and Br^- can be oxidized by OH radicals or O_3 at the air-water interface with mechanisms different from those in the bulk phase[113]; the dynamics of dissociation reactions at alumina-water interfaces are different at low and high water coverage[114].

Previous experimental observations can shed some light on the detailed structure and bonding information of the hydrated interface at the molecular level[72,73]. Spectrographic studies suggest highly ordered structures of water molecules and dissociation of hydration water at the gas/solid interface.[74,75]. Computer simulation provides an alternative way to better understanding of hydration phenomena of ions, ion pairs, and solid-liquid interfaces[81-83], such as the role of hydration energy and structural change with reduced water activity[84,85], which shows a high degree of positional ordering parallel to the surface. The comparison between dissociative and associative adsorption of water on the calcite surface[88-90] argued that the water dissociation is strongly disfavored even on surface defects of vacancies, except near a CO_3^{2-}, where water molecules can be disassociated into protons and hydroxides.

4.2 Free Energy of Hydrolysis of Basic Ions

4.2.1 Computational Model

Here we present the free energy change of hydrolysis for several multivalent basic ions (S^{2-}, CO_3^{2-}, SO_3^{2-}, HPO_4^{2-}, SO_4^{2-}, PO_4^{3-}) and monovalent basic ions (CN^-, HS^-) in the presence of different number of water molecules (*n*) in the range from 1 to 20, as shown **Equation 4.1**. *X* stands for the basic ion, *m* is the valence, *n* is the number of water molecules:

$$X^{m-} + nH_2O \Leftrightarrow HX^{(m-1)-} + OH^- + (n-1)H_2O \qquad 4.1$$

The geometric configurations of hydrated ions are shown in **Figure 4.1**. Number of *m* mobile cations (Na^+) are included in the system, in order to balance the anionic charges. The free energy changes are obtained via calculating the energetics difference between reactants and products by Quantum Modeling (QM). Next section, we decompose the free energy change into enthalpic and entropic components. This procedure allows one to identify the driving forces governing the free energy change of **Equation 4.1**.

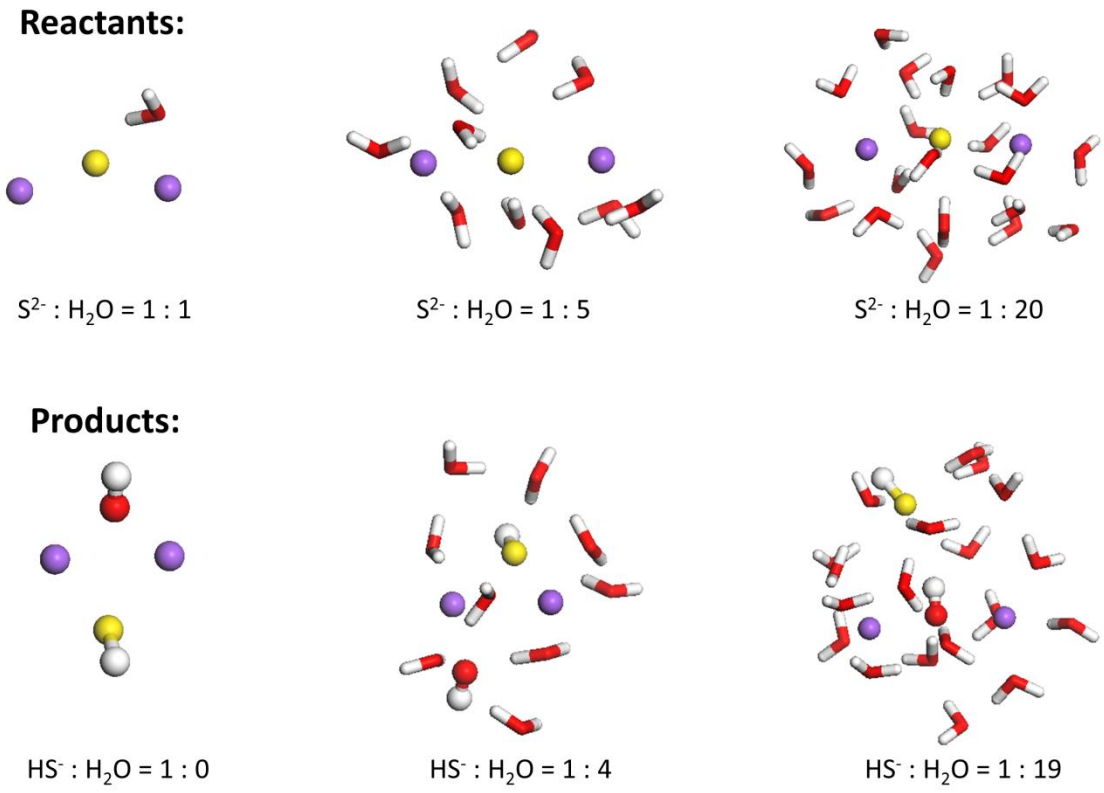

Figure 4.1: Simulation snapshots of reactants and products of hydrolysis of S^{2-} with different numbers of water molecules present. While the example consider the sulfur anion, S^{2-} could be replaced by all other divalent basic ions, but the choice of ion will affect the geometry of the hydration and the hydrolysis process. In the S^{2-} ion system simulations, the reactants S^{2-} to H_2O ratio is selected to be 1:1, 1:2, 1:3,1:4, 1:5, 1:6, 1:7, 1:8, 1:10, 1:15, 1:20 respectively, and for the products the ratio of HS^- to H_2O ratio is 1:0, 1:1, 1:2, 1:3,1:4, 1:5, 1:6, 1:7, 1:9, 1:14, 1:19, correspondingly. Shown in the figure are the reactants with a ratio of S^{2-}:H_2O at 1:1, 1:10, 1:20 and the corresponding products with a ratio of HS^-:H_2O of 1:0, 1:9, 1:19. **Figure 4.2** and **Figure 4.3** show the simulation snapshots of trivalent (PO_4^{3-}) and monovalent (HS^-) basic ions.

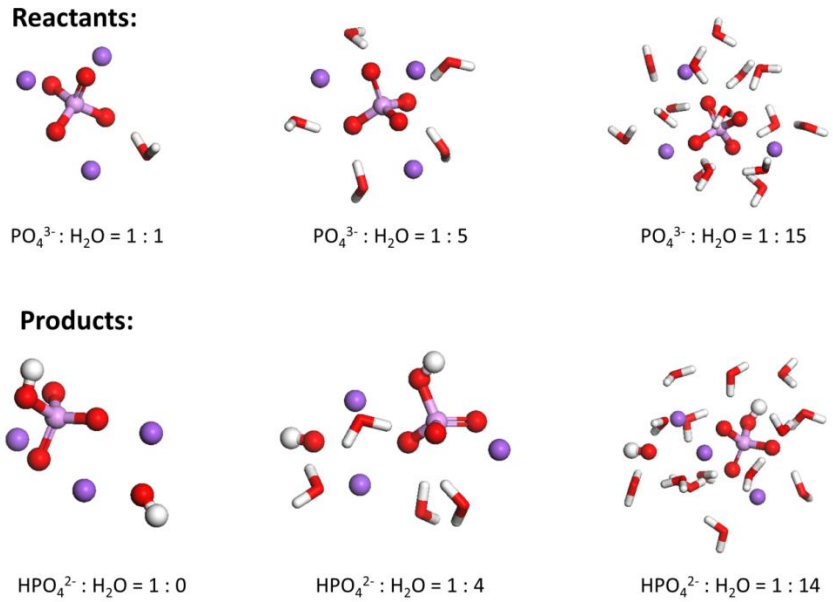

Figure 4.2: Simulation snapshots of reactants and products of hydrolysis of PO_4^{3-} with different amount of water molecules as samples

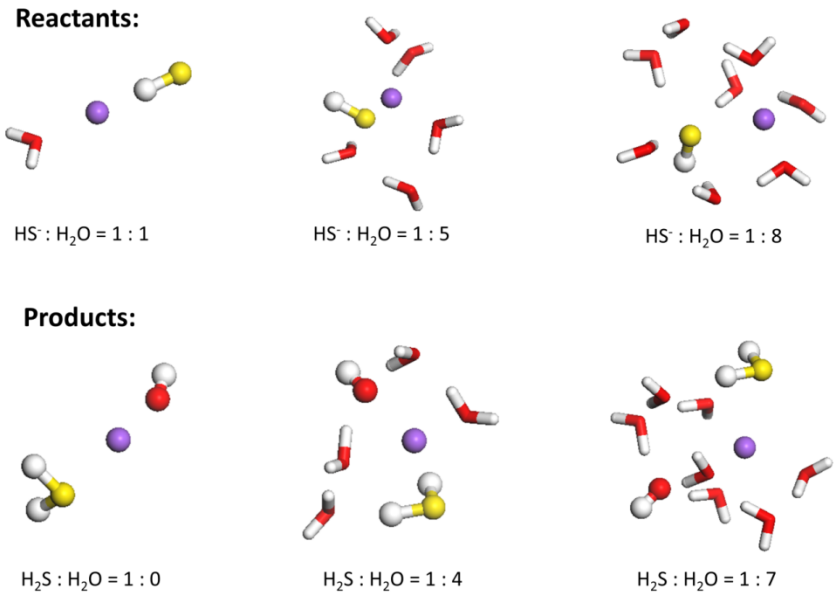

Figure 4.3: Simulation snapshots of reactants and products of hydrolysis of HS^- with different amount of water molecules as samples

4.2.2 Computational Methods

All molecular dynamics simulations were performed using Materials Studio[92], which is a modeling and simulation environment to study atomic and molecular structure in material science and chemistry. Geometry and partial charges on all atoms of ions in gaseous phases were calculated by density functional theory code DMol^3.[93] Geometry optimizations and population analysis of the ions were obtained according to Generalized Gradient Approximations (GGA) DFT formulation which includes the effect of charge-density inhomogeneity, and the HCTH functional[104]. The "triple numerical plus polarization" (TNP) basis set was utilized in the present work. TNP is the best accuracy and the most expensive basis set in the DMol^3 code. It includes additional polarization functions on all atoms. The quality of self-consistent field (SCF) convergence tolerance was set as "fine" with a convergence tolerance 1×10^{-5} hartree on total energy, 2×10^{-3} hartree/Å on the gradient, and 5×10^{-3} Å on the displacement in our calculations. The chemical reaction energy of $X^{m-} + nH_2O \Leftrightarrow HX^{(m-1)-} + OH^- + (n-1)H_2O$ in a vacuum connecting ground states was calculated by the energy difference between reactants and products. All the reactants and products are optimized to the local minimum without imaginary frequency. The free energy change at finite temperatures was computed according to the various translational, rotational and vibrational components.

To determine the free energy of reaction from QM calculations, the thermodynamic cycle, shown as **Figure 4.4**, was employed. If the heat capacities of the reactants and products between the two temperatures are known, the enthalpy of reaction at temperature T_1 can be calculated from the enthalpy of reaction at T_0. ΔS is given by $\Delta S = \Delta S_{vib} + \Delta S_{trans} + \Delta S_{rot}$. The Gibb's free energy difference is given by $\Delta G(n) = \Delta H(n) - T\Delta S(n)$.

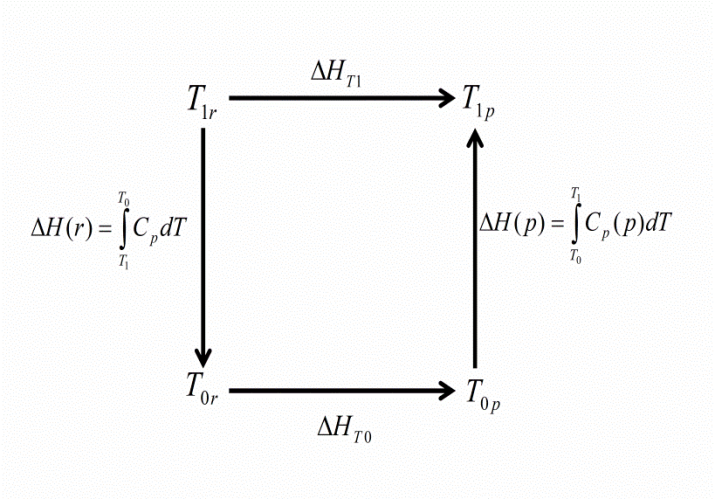

Figure 4.4: Chemical reaction thermodynamic cycle between different temperatures.

4.2.3 Reaction Free Energy of Hydrolysis of Basic Ions with Different Number of Water Molecules

The free energy differences between reactants and products of hydrolysis of all basic ions at 298.15K are calculated for different numbers of water molecules present. The number of water molecules is denoted by (*n*). In the simulation, the reactants trivalent basic ion X^{3-} : H_2O ratios are selected to be from 1:1 up to 1:15 and products HX^{2-} : H_2O ratios are from 1:0 up to 1:14; the reactants divalent basic ion X^{2-} : H_2O ratios are from 1:1 up to 1:20 and products HX^{-} : H_2O ratios are from 1:0 up to 1:19; the reactants monovalent basic ion X^{-} : H_2O ratios are from 1:1 up to 1:10 and products HX : H_2O ratios are from 1:0 up to 1:9, from dense to dilute solution, respectively. The selection of the maximum number of water molecules depends on the size of *n*, for which the energy difference between the reactants and products becomes stable.

Figure 4.5 (a), **(b)**, and **(c)** present the reaction free energies ΔG of **Equation 4.1** for the hydrolysis of these basic ions with different number of water molecules. For the trivalent and divalent basic ions, the reaction free energies ΔG increase rapidly with the increase in the

number of water molecules, then they reach a plateau at a large number of water molecules. The smaller value of the reaction free energy at low values of *n*, means a greater degree of the chemical reaction in the forward direction. The present analysis shows that the hydrolysis degree of multi-valence basic ions is enhanced significantly with reduction of the number of water molecules. With a small number of ambient water molecules, the relatively dry system becomes more energetically favorable to form products $HX^{(m-1)-}$ and OH^- ion hydrations, whereas reactants X^{m-} ion hydration occurs in relative wet condition. Conversely, for the monovalent basic ions, ΔG decreases rapidly with the increase in the number of water molecules and then touches down to a flat bottom. Hydrated reactants X^- ions prefer to exist in relative dry condition. A small number of water molecules inhibits their hydrolysis. In other words, trivalent and divalent ions can hydrolyze much more H_2O into OH^- ions, while monovalent ions can hydrolyze much less H_2O into OH^- ions under relatively dry condition. The hydrolysis degree of all basic ions holding only a few water molecules is significantly different from the degree of hydrolysis of basic salts in bulk water; in other words, the hydrolysis reaction has a moisture-effect characteristic, which was first found in anionic, strong based exchange resins, whose affinity to CO_2 is strongly affected by the presence of absence of water [18,26,115].

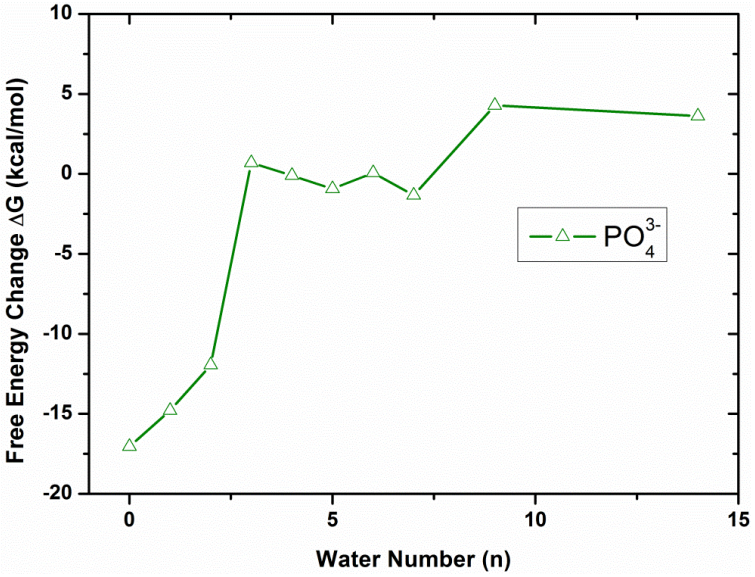
Free Energy Change ΔG (kcal/mol)
Water Number (n)
PO4 3-

(a)

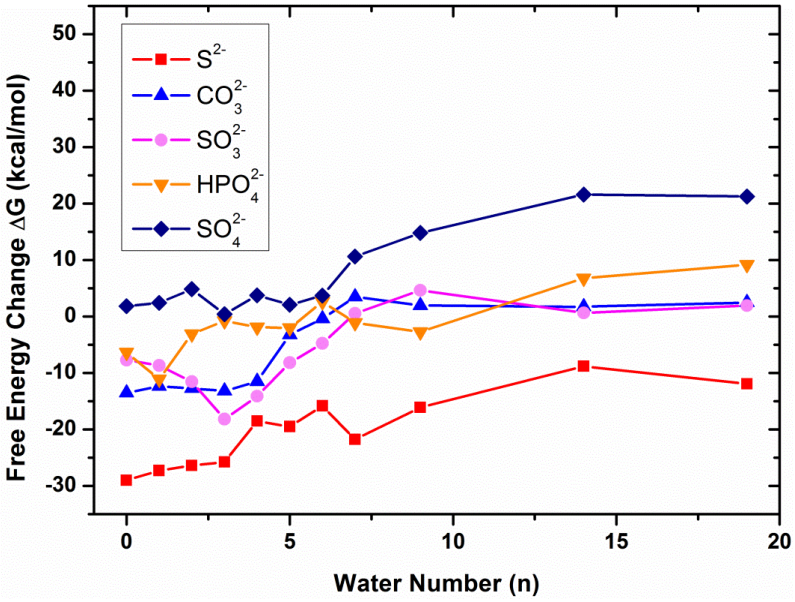
Free Energy Change ΔG (kcal/mol)
Water Number (n)
S2-
CO3 2-
SO3 2-
HPO4 2-
SO4 2-

(b)

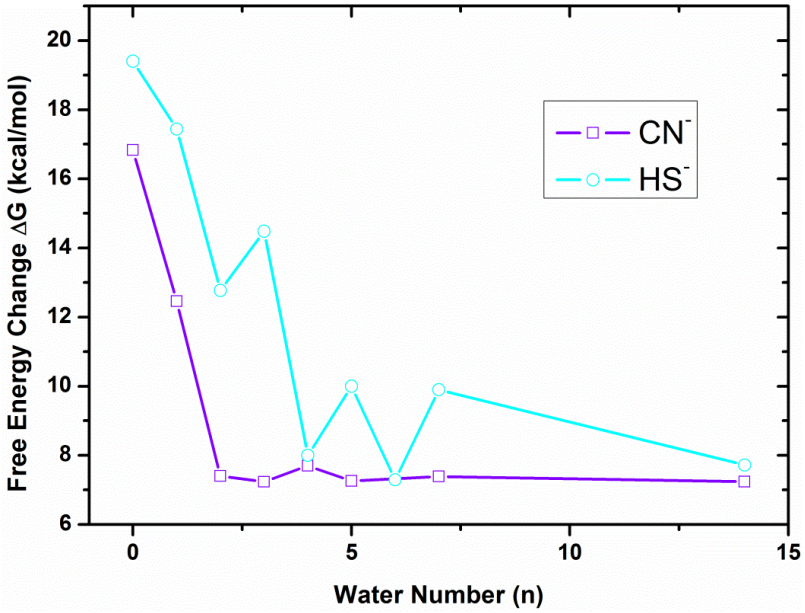

(c)

Figure 4.5: Equation 4.1 free energies of hydrolysis of basic ions change with water numbers. (a) trivalent basic ion PO_4^{3-}, (b) divalent basic ions S^{2-}, CO_3^{2-}, SO_3^{2-}, HPO_4^{2-}, SO_4^{2-}, (c) monovalent basic ions CN^-, HS^-.

The hydration shells around ions dissolved in water can be separated into two regions: a hydration shell, where the water is immobilized and electrostricted, and bulk water, where water molecules are still attracted by the Coulomb electric field of the ion, but they are mobile and not bound to the ion. Even farther away from the ion the water is essentially unaffected by its presence. The reason of the significantly different hydrolysis degree at different number of waters present is the energetic change in the hydration shell, which determines the energy levels of the reactants and products when a limited number of water molecules are present. Fewer water molecules could result in a different geometric configuration of the inner hydration shell, leading to different energy levels of ion hydration. Energy states can be very different than in the bulk water changing the free energy of the hydrolysis reaction. Shown in **Figure 4.5**, for all the basic

ions studied, the energetic levels between the reactants and the products are highly dependent on the number of water molecules when this number is below a critical threshold (the critical numbers in trivalent and divalent ion hydrations are less than about 15 molecules, while in monovalent ion hydration shells they are less than about 6 molecules). With the increase of the water molecule number, the energy difference asymptotically approaches stable values due to the Coulomb potential of the basic ions in free water.

4.2.4 Reaction Free Energy of Hydrolysis from Experiment and Modeling

In terms of the basic strength of these ions, the larger value of the reaction free energy means a smaller degree of hydrolysis and weaker basicity. The reaction free energy from modeling for large values of *n*, approximates the free energy for the bulk solution and therefore it can be compared with experimental results of hydrolysis equilibrium constants of ions in aqueous solution according to $\Delta G = -RTlnK$ at room temperature, shown in **Figure 4.6** and

Ions	Experimental Results (kcal/mol)	Modeling Results (kcal/mol)	Standard Deviation
PO43-	2.117	3.948	0.328
S2-	-6.817	-10.361	1.567
CO32-	5.052	2.423	0.679
HPO42-	9.266	9.181	0.171
SO32-	9.266	6.835	0.248
SO42-	16.472	21.449	0.168
CN-	6.274	7.434	0.162
HS-	9.544	9.546	1.139

Table 4.1. Based on the quantum calculations for large *n*, the descending order of the basicity of divalent ions is $S^{2-} > SO_3^{2-} > CO_3^{2-} > HPO_4^{2-} > SO_4^{2-}$ and for monovalent ions the ranking is $CN^- > HS^-$. This is consistent with the experimental results for basicity in aqueous

solutions, except that experimentally in liquid water $CO_3^{2-} > SO_3^{2-}$. Although on the same order of magnitude, there is some disagreement. PO_4^{3-} and SO_4^{2-} have relative large errors. The error of the present quantum modeling may result from *n* not being large enough to have reached the bulk water limit, and also searching for lowest energy state by QM when *n* is large.

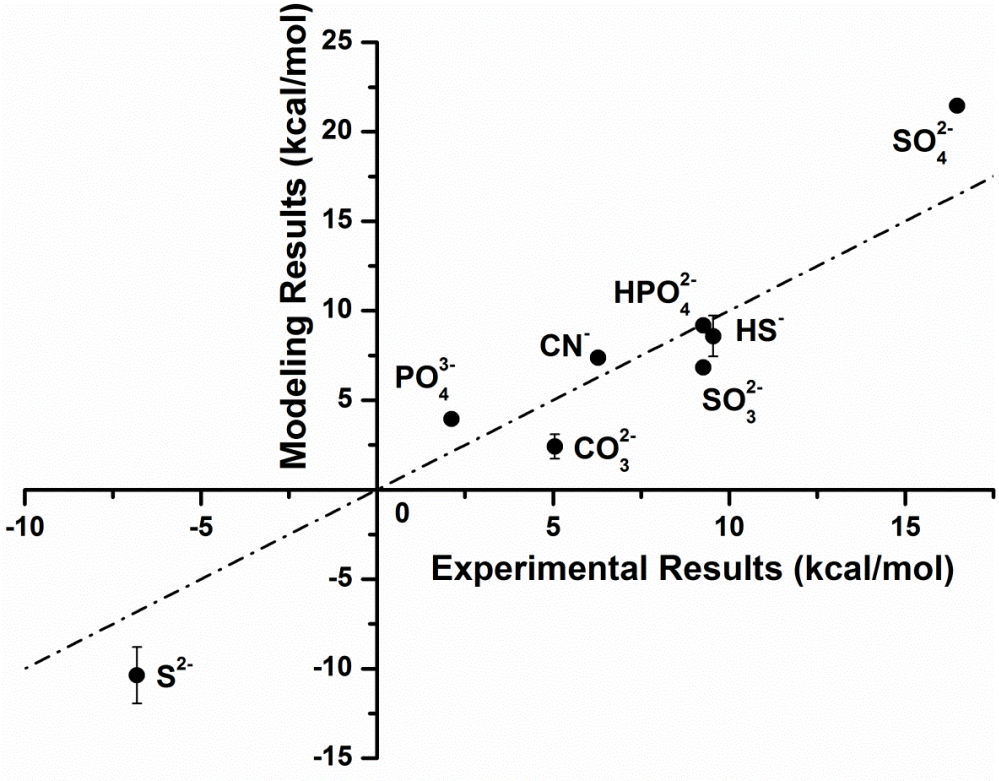

Figure 4.6: Reaction free energy from experiment and modeling

Ions	Experimental Results (kcal/mol)	Modeling Results (kcal/mol)	Standard Deviation
PO_4^{3-}	2.117	3.948	0.328
S^{2-}	-6.817	-10.361	1.567
CO_3^{2-}	5.052	2.423	0.679
HPO_4^{2-}	9.266	9.181	0.171

SO_3^{2-}	9.266	6.835	0.248
SO_4^{2-}	16.472	21.449	0.168
CN^-	6.274	7.434	0.162
HS^-	9.544	9.546	1.139

Table 4.1: Reaction free energy from experiment and modeling

4.2.5 Decomposition of Free Energy

Figure 4.7 (a), (b) and **(c)** show the enthalpic component $\Delta H(n)$, and in **Figure 4.7 (d)**, **(e)** and **(f)** the entropic component $T\Delta S(n)$ of the reaction free energy $\Delta G(n)$. Note that these components sum up to the reaction free energy via $\Delta G(n) = \Delta H(n) - T\Delta S(n)$. The enthalpies for all basic ions are consistent with the trends of the change in the reaction free energies with the number of water molecules. The entropy differences between reactants and products for all ions are essentially invariant as the number of water molecules changes. Hence, the different degrees of hydrolysis of basic ions with different water numbers are based primarily on enthalpic effects.

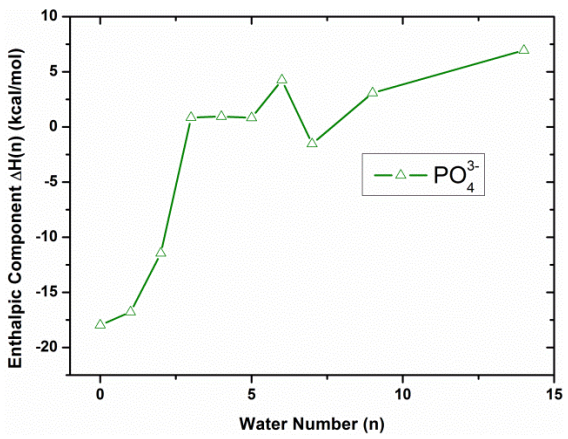

(a)

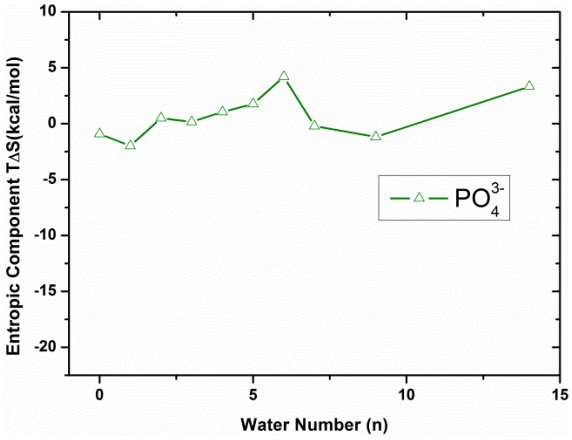

(d)

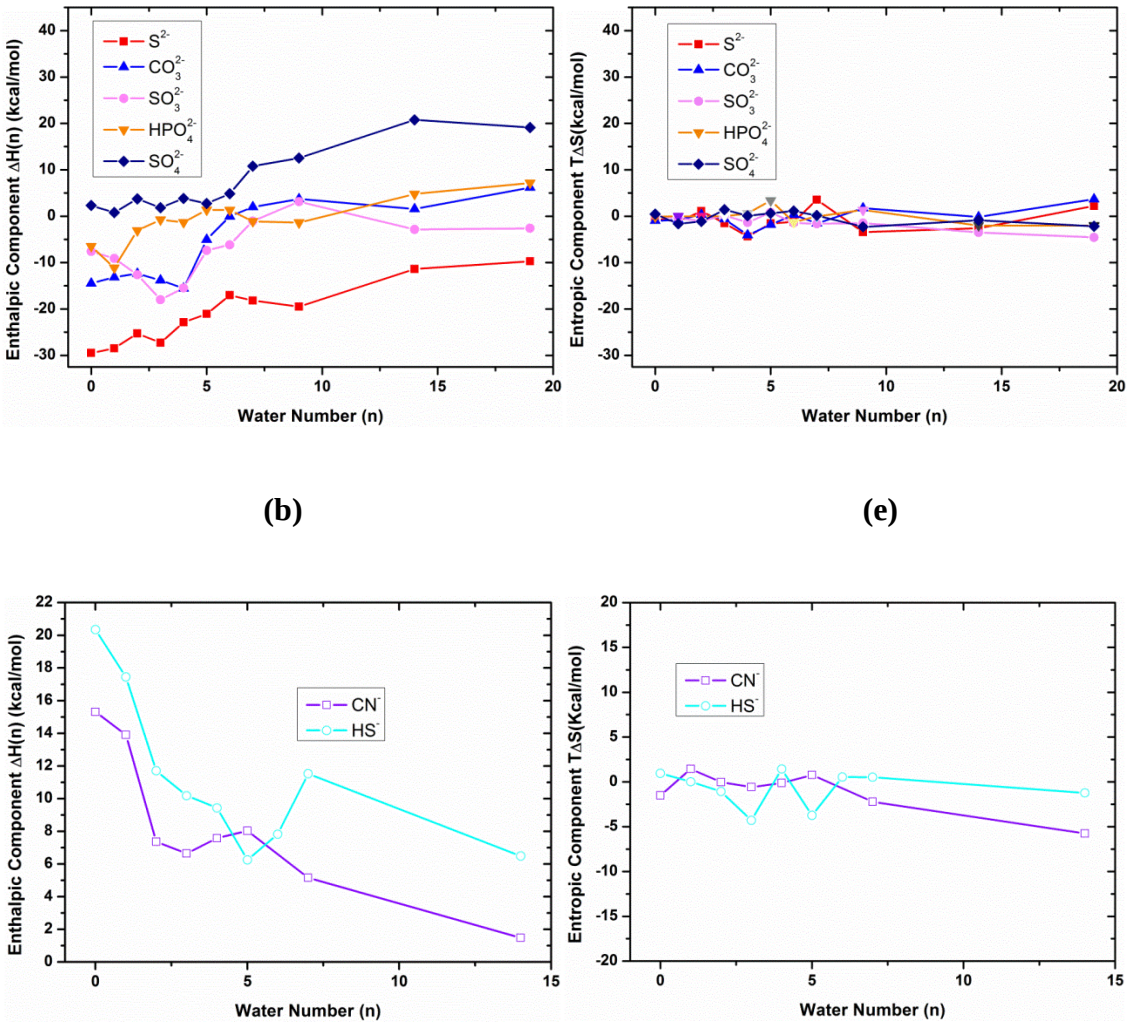

Figure 4.7: Decomposition of the reaction free energy of Eq. 1 into enthalpic components (a, b and c), and entropic components (d, e and f). The enthalpy and entropy are plotted as the energy difference with respect to the number of water molecules.

The effect of moisture on the chemical reaction and basicity of divalent basic ions, which is explained by the impact additional water has on the hydration energy of ions, implies that it is easier to hydrolyze H_2O into a larger amount of OH^- ions upon relatively dry condition. This discovery has been applied to the design of efficient absorbents for carbon dioxide[18] as

introduced in Chapter 1, Chapter 2 and Chapter 3, moreover, with the new insights from this analysis can be generalized to other acidic gases. Such sorbents only consume low-cost water instead of expensive energy for regeneration. A specific implementation of such a sorbent system utilizes anionic ion exchange resins (IER) for managing the moisture in contact with the anions contained in the material. If these resins are prepared in the carbonate state, the ratio of CO_3^{2-} ions to OH^- and HCO_3^- ions is controlled by the amount of water present, which in turn responds to the humidity conditions in ambient air. This moisture-driven chemical reaction is useful in a practical implementation for capturing CO_2 from ambient air[18]. The substitution of water that evaporates for energy has significant cost advantages and represents a significant advance in air capture technology.

4.3 Summary

In Chapter 4, we demonstrate through quantum modeling a series of unconventional chemical reactions, where the degree of hydrolysis of basic salts (S^{2-}, CO_3^{2-}, SO_3^{2-}, HPO_4^{2-}, SO_4^{2-}, PO_4^{3-}, CN^-, HS^-) containing several water molecules is significantly different from that in bulk water and can be controlled by adding or removing water. The reaction free energy of the hydrolysis of basic salts were decomposed to enthalpic component and entropic component. The enthalpy change due to a change in the number of water molecules determines the hydrolysis degree of basic salts. This unique mechanism sheds some light on a vast number of chemical processes of hydrated ion pairs in nanoscopic pores and in the natural atmosphere. The finding also suggests that the multiple valence acidic ions can hydrolyze H_2O to create larger amount of protons with the decrease of water amount.

The discovery also has wide potential applications, including on design options for more efficient novel absorbents to absorb acidic gases by modifying the water content of their environment rather than using traditional energy-consuming sorbent material. Using Quantum Mechanics, this discovery theoretically elucidated the underlying mechanism of the moisture swing CO_2 capture sorbent which was demonstrated in Chapter 1. The conversion between absorption and desorption of this new efficient sorbent can be switched only by low-cost water quantities instead of consuming extra costly energy to regenerate. The novel technology for direct air capturing CO_2 can help dealing with the critical issue of global warming.

Chapter 5 Humidity Effect on Diffusion and Structure of a CO_2 Sorbent

5.1 Introduction

This chapter is related to the paper "Humidity Effect on Diffusion and Structure of a Moisture-swing CO_2 sorbent", which is to be submitted.

Chapter 1 introduced a moisture swing CO_2 capture sorbent which is an Ion Exchange Resin (IER). This resin after washing with a carbonate solution can absorb CO_2 from ambient air when the surrounding is dry; It will release this CO_2 again when the surrounding is wet. This is depicted in **Equation 1.5-1.8**. The quaternary ammonium cations are attached to the polymer backbone of the IER, while H_2O molecules and three kinds of anions CO_3^{2-}, HCO_3^-, OH^- are moveable within the resin with different diffusion rates. This chapter describes the transport properties of anions and water molecules under different moisture surroundings regarding mean square displacement (MSD) and radial distribution functions (RDF).

The diffusions of movable anions and water molecules in IER are essential to determine the absorption efficiency of the sorbent. By studying the diffusivity and structures of functional substances under different moisture concentrations can help us to design a more efficient sorbent for CO_2 capture and understand the underlying working mechanisms. MD simulations are especially appropriate for studying complex polymer systems[116-120] and water structures[121-123], since it can be applied to expose nano-structure features without a priori structural model. Researchers have calculated the diffusion of molecules in polymer system[124-128] and investigated the moisture effect on epoxy resins by MD simulation. Lin[129] investigated the diffusion

coefficient and the activation energy of epoxy resin under moisture environment and showed that the results from MD simulations and experiments are in reasonable agreement. Wu[130] studied the influences of absorbed water on structures and properties of crosslinked resins including the diffusion coefficient of water, radial distribution function, geometry configuration and mobility of polymer network chains. Chang[131] performed MD to study the hygroscopic properties of resin materials regarding diffusivity and swelling strains respect to temperature and moisture concentration. Lee[132] simulated the distribution and diffusion of water in epoxy molding compound, considering the effect of water content.

Although the diffusion of moisture in polymer has been studied by experiments and computer simulations, the transport properties of anion exchange resin (IER) for moisture-swing CO_2 capture in air have not been studied in this type of research, since IERs were previously used for water treatment [133-135]. Thermodynamic[29] and kinetic[136] investigations have been carried out to explain the underlying mechanism of CO_2 sorbent of moisture swing[115], but the diffusive and transport characteristics remain unclear at molecular level. In this study, for the first time, MD simulation was carried out to investigate the diffusivity and structures of ions and water molecules in a CO_2 capture sorbent under various humidity conditions.

5.2 MD Simulation

5.2.1 Models of Ion Exchange Resin

The IER in the simulation is composed of a polystyrene backbone with quaternary amine ligands attached to the polymer. These quaternary amine groups carry a permanent positive charge. They can be depicted as NR_4^+, in which R is an organic carbon chain, at least one of

these is attached to the polymer matrix. The positive ions fixed to the polymer backbone cannot release a proton. Therefore the resulting resin is a strong base resin.

A model of oligomer containing eight side chains with eight quaternary ammonium ions was built for the MD simulation, which has been introduced firstly in **Chapter 2**. A oligomer includes two quaternary ammonium ions is shown in **Figure 5.1**. Four oligomers, each containing eight quaternary ammonium ions, were packed in an amorphous cell. The periodic boundary conditions was applied to eliminate surface effects. In this study, two IER systems containing different classes of anions were established in charge balance. System 1 has four oligomers attaching sixteen carbonate ions, and the other one system 2 has four oligomers attaching sixteen bicarbonate ions and sixteen hydroxide ions. System 1 and system 2 stand for reactant and product of **Equation 2.2** $CO_3^{2-} \cdot nH_2O \Leftrightarrow HCO_3^- \cdot m_1H_2O + OH^- \cdot m_2H_2O + (n - 1 - m_1 - m_2)H_2O$ respectively, shown in **Figure 5.2**.

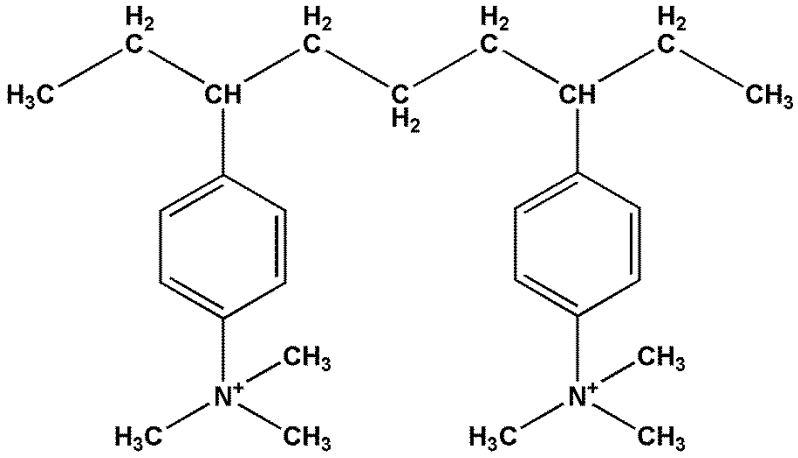

Figure 5.1: Chemical structure of IER containing two side chains

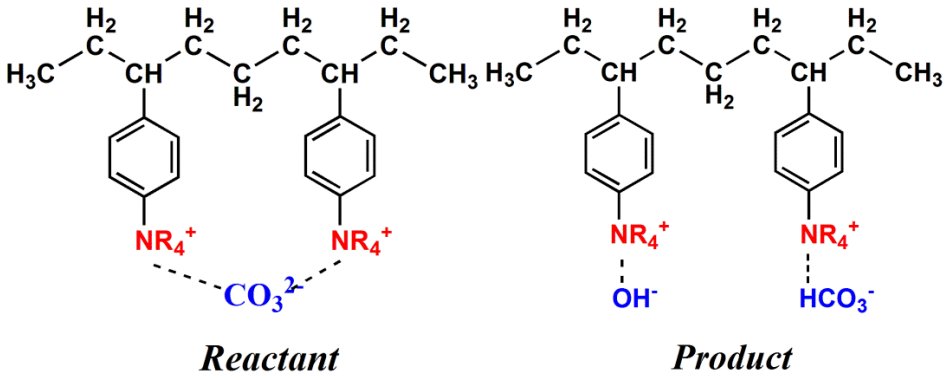

Figure 5.2 Chemical structures of reactant system 1 and product system 2

System 1 (S1) and system 2 (S2) are solvated with different numbers of water molecules. In the carbonate ion system (S1) simulations, the CO_3^{2-} : H_2O ratio is selected to be 1:5, 1:10 and 1:15 (total water molecule numbers are 80, 160 and 240 in the computational cell) respectively, and for the bicarbonate and hydroxide ion system (S2), HCO_3^- : H_2O ratio or OH^- :H_2O ratio is tested at 1:4,1:9 and 1:14 (total water molecule numbers are 64, 144, and 244 in the computational cell) respectively, from low to high humidity conditions. These cases have one-to-one correspondence, since one water molecule reacts with one carbonate ion to form a bicarbonate and a hydroxide ion. The geometry configurations of S1 containing 80 water molecules and S2 containing 64 water molecules are shown in **Figure 5.3**.

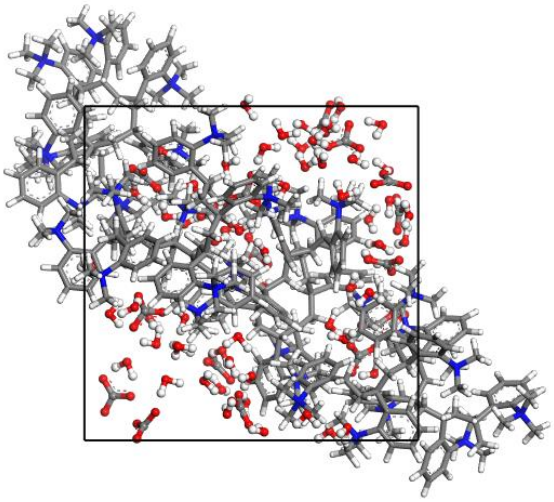

(a)

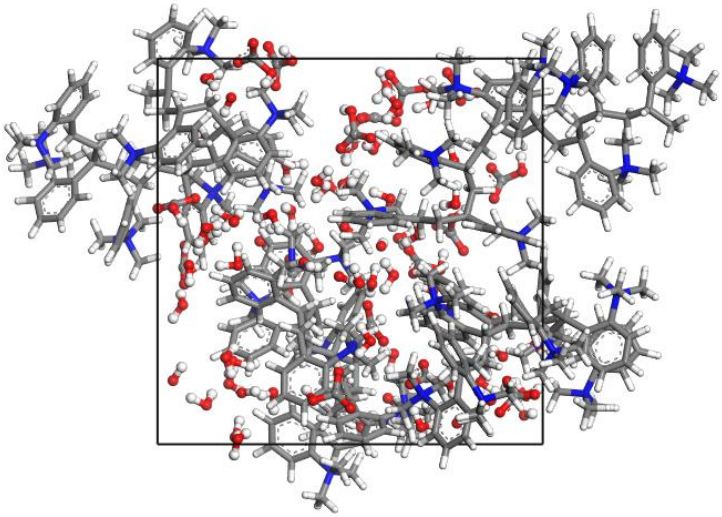

(b)

Figure 5.3: Geometry configurations of IER with ion species and water molecules. **(a)** S1 contains 4 oligomers, 32 quaternary ammonium ions, 16 carbonate ions, and 80 water molecules. **(b)** S2 contains 4 oligomers, 32 quaternary ammonium ions, 16 bicarbonate ions, 16 hydroxide ions and 64 water molecules.

5.2.2 Simulation Procedure

All molecular dynamics simulations were carried out in Materials Studio,[92] The COMPASS Force Field was used for all geometry optimizations and MD simulations. The COMPASS uses an *ab initio* force field optimized for condensed-phase applications. This force field was assigned to all atoms in the carbonate ion, bicarbonate ion, hydroxide ion, and water molecule.

Three cases of S1 (CO_3^{2-}:H_2O ratio is selected to be 1:5, 1:10 and 1:15) and three cases of S2 (HCO_3^-:H_2O ratio is tested at 1:4, 1:9 and 1:14) were built in amorphous cells. Minimizations were carried out by the Quasi-Newton procedure, where the electrostatic and van der Waals energies were calculated by the Ewald summation method (the Ewald accuracy was 0.001kcal/mol, and the repulsive cutoff for van der Waals interaction was 6 Angstrom). In order to achieve a relaxed structure, the systems were further equilibrated by NVE ensemble simulation with 100 ps, and then an NPT ensemble was performed to obtain the relevant density values with different water numbers at standard state condition. The system achieved equilibrium after running 200 ps in NVT ensemble. Finally to estimate the diffusivity and Structure of molecules, NVT ensembles for 0.5 ns were run with different densities at 298 K. A time step of 1.0 fs was used in all simulations. NPT ensemble used Nose thermostat and Berendsen barostat and NVT ensemble used Nose thermostat.

The diffusion coefficients for all ions and molecules were calculated from the Einstein relation[137] as **Equation 5.1**

$$D = \frac{1}{6N} \lim_{t\to\infty} \frac{d}{dt} \sum_{i=1}^{N} \langle |r_i(t) - r_0(t)| \rangle \qquad 5.1$$

where *D* is the diffusion coefficient, $r_i(t)$ is the coordinate of the center of the mass of the *i*th H_2O molecule and *N* is the number of calculated molecules in the system. The value of mean square displacement (MSD) of molecules calculated in MS is the average over a time interval for all molecules in a set. Therefore, **Equation 5.1** can be simplified to $D = a/6$, where *a* denotes the slope of the best-fit line of MSD versus time.

The interactions of molecules and ions in IER were examined by calculating radial distribution functions (RDFs) of atoms of interest. These functions, also referred to as pair correlation functions, provide insights into the structure of studied models. In a cell with volume V, for two groups of atoms A and B, they can be determined by

$$g_{AB}(r) = \frac{V \times \langle \sum_{i \neq j} \delta(r - |r_{Ai} - r_{Bj}|) \rangle}{(N_A N_B - N_{AB}) 4\pi r^2 dr} \qquad 5.2$$

Where i and j refer to the ith and jth atoms in group A and group B. N_{AB} is number of atoms are in both groups A and B, and the angle bracket implies averaging over different configurations. For a single group of atoms, accordingly, **Equation 5.2** can be simplified as

$$g_{AB}(r) = \frac{V \times \langle \sum_{i \neq j} \delta(r - |r_{ij}|) \rangle}{(N^2 - N) 4\pi r^2 dr} \qquad 5.3$$

these functions give the probability of finding an atom at a distance r from another in completely random distribution. They may be employed to to investigate the interactions between quaternary ammonium cations and ions under different humidity conditions, therefore, analyze the role of water in IER systems.

5.3 Results and Discussion

5.3.1 Humidity Dependence of Diffusivity

Molecules diffusions in IER were studied under three relative humidity conditions (40%, 50%, 60%). The one-to-one corresponding humidity condintons to the ratios of CO_3^{2-} : H_2O are 1:5, 1:10 and 1:15 (S1), and the ratios of HCO_3^- : H_2O are 1:4,1:9 and 1:14 (S2) respectively[115]. **Figure 5.4** shows time-averaged MSDs of water molecules in S1 and S2 versus time with respcet to the different humidity conditions. **Figure 5.5** shows the time-averaged MSDs of ion CO_3^{2-} in S1, and ions HCO_3^-, OH^- in S2 versus time with respect to different humidity conditions. Here, the slope of the plots are proportional to the diffusion coefficient in the system, therefore, the diffusion coefficients (D) were calculated. The diffusion coefficients of water molecules and ion species are shown in **Figure 5.6**.

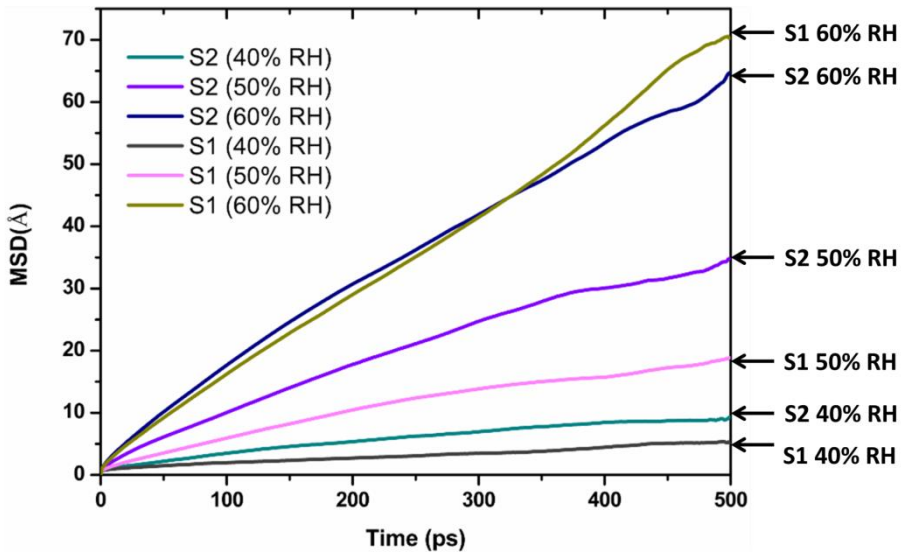

Figure 5.4: MSDs of water molecules in S1 and S2 versus time with respect to different humidity conditions.

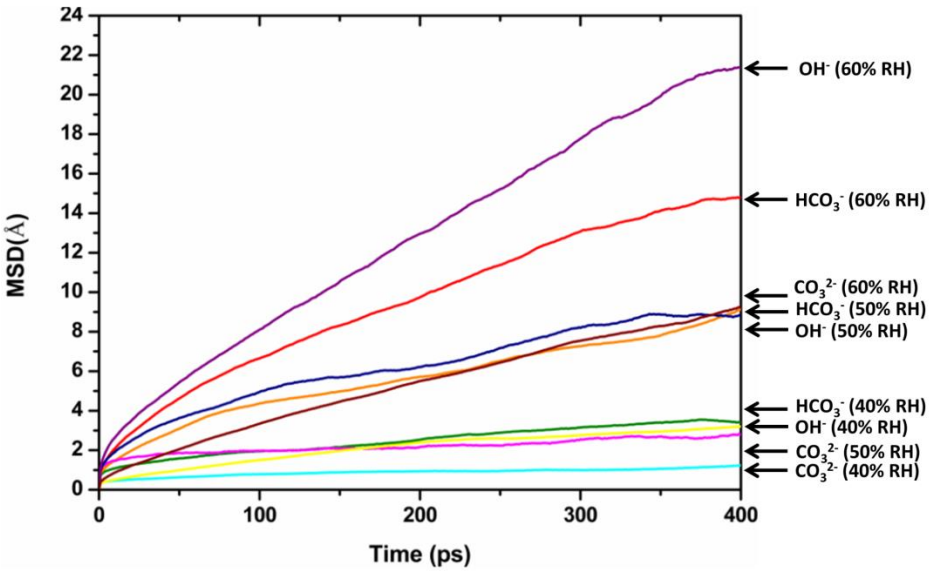

Figure 5.5: MSDs of CO_3^{2-} ion in S1, and HCO_3^-, OH^- ion in S2 versus time with respect to different humidity conditions.

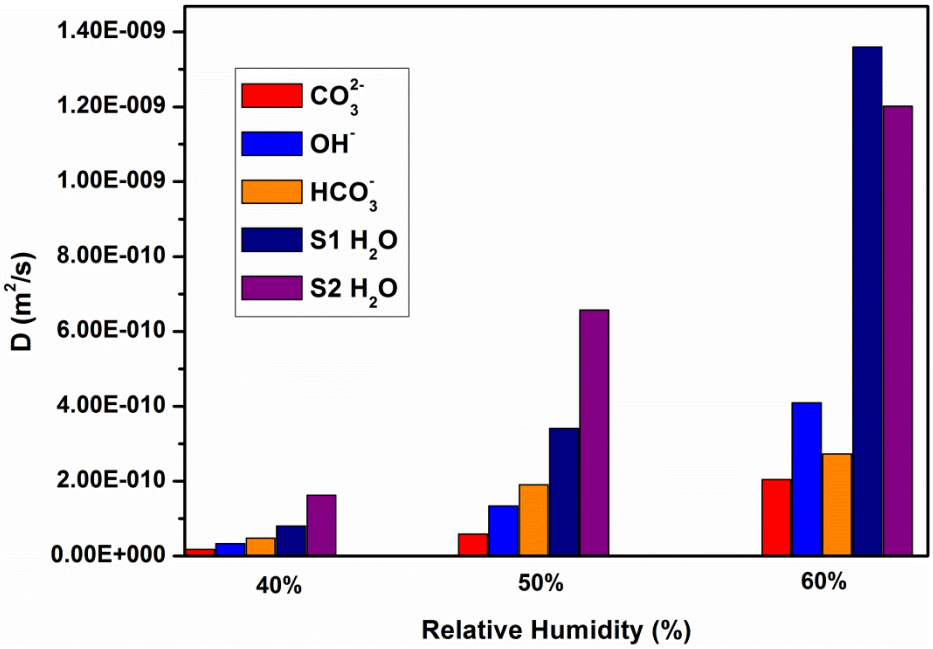

Figure 5.6: Diffusion coefficients of water molecules and ion species at various humidity conditions.

In general, the diffusion coefficients of water molecules and all ion species increase as the humidity increases. A higher humidity level means a higher hydration level. More water molecules are uncoordinated to NR_4^+ groups, and these waters can break NR_4^+-CO_3^{2-}, NR_4^+-HCO_3^-, and NR_4^+-OH^- pairs at a higher level of hydration. Higher water content also leads to a better connected water-channel network, which can also stimulate water transport.

From a comparison of different ion species and water molecules under the same humidity condition, it is clear that the motilities of ion species are much lower than those of water molecules. This is reasonable, considering the strong electrostatic attraction between negative charged ions and NR_4^+ end-groups. Note that although NR_4^+ groups can exhibit local mobility, they are attached to the polystyrene backbone and therefore do not diffuse through the system. By comparison, water is much less restricted to move within the simulation box, although water molecules can create relative weak H-bonds to NR_4^+ groups. Based on observation of local dynamics in the simulations, the water molecules and ion species which are farther away from backbones with NR_4^+ group are much more mobile than those situated closer to the walls of the backbones. The quaternary ammonium cations NR_4^+ tend to immobilize and stabilize water molecules and ion species and thus reduce local mobility.

From the comparison of the diffusion coefficient of ion species in two systems, the results show the mobility of carbonate ions is lower than those of bicarbonate ions and also hydroxide ions, for all humidity levels considered herein. The reason is that the carbonate ion has higher valence which leads to a larger Coulombic force with NR_4^+ groups. The diffusion coefficient of a bicarbonate ions is slightly higher than that of hydroxide ions under the 40% and 50% relative humidity conditions, shown in **Figure 5.5** and **Figure 5.6**; . The reason is that the bicarbonate ions have a larger van der Waals force with backbone systems than hydroxide ions,

which tends to immobilize bicarbonate ions more than hydroxide ions. However, when the relative humidity level raises to 60%, the mobility of hydroxide ion is higher than that of bicarbonate ions. Since the size of hydroxide ion is smaller than the bicarbonate ion, the well-formed hydration shell may be created first when the water amount is up to a certain level, and then these floating ion hydrations could increase the mobility of hydroxide ions significantly.

5.3.2 Structure of Molecular System

The intermolecular RDFs for two pairs of atoms under four different humidity conditions (CO_3^{2-}:H_2O = 1:70, CO_3^{2-}:H_2O = 1:50, CO_3^{2-}:H_2O = 1:30, CO_3^{2-}:H_2O = 1:10) are shown in **Figure 5.7**. One is nitrogen atoms in NR_4^+ and carbon atoms in CO_3^{2-} (N-C), the other one is nitrogen atoms in NR_4^+ and carbon atoms in HCO_3^- (N-C). The difference of this model from the one of diffusion analysis, is all anions (CO_3^{2-}, HCO_3^-,OH^-) are built in a single system with different water molecules. The ratio of CO_3^{2-}:HCO_3^-:OH^- are 1:1:1 under the condition of neutral balance. There are indications from the molecular modeling, that the change of the number of water molecules can influence the precipitation rates of ionic species on the solid surfaces of the IER.

In a wet surrounding (CO_3^{2-}:H_2O = 1:70, CO_3^{2-}:H_2O = 1:50), the hydration clouds of all ions are so large such that the anions can hardly approach the cations RH_4^+, shown in **Figure 5.7 (a)** and **Figure 5.7 (b).** The probabilities of the appearance of CO_3^{2-} and HCO_3^- ions near the NR_4^+ groups are a little higher than that averaged in the whole system, because the atomic forces between NR_4^+ groups and anions are larger than the ones between water molecules. The probability of appearance of HCO_3^- ions in the vicinity of RH_4^+ cations are higher than CO_3^{2-} ions.

With less water molecules (CO_3^{2-}:H_2O = 1:30) available, the optimal approach distances of CO_3^{2-}-NR_4^+ and HCO_3^--NR_4^+ both become smaller. This, in turn, gives an energetic advantage to the mono-valent HCO_3^- ion over the divalent CO_3^{2-} ion that does not match the NR_4^+ single cationic charge. The presence of competition for one CO_3^{2-} ion is between the two monovalent NR_4^+ cations. Therefore, the NR_4^+ quaternary ammonium cations do not comfortably accommodate carbonate ions into the structure. The part of unfitted CO_3^{2-} ions containing hydration water are more likely to be located at 4.3 Å and 7.0 Å. On the other hand bicarbonate ions can easily fit to NR_4^+ cations and the favorable distance between them is at 4.5 Å, shown as **Figure 5.7(c)**. As a result, as the humidity level decreases, the HCO_3^- ions are more likely to precipitate than CO_3^{2-} ions, and favors a more alkaline surrounding. The larger amount of OH^- ions in dry condition is more conducive to capture CO_2. This discovery may provide an explanation for the underlying mechanism of IER absorbs CO_2 in dry and release CO_2 in wet.

At even lower humidity (CO_3^{2-}:H_2O = 1:10), both carbonate ions and bicarbonate ions precipitate completely. One obvious peak shows at distance of 4.5 Å, shown as **Figure 5.7(d)**. The sharp peak at distance around 4.5 Å is an indication of the strong columbic force and van der Waals force of NR_4^+ cations associated with CO_3^{2-} anions in S1 or HCO_3^- anions in S2. The attracted CO_3^{2-} anions and HCO_3^- anions are more likely to be located in the vicinity of the NR_4^+ groups on the IER network in the dry condition. Under this condition, the mechanism of CO_2 capture by IER was explained elsewhere[115]. The intermolecular RDFs for two pairs of atoms under more humidity conditions (CO_3^{2-}:H_2O = 1:5 to CO_3^{2-}:H_2O = 1:70) are provided in supplementary materials.

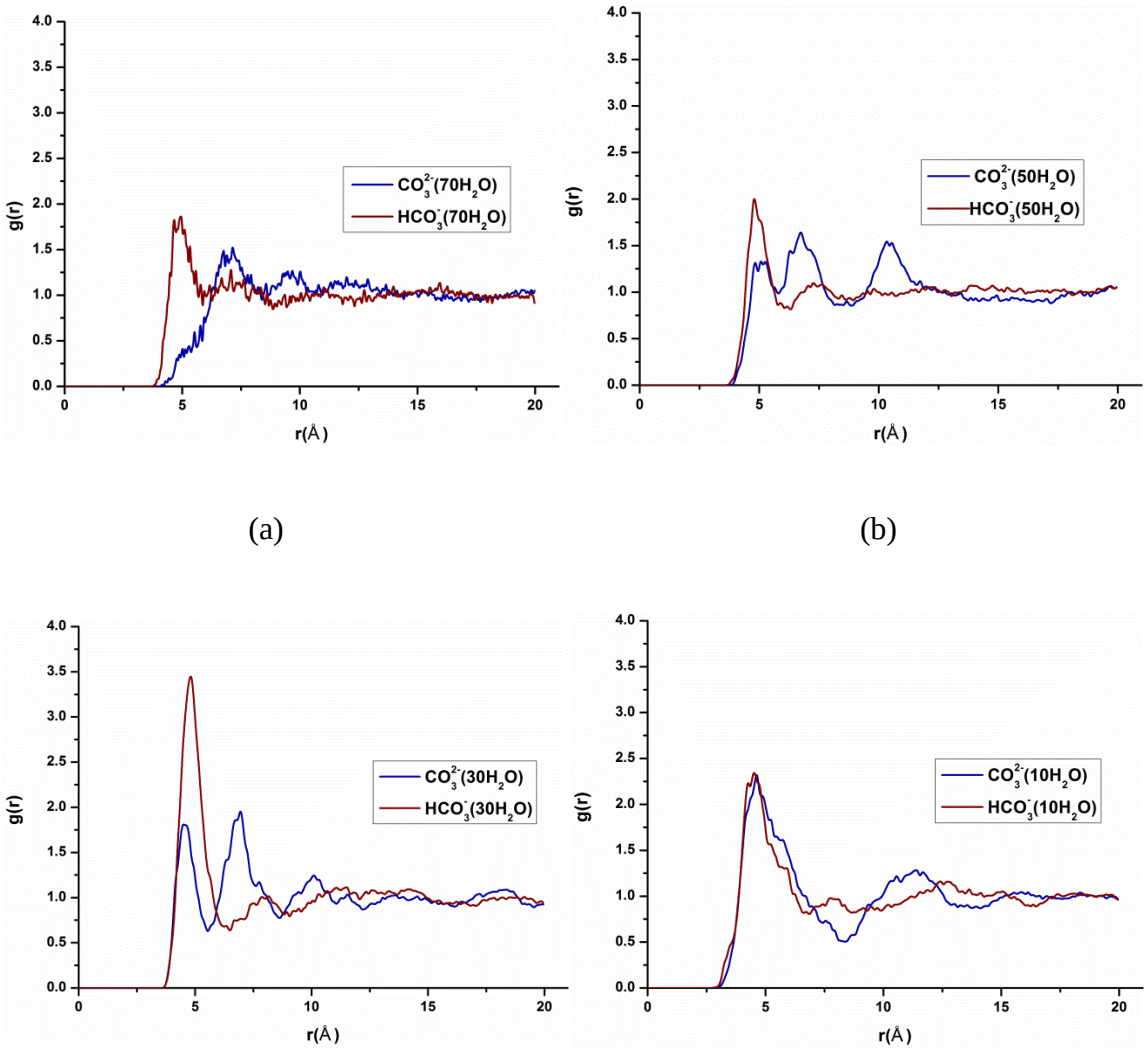

Figure 5.7: Intermolecular radial distribution functions between 1) Navy color: N atoms in NR_4^+ and C atoms in CO_3^{2-} of S1. 2) Red color: N atoms in NR_4^+ and C atoms in HCO_3^- of S2. These two RDFs are calculated under three humidity conditions: a) CO_3^{2-}:H_2O = 1:70, b) CO_3^{2-}:H_2O = 1:50, c) CO_3^{2-}:H_2O = 1:30, and d) CO_3^{2-}:H_2O = 1:10

In summary, the work in this Chapter reports the results of MD simulations of moisture-swing CO_2 sorbent with carbonate ion system and bicarbonate ion system under different humidity conditions. The transport characteristics and structures of ion species are explored with

different numbers of water molecules. The diffusion coefficients of water molecules and anions provide helpful insights, from a molecular level perspective, for designing a CO_2 sorbent with better dynamic performance. The CO_2 capture efficiency can be enhanced according to increase the ion diffusion rates, which could be realized by using different support materials with different characteristics like hydrophobicity and cation species. The molecular structure analysis states the different precipitation rates of carbonate ions and bicarbonate ions. In a drier surrounding, bicarbonate ion that precipitates out first leaves behind a more alkaline solution, which may promote the absorption of CO_2. This finding may provide an elucidation for the working mechanism of moisture-swing CO_2 sorbent.

Chapter 6 Kinetic Analysis of an Anion Exchange Sorbent

This chapter is derived from the paper "Kinetic Analysis of an Anion Exchange Sorbent for CO_2 Capture from Ambient Air", which is to be submitted.

Chapter 2 studied the underlying mechanism of a moisture swing sorbent for CO_2 capture from air. Chapter 3 calculated the effects of sorbent parameters on the working performance of nanoporous CO_2 sorbent. Chapter 4 discovered the hydrolysis of a series of basic salts in nanopores and ambient air surroundings. Chapter 5 presented the structure and diffusivity of molecules in moisture swing CO_2 sorbent. This chapter reports a preparation method of a new moisture swing sorbent for CO_2 capture from air, by using polyvinyl chloride as binder and ion exchange resin powder. The resin, with quaternary ammonium cations attached to the polymer structure and carbonate groups as mobile counter-ions, can absorb CO_2 when dry and release CO_2 when wet. The membrane structure, kinetic model of absorption process, performance of desorption process and the diffusivity of water molecules of the moisture swing sorbent are studied. It has been proved that the kinetic performance can be improved by using thin binder and hot water treatment. The impressive is this new CO_2 sorbent has the fastest CO_2 absorption rate among all air capture sorbents which have been reported by other literatures up to date.

6.1 Background

In order to compensate for CO_2 emission to ambient air, moisture swing sorbent for air carbon dioxide capture was first suggested by Lackner in 2009[18], which provides a novel approach to absorb CO_2 in dilute streams. The absorption/desorption process of this CO_2 sorbent is driven by moisture swing involving ion hydration/dehydration in an ion exchange resin[115]. This isothermal[26,28] and kinetic[136] performance of the resin-based sorbent (I-200) has been revealed systematically.

Increasing absorption capacity is a significant task for thermal-swing CO_2 sorbent[24] due to the high cost on the regeneration of sorbent. Kinetics improvement is a more interesting factor for moisture-driven sorbent due to the low cost of the regeneration part[136]. The energy consumption and cost can be reduced significantly according to increase the absorption rate of CO_2 sorbent. The objective of this study is to propose a new moisture swing CO_2 sorbent (P-100) by using ion exchange resin (IER) with polyvinyl chloride (PVC) as a binder. Note that P-100 means the binder of the absorbent is made by PVC with the thickness 100 micron. The kinetic characterization of the new CO_2 sorbent has been enhanced significantly comparing to sorbent I-200[26], which is manufactured and named by Snowpure LLC, California. I-200 is manufactured by coextrusion of a matrix polymer (polypropylene) and IER comprising quaternary ammonium functional groups. The preparation process of this new sorbent is introduced first. The analysis of kinetic performance is presented next based on the SEMs of sorbent structures, CO_2 absorption/desorption and water diffusion experiments.

6.2 Materials and Preparation Process

6.2.1 Materials

A heterogeneous ion-exchange material in the form of a flat sheet is produced in this air capture CO_2 study. The material includes: 1) an Ion Exchange Resin (IER)[18], which is composed of a polystyrene backbone with quaternary amine ligands attached to the polymer. The resin can be made up from 20% to 60% of the weight of the membrane. 2) Polyvinyl chloride (PVC) is a widely produced synthetic plastic polymer which was used as a binder. 3) Tetrahydrofuran is an organic compound with the formula $(CH_2)_4O$ which was employed a solvent to mix IER and PVC. Note that Tetrahydrofuran can only dissolve PVC.

6.2.2 Preparation of Anion-exchange Sorbent

Heterogeneous anion-exchange sorbents were prepared by a solution dip-coating technique[138]. For sorbent preparation, the IER particles were ground in a ball mill and then filtered by using a mesh with 44~74 micrometer openings first. Then, the PVC solid was dispersed into THF solvent in a glass reactor which was equipped with a mechanical stirrer for more than 5 hours. The PVC solid to THF solvent ratio is 1:20. Next, powdered resin particles (44~74um) were added into the PVC and THF solution. The mechanical stirrer stirred vigorously at room temperature for 30 min to mix PVC and THF uniformly. The resin to PVC weight ratio is 1:1 and the total solid to THF solvent ratio is 1:10 (w/v) [139]. After the mixing was complete, the dip coating method was used to coat material on a dry clean glass plate. This process generated anion-exchange sorbents whose thickness was 100 micron. They were dried at an ambient temperature 25℃ for 30 min, and then the almost dried sorbents were immersed in

distilled water. Lastly, the produced sorbents were heated in 90℃ hot water for 48 hours. Afterwards, they were ready-to-use.

6.2.3 The Absorption Capacity of CO_2 Sorbent

The Mohr method was used to determine the effective resin's ion charge density ρ_c of the P-100 sorbent is 1.58 mol/kg. CO_2 capacity Q_{est} was 17.69 L/kg estimated by ρ_c at standard condition. The CO_2 capacity Q_∞ was also measured by experiments, and the value was 16.4L/kg. The effective charge density and CO_2 capacity of sorbent can be both enhanced according to increase the weight ratio of resin to PVC during the preparation process.

6.3 Experimental Methods

6.3.1 Absorption Experiment

The experimental device with humidity control was set up to measure the half-time (the time when the absorbent reaches half of its capacity) of CO_2 absorption by P-100 sorbent. A layout of the device is shown in **Figure 6.1**. The CO_2 concentration changes were recorded with two infrared gas analyzers (IRGA). Measurements were taken once per second. The sorbent samples were treated by hot water under different water temperatures for 48 hours (25℃ warm water (P-100-25C), 50℃ hot water (P-100-50C), 90℃ hot water (P-100-90C)). Three P-100 samples and an I-200 sample, containing the same resin load, were immersed in 1.0 M sodium carbonate solution for 2-4 hours[26]. The solution was stirred to enhance ion exchanges rate. Samples were washed by 1.0 M sodium carbonate solution for 4-5 times until no bicarbonate ions could be detected on them, and then washed by plenty of DI water to flush away the sodium carbonate solution residues on samples. Wet and fresh samples (each one containing 0.30g IER) were put into a sealed chamber one by one and flushed with 2L/min zero CO_2 dry air, and the air

water concentration of air at outlet was measured to determine whether the samples were sufficiently dried. The drying process continued until the water concentrations of inlet and outlet were same, with 1% error. 1 L/min Air, containing 400 PPM CO_2, went through a dew point generator with 30% relative humidity, flowed over sorbent samples. The entire absorption process would last until CO_2 concentrations were same at inlet and outlet, with 1% error.

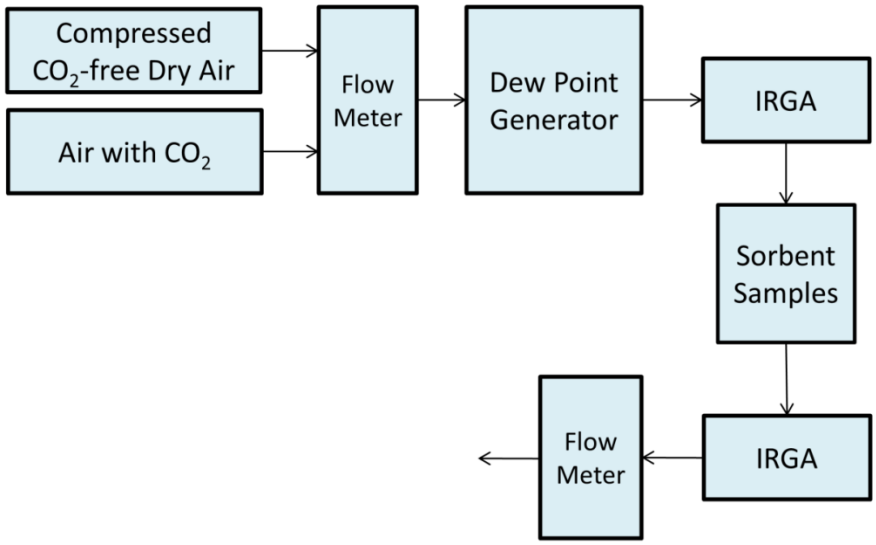

Figure 6.1: Schematic of Experimental Device. We can track the absorption of carbon dioxide by measuring the carbon dioxide content of the gas in the chamber of sorbent sample. The device can control the water vapor level in the closed gas circulation system by dew point generator. We can determine the absorption time of CO_2 by sorbent in the test sample chamber.

6.3.2 Desorption Experiment

The absorbed CO_2 was released when the sorbent P-100 or I-200 was exposed to a high humidity surrounding or liquid water surrounding. Meanwhile, the sorbent kept on absorbing water vapor from air when it was put into a higher humidity surrounding until it reached tan

equilibrium state. The absorbed water molecules lead to the sorbent weight increase. This experiment was to point out the reason of this sorbent owning better kinetic characteristics by analyzing the equilibrium time of the increase of sorbent weight and CO_2 desorption process. The diffusion coefficients of water molecules in four samples were calculated by the weight changes of samples. Diagram of the experimental device is shown as **Figure 6.2**

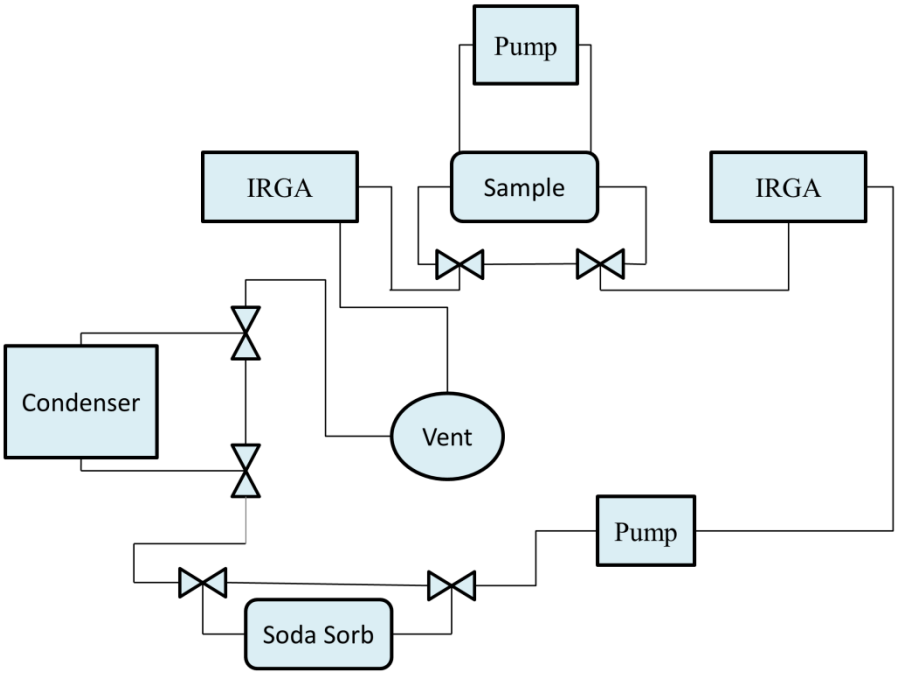

Figure 6.2: Schematic of Experimental Device. The total amount of carbon dioxide on the sample and in the gas volume is constant. We can track the absorption and desorption of carbon dioxide by measuring the carbon dioxide content of the gas. The device can control the water vapor level in the closed gas circulation system. We can determine and characterize the process of CO_2 absorption/desorption and weight change of sorbent in the test sample chamber

Four samples (25℃ warm water treated P-100, 50℃ hot water treated P-100, 90℃ hot water treated P-100, and I-200) containing the same resin load, were first exposed to pretreated air without water vapor for two hours, in order to completely dry and load the samples. Next, set a same initial environment of dew point 15 ˚C and 400 ppm CO_2 in the closed experimental device for four samples. The weight change of each sample and the CO_2 concentration change in the chamber due to CO_2 released from each sample were measured separately. A humidity controller was employed to maintain a constant humidity in the chamber through PID control. The CO_2 concentration increase was recorded every second by infrared gas analyzers (IRGA).

6.4 Results and Discussion

6.4.1 Sorbent Structure Analysis

The structures of the P-100 sorbents treated by hot water with different temperatures were studied by SEM (Agilent Technologies, SE 1000V) as shown in **Figure 6.3**. Obviously, exposed to a hot-water treatment, anion-exchange resin particles swelled and expanded pushing away the PVC binder, resulting in the formation of narrow cavities between anion exchange particles and PVC matrix and larger amount of pores in PVC materials.

The following **Figure 6.4**, micro-structure schematic of P-100 sorbent can express the percolation of P-100 sorbent clearly. After treatment of 50 ˚C hot water, some small islands of interconnected particles appear; After treatment of 90˚C hot water, these connections grow and form extended pathways. More and more ion exchange resin particles are connected by channels if the connections keep growing. The chance of the appearance of percolation threshold can increase the speed and range of air diffusion inside the sorbent. According to the observation of SEM, much more resin particles in new sorbent P-100 are exposed into air than the ones held by

I-200[26] due to the thinner thickness of membrane and the more continuous channels inside the sorbent. Moreover, reaching the percolation threshold may further promotes the conduction level between surrounding air and resin particles. Therefore, treating P-100 by high temperature water may promote resin particles to be exposed to ambient air surrounding, thereby further improve the working performance of this moisture-swing CO_2 sorbent.

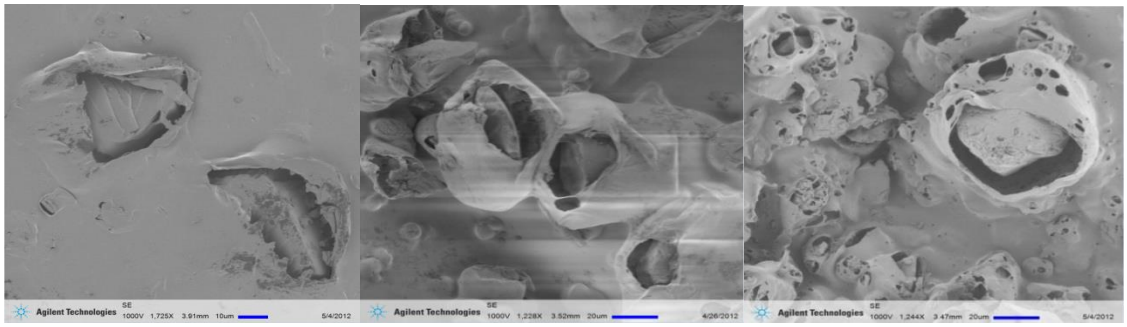

(A) (B) (C)

Figure 6.3: SEMs of P-100 sorbents treated with different hot water temperatures. (A) 25°C water treated sample P-100-25C, (B) 50°C water treated sample P-100-50C, and (C) 90°C water treated sample P-100-90C

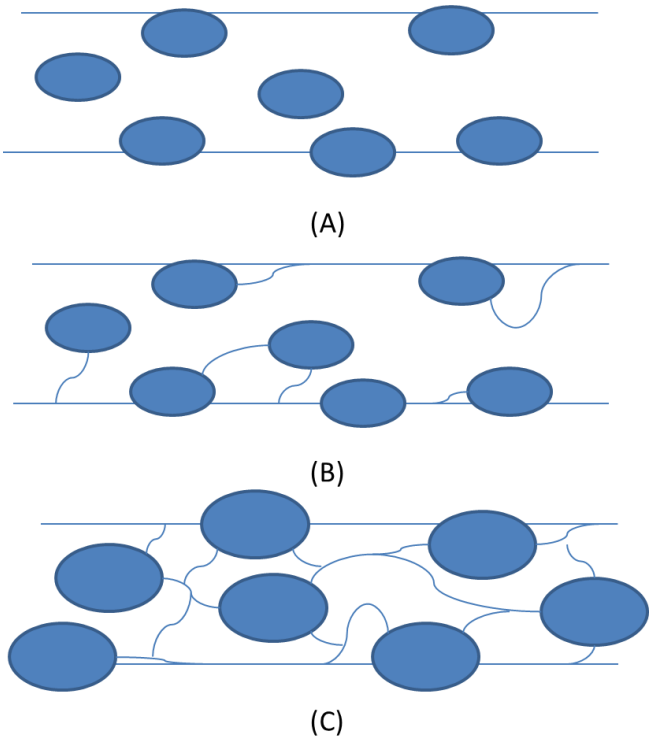

Figure 6.4: Schematic micro-structure of P-100 ion exchange sorbent (A) 25 ˚C water treated P-100-25C, (B) 50 ˚C water treated P-100-50C, (C) 90 ˚C water treated P-100-90C

6.4.2 Absorption Half-time

The kinetic characteristics are significant factors for moisture-swing CO_2 capture sorbent. Absorption kinetics of the sorbent are determined by mass diffusivity in the materials, heat transfer into and out of the pores, and intrinsic chemical reaction rates[20,136,140]. As a preliminary assessment of the CO_2 absorption kinetics of these air capture sorbents, absorption half time is an assessment factor[20] to evaluate the absorption rate of CO_2 sorbent. The absorption half time of moisture swing sorbent can be expressed by **Equation 6.1**:

$$T_{half-time} = \frac{T_{CO_2}}{2} = T_{H_2O} + T_{reaction} \qquad 6.1$$

T_{CO_2} is the time for CO_2 absorption by sorbent from fresh-empty status to full-loaded status, T_{H_2O} is the absorption time for water on sorbent; $T_{reaction}$ is the time of intrinsic chemical reaction. The half times of sample P-100-25C, P-100-50C, P-100-90C, and sample I-100 were measured by experimental device in **Figure 6.1**.

Figure 6.5 displays the half times of the four different samples under simulated air capture condition (30% relative humidity, 400ppm). Other half times of current air capture CO_2 sorbents[20,141] in literatures have also been presented.

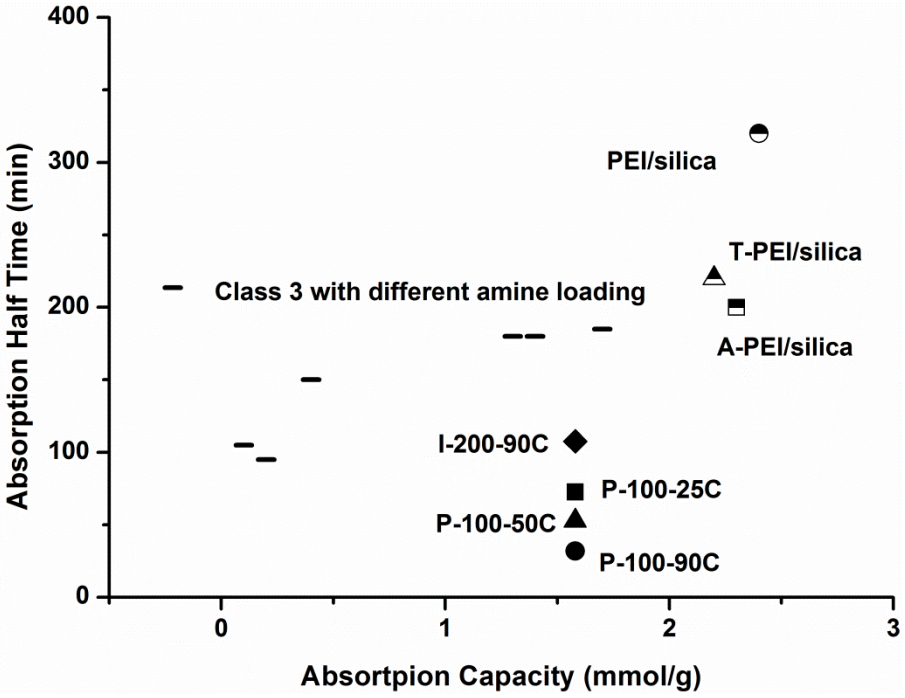

Figure 6.5: Comparison of CO_2 absorption half times and capacities of different sorbents

The sample P-100-90C has the best kinetic characteristics comparing with the other three moisture swing CO_2 sorbents. The 31.8 min half time is also the shortest half time in all air capture sorbents which have been reported by other literatures up to date. Obviously, the kinetics

of P-100-90C treated by 90 ˚C hot water is better than the other two P-100 sorbents, because the treatment by high temperature water enlarges the surface of resin to be exposed to the ambient air. This leads to the absorption rate of water molecules on IER is much faster than the other two P-100 samples, meaning the smaller T_{H_2O} value. More existing water molecules on P-100-90C sorbent can produce more OH^- ions[115] which can absorb a larger amount of CO_2 under the same time range. The higher reaction rate means the smaller $T_{reaction}$ value.

I-200 moisture swing CO_2 sorbent was also already treated by 90˚C hot water but still had a longer half time than those of three P-100 samples. The reason is the thickness of I-200 sorbent is 640 microns which is much thicker than the 100 microns thickness of P-100 sorbent. Much more time is consumed by water vapor to permeate into I-200 sorbent to contact with the inside resin particles, which is wrapped by polypropylene matrix binder.

6.4.3 Absorption Kinetic Model of Sorbent

The kinetic absorption of P-100-90C sorbent was analyzed by Lagergren pseudo first-order model[142], which has been most frequently employed to present absorption dynamic process under various conditions.

$$\frac{dq}{dt} = k(q_e - q) \qquad 6.2$$

q is absorption quantity at time t, k is constant number, q_e is equilibrium isotherm absorption capacity. Integrating **Equation 6.2** with boundary conditions (a) t=0, q=0; (b) t=t, q=q_e

$$q = q_e(1 - e^{-kt}) \qquad 6.3$$

Experimental data of absorption amount of CO_2 by P-100-90C sorbent was recorded per second according to the experimental device **Figure 6.1**. *k* values were determined by **Equation 6.3**. **Figure 6.6** shows that pseudo first order model fits the absorption kinetic data of ion-exchange P-100-90C sorbent with the coefficient of determination 0.98.

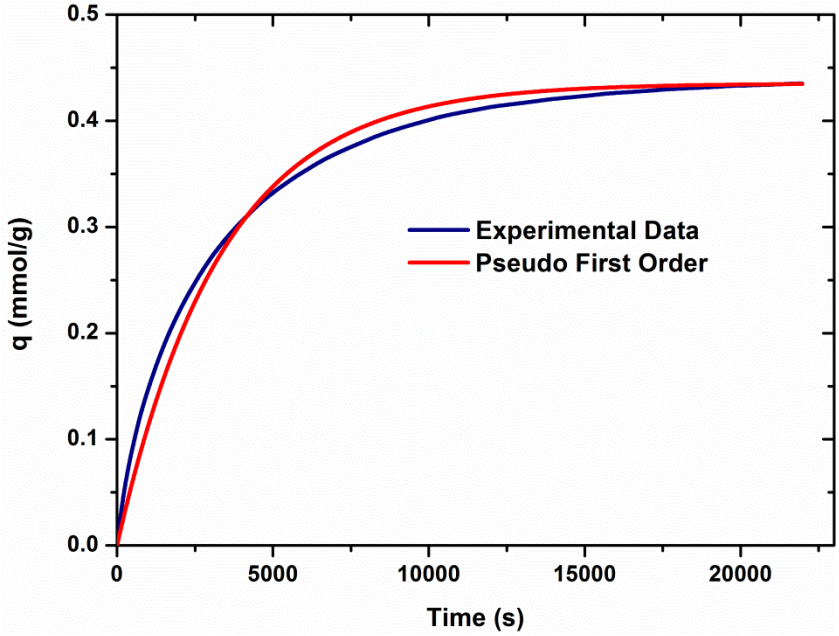

Figure 6.6: Comparison of kinetic model and experimental data of absorption performance

6.4.4 Desorption Kinetic Performance

A moisture swing CO_2 sorbent can release CO_2 back to the air in a wet surrounding[18]. The desorption kinetic characteristics of moisture swing sorbents are mainly influenced by the diffusion rate of water molecules in sorbent, T_w , and the diffusion rate of desorbed CO_2 from

inside of sorbent to ambient air, T_c. This study focuses on analyzing the impact of these two factors on the desorption rate.

To determine the diffusion coefficients of water molecules in the four sorbents, the moisture uptake percentage, was determined from the **Equation 6.4**

$$Moisture\ Uptake\% = \frac{M_t}{M_d} \times 100\% \qquad 6.4$$

Where M_t is the total amount of water content absorbed by sorbent samples at time *t*, M_d is the original weight of the dry samples. The diffusivity *D*, was determined from the slope (*K*) of the initial linear region of the percentage moisture uptake $\frac{M_t}{M_d}$ versus $\sqrt{t}$ curve[129,143].

$$D = \frac{\pi}{16}\left(\frac{h}{M_\infty/M_d}\right)^2 K^2 \qquad 6.5$$

Where *h* is the thickness of the sample, *t* is exposure time and M_∞ is the maximum moisture gain.

Figure 6.7 7 illustrates the desorption process of four sorbents. Four samples are comparable because they have same weight of resin particles about 0.30g. The same weight of resin particles can maintain the equilibrium concentration of CO_2 is between 1900ppm and 2000ppm under the same condition of dew point 15℃ in the experimental device, shown as **Figure 6.2**. . The samples increasingly absorb water molecules over time, which leads to their weights reach to equilibrium values under the certain water vapor partial pressure. Absorbed water molecules is conducive to desorb CO_2 from full loaded sorbent. The released CO_2 from sorbent increases the CO_2 concentration in device. The diffusion coefficients of water, as well as equilibrium times of T_w and T_c in four sorbents have been listed in Table 1.

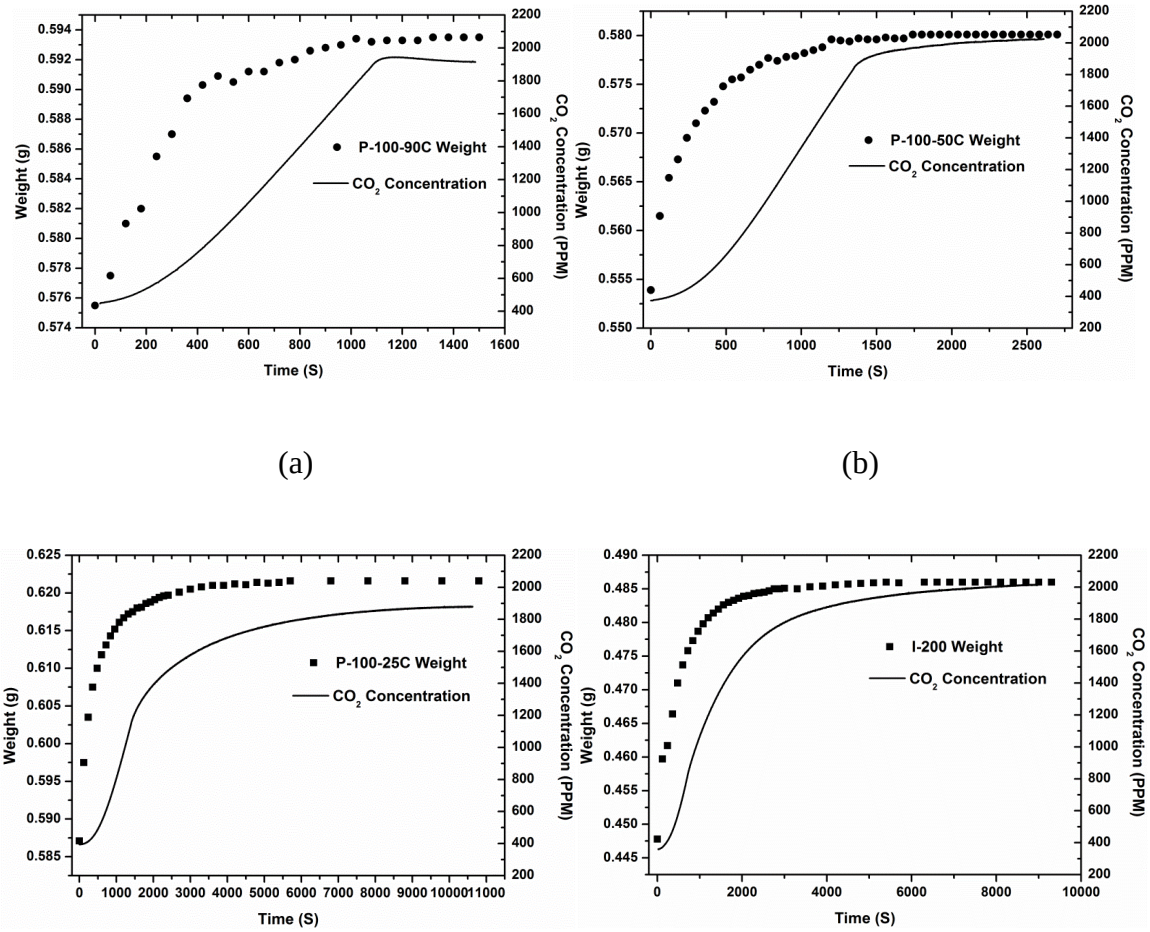

Figure 6.7: CO_2 desorption process of four sorbents (a) P-100-90C Sorbent, (b) P-100-50C Sorbent, (c) P-100-25C Sorbent, (d) I-200 Sorbent. Left Y-axis is sorbent weight, and right Y-axis is CO_2 concentration.

	D(m^2/s,× E-12)	T_w (s)	T_c(s)	ΔT (s)
(a)P-100-90C	6.503	1020	1086	66
(b)P-100-50C	2.536	1740	2462	722
(c)P-100-25C	1.842	7200	10628	3428
(d)I-200	58.464	6300	8970	2670

Table 1. Diffusion coefficients of water, equilibrium times of water and CO_2 in four samples

Comparing **Table 1** (a), (b) and (c), the diffusion rate of water is higher for the sorbents are treated by higher temperature water. The higher diffusion rate is due to sorbent has more pores in PVC matrix, larger narrow cavities between IER particles and PVC binder, and also expanded channels in IER particles. These characteristics greatly promote the diffusion rates of H_2O and CO_2 in sorbent. Water with high diffusion rate can reach to HCO_3^- ions more quickly and released CO_2 can escape from sorbent more rapidly. For P-100-90C sorbent, the equilibrium time difference ΔT between T_w and T_c is smallest ΔT=66s. It means the desorbed CO_2 diffuses out of the sorbent requiring 66s after water increase reaches to equilibrium on sorbent. However, ΔT of P-100-25C is as long as 3428s. It shows even though ample water provides surrounding for HCO_3^- ions to release CO_2, the released CO_2 is still trapped in sorbent for some time. The narrow channels in IER of P-100-25C also slow down the CO_2 diffusion rate because of relative high CO_2 partial pressure around bicarbonate ions, which is not conducive for desorption.

Comparing (a) and (d), both sorbents has been treated by 90°C hot water. Resins on the two sorbents have similar structural features. Though the diffusion coefficient of water in I-200 is much larger than the one of P-100-90C, the water equilibrium time of P-100-90C is much smaller than those of I-200 due to the different binder materials of two sorbents. The hydrophilic polypropylene binder may also contribute to the initial water diffusion for I-200 more than the hydrophobic PVC binder for P-100-90C. Also, the polypropylene of 640 micron thickness takes more time for water diffusion than the 100 micron PVC.

I-200 also has longer time for CO_2 release to ambient air. 44~74um resin particles are inlayed in 640 micron polypropylene of I-200 sorbent. The narrow, tortuous and long paths between resin particles and polypropylene are against to CO_2 diffusion, however, same 44~74um rein particles can almost penetrate the 100 micron PVC for P-100-90c sorbent, contacting with

atmosphere directly is benefit to desorption performance. Hydrophilic polypropylene binder attracts part of absorbed water molecules attaching to it in I-200 sorbent, which water can not contact to functional IER particle to release CO_2 immediately.

6.5 Conclusion

This Chapter introduces a new moisture swing CO_2 sorbent by using a new polymer material PVC as binder for the IER. The preparation process, sorbent structure, kinetic model, absorption and desorption characteristics are analyzed. The CO_2 absorption rate is nearly three times as fast as the one of polypropylene CO_2 sorbent, and also three to ten times as fast as amine-tethered solid sorbents. This fast absorption/desorption rate is with the benefit of a thin binder for IER. This new sorbent provides a way of designing a moisture swing CO_2 sorbent with a high absorption rate in the future.

Chapter 7 Conclusions and Future Work

7.1 Concluding Remarks

In this dissertation, by using nanomaterials or anionic exchange resins, we control the water activity and thereby modify ion hydration states inside nanoscale spaces. We have demonstrated in simulations and experiments that the nanoconfined ion hydration in nanomaterials can absorb CO_2 from ambient air when the surrounding is dry while it will release CO_2 when the surrounding is wet.

The dissertation begins with an explanation of the molecular mechanism that underly the moisture swing in ion exchange based sorbent for CO_2 capture from air. The calculated free energy change during the hydration of ions shows that the sorbent system energetically prefers a combination of bicarbonate and hydroxide ions over carbonate ions in a dry environment. The large hydroxide ion is more attractive for absorbing CO_2 as it readily reacts with CO_2 to form bicarbonate. The higher degree of hydrolysis of carbonate ions that exists in a relative dry environment cannot be produced or observed in an aqueous solution. In the presence of large amounts of water the reaction reverses bicarbonate and hydroxide from carbonate and water. This counterintuitive phenomenon is verified by both simulation and experiment. It can be applied to other basic and acidic ions. The molecular dynamic calculations that verify the moisture swing can also be used to shed light on the fundamental chemical reactions between ions and water molecules in a confined space of nanoporous materials. Based on this discovery, a nano-structured CO_2 sorbent is developed to capture CO_2 from dry ambient air spontaneously, while it releases CO_2 in a wet surrounding for regeneration. The conversion between absorption and desorption of this novel sorbent can be driven just with inexpensive water quantities instead

of expensive heat energy. The novel CO_2 sorbent is designed for dealing with the global warming.

In the subsequent chapters we study the effects of nanopores size, the characteristics of the confining layers, the ion charge density and the temperature on the efficiency of the moisture swing CO_2 capture system. We do this by analyzing how the concentration of hydroxide ions changes as the function of the water quantity present. In parallel CO_2 absorption experiments are carried out on nanomaterials to verify the working principles and parameter effects. The methodology of combining MD for analyzing complex systems with QM for simple chemical transitions, allows us to calculate transition energies for dry and wet equilibria, by transitioning from a physical state to a hypothetical near vaccum state, where chemical reactions can occur without interference of large numbers of molecules. This technique provides a more efficient way to study this and similar problems.

The higher degree of the hydrolysis reaction between carbonate ion and water molecules at solid/water interface in a relative dry environment, is also applicable to some other weak base and weak acid ions. We have demonstrated this to be the case for some divalent and trivalent base ions, and shown that the opposite is true for certain univalent ions. A better understanding of the underlying mechanism and extensive parametric studies will help a developed design of more efficient energy-saving water-driven CO_2 capture absorbent. The parametric optimization investigation may be carried out in the future.

Through quantum mechanical modeling we have demonstrated a series of unconventional chemical reactions. The degrees of hydrolysis of basic salts (S^{2-}, CO_3^{2-}, SO_3^{2-}, HPO_4^{2-}, SO_4^{2-}, PO_4^{3-}, CN^-, HS^-) containing several water molecules are significantly different from those in bulk

water. The hydrolysis degrees can be controlled by adding or removing water. Moreover, the reaction free energy of hydrolysis of basic salts were decomposed to enthalpic component and entropic component. The enthalpy change with different number of water molecule are dominant component in the free energy change of hydrolysis of basic salts. This unique mechanism sheds some light on a vast number of chemical processes of hydrated ion pairs in nanoscopic pores and in the natural atmosphere. The finding is also suggested that the multiple valence acidic ions can hydrolyze H_2O to create larger amount of protons with the decrease of water amount. Furthermore, the discovery also has wide potential applications, like design novel absorbents to capture acidic gases against traditional sorbents.

In order to discover other mechanisms which can drive the moisture swing sorbent to capture CO_2 in dry and lease CO_2 in wet, the transport abilities and structures of ion species under different amount of water molecules were explored. We report the results of MD simulations of IER with carbonate ion system and bicarbonate ion system under different humidity conditions. The diffusion coefficients of water molecules and anions provided us critical information from molecular level, which can be used to design better CO_2 sorbent with benefit of improved dynamic performance. The molecular structure analysis states the different degrees of precipitation of carbonate ions and bicarbonates. In dry surrounding, bicarbonate that precipitates out first leaves behind a more alkaline solution may promote the absorption of CO_2.

Besides atomic modeling, we produce a new moisture swing CO_2 sorbent by using a new binder PVC. A better kinetic characteristics of this new sorbent is described and analyzed. Its fast absorption/desorption rate is with the benefit of a thin bind holder for IER. This new sorbent provides a way of designing a moisture swing CO_2 sorbent with a high absorption rate in future.

7.2 Recommendations for Future Work

For the study of moisture swing CO_2 sorbent, a more comprehensive model which includes CO_3^{2-} ions, HCO_3^- ions, OH^- ions, NR_4^+ ions, H_2O, CO_2 and IER backbones, should be built for calculating the diffusion coefficients of molecules with chemical reactions. ReaxFF in Molecular Dynamics can be applied to model this kind large system with chemical reactions because of the requirement of breaking and forming bonds. The diffusion coefficients provided from molecular level calculation can be used to design high efficient CO_2 sorbent.

The optimal parameters for a CO_2 sorbent could be found in the future. For example, more detailed calculations could determine the optimal layer distance of the confining layers, and it could be used to choose a nanoporous material containing appropriate pore size. The optimal distance of cations can be applied to choose the most suitable charge density of IER for CO_2 capture. These information can help us to design next generation CO_2 sorbent with high capacity and fast absorption rate, which can greatly save costs.

The activation energy change with the change of the number of water molecules is also an interesting study. The proton transfer in hydration shells may decrease the activation energy level thereby increase the rate of chemical reaction which is also being explored currently.

Finally, the study in this dissertation belongs to chemical physics. The study content is the interaction of water molecule with ions, which are usually hydrated carrying from several to several tens of water molecules when present in the natural atmosphere or on solid porous surfaces. Interfaces with hydrated ions play an important role in a wide range of natural and fundamental processes, such as environmental chemistry, electrochemistry and corrosion. More related work in this field can also be studied by using the knowledge of chemical physics to

explain results and guide future investigation. We can explore chemical structures and reactions at the quantum mechanical level, elucidate the structure and reactivity of gas phase ions, and discover accurate approximations to make the physics of chemical phenomena computationally accessible. We also hope this study can open a vast scope of new chemistry in atmospheric and nanoconfined water.

Bibliography

1 Goddard Institute of Space Studies NASA 2016.

2 IPCC. Intergovernmental Panel on Climate Change 2007, Fourth Assessment Report. *Synthesis Report (Cambridge Univ Press, New York)* (2007).

3 Kharecha, P. A. & Hansen, J. E. Implications of “peak oil” for atmospheric CO2 and climate. *Global Biogeochem. Cycles* **22** (2008).

4 Tavoni, M. & Van der Zwaan, B. Nuclear versus coal plus CCS: a comparison of two competitive base-load climate control options. *Environmental Modeling & Assessment* **16**, 431-440 (2011).

5 Spector, N. A. & Dodge, B. F. Removal of carbon dioxide from atmospheric air. *Transactions of the American Institute of Chemical Engineers* **42**, 827-848 (1946).

6 Astarita, G. Mass transfer with chemical reaction. (1967).

7 Carey, R., Gomezplata, A. & Sarich, A. An overview into submarine CO 2 scrubber development. *Ocean Engineering* **10**, 227-233 (1983).

8 DallBauman, L. & Finn, J. E. Adsorption processes in spacecraft environmental control and life support systems. *Stud. Surf. Sci. Catal.* **120**, 455-471 (1999).

9 Thomson, A. M., Izaurralde, R. C., Smith, S. J. & Clarke, L. E. Integrated estimates of global terrestrial carbon sequestration. *Global Environmental Change* **18**, 192-203 (2008).

10 Lehmann, J., Gaunt, J. & Rondon, M. Bio-char sequestration in terrestrial ecosystems–a review. *Mitigation and adaptation strategies for global change* **11**, 395-419 (2006).

11 Coale, K. H. *et al.* Southern Ocean iron enrichment experiment: carbon cycling in high-and low-Si waters. *science* **304**, 408-414 (2004).

12 Schuiling, R. & Tickell, O. (2010).

13 Schuiling, R. & Krijgsman, P. Enhanced weathering: An effective and cheap tool to sequester CO2. *Climatic Change* **74**, 349-354 (2006).

14 Lackner, K., Ziock, H.-J. & Grimes, P. *Carbon Dioxide Extraction from Air: Is It An Option?* , (1999).

15 Stolaroff, J. K., Keith, D. W. & Lowry, G. V. Carbon dioxide capture from atmospheric air using sodium hydroxide spray. *Environmental science & technology* **42**, 2728-2735 (2008).

16 Mahmoudkhani, M., Heidel, K., Ferreira, J., Keith, D. & Cherry, R. S. Low energy packed tower and caustic recovery for direct capture of CO 2 from air. *Energy Procedia* **1**, 1535-1542 (2009).

17 Zeman, F. S. & Lackner, K. S. Capturing carbon dioxide directly from the atmosphere. *World Resource Review* **16**, 157-172 (2004).

18 Lackner, K. S. Capture of Carbon Dioxide from Ambient Air. *Eur. Phys. J. Spec. Top.* **176**, 93-106, doi:10.1140/epjst/e2009-01150-3 (2009).

19 Li, W. *et al.* Steam‐Stripping for Regeneration of Supported Amine‐Based CO2 Adsorbents. *ChemSusChem* **3**, 899-903 (2010).

20 Choi, S., Drese, J. H., Eisenberger, P. M. & Jones, C. W. Application of Amine-Tethered Solid Sorbents for Direct CO2 Capture from the Ambient Air. *Environmental Science & Technology* **45**, 2420-2427, doi:10.1021/es102797w (2011).

21 Ge, J.-J., Trachtenberg, M. C., McGregor, M. & Cowan, R. Enzyme-based facilitated transport: Use of vacuum induced sweep for enhanced CO 2 capture. Report No. 0148-7191, (SAE Technical Paper, 2001).

22 Baciocchi, R., Storti, G. & Mazzotti, M. Process design and energy requirements for the capture of carbon dioxide from air. *Chemical Engineering and Processing: Process Intensification* **45**, 1047-1058 (2006).

23 Lackner, K. S. The thermodynamics of direct air capture of carbon dioxide. *Energy* **50**, 38-46 (2013).
24 Socolow, R. *et al.* Direct air capture of CO2 with chemicals: a technology assessment for the APS Panel on Public Affairs. (American Physical Society, 2011).
25 Keith, D. W., Ha-Duong, M. & Stolaroff, J. K. Climate strategy with CO2 capture from the air. *Climatic Change* **74**, 17-45 (2006).
26 Wang, T., Lackner, K. S. & Wright, A. Moisture Swing Sorbent for Carbon Dioxide Capture from Ambient Air. *Environmental Science & Technology* **45**, 6670-6675, doi:10.1021/es201180v (2011).
27 House, K. Z. *et al.* Economic and energetic analysis of capturing CO2 from ambient air. *Proceedings of the National Academy of Sciences* **108**, 20428-20433 (2011).
28 Wang, T., Lackner, K. S. & Wright, A. B. Moisture-swing sorption for carbon dioxide capture from ambient air: a thermodynamic analysis. *Phys. Chem. Chem. Phys.* **15**, 504-514, doi:10.1039/c2cp43124f (2013).
29 Wang, T., Lackner, K. S. & Wright, A. B. Moisture-Swing Sorption for Carbon Dioxide Capture from Ambient Air: A Thermodynamic Analysis. *PCCP* **15**, 504-514, doi:10.1039/c2cp43124f (2013).
30 Carlon, H. R. New measurements of the ion content of evaporation‐humidified air. *The Journal of Chemical Physics* **76**, 5523-5529, doi:doi:http://dx.doi.org/10.1063/1.442907 (1982).
31 Steinbach, P. J. & Brooks, B. R. Protein hydration elucidated by molecular dynamics simulation. *Proceedings of the National Academy of Sciences* **90**, 9135-9139 (1993).
32 Israelachvili, J. & Wennerstrom, H. Role of hydration and water structure in biological and colloidal interactions. *Nature* **379**, 219-225 (1996).
33 Jungwirth, P. & Tobias, D. J. Specific Ion Effects at the Air/Water Interface. *Chem. Rev.* **106**, 1259-1281, doi:10.1021/cr0403741 (2005).
34 Caleman, C., Hub, J. S., van Maaren, P. J. & van der Spoel, D. Atomistic simulation of ion solvation in water explains surface preference of halides. *Proceedings of the National Academy of Sciences* **108**, 6838-6842, doi:10.1073/pnas.1017903108 (2011).
35 Laskin, A. *et al.* Reactions at Interfaces As a Source of Sulfate Formation in Sea-Salt Particles. *Science* **301**, 340-344, doi:10.1126/science.1085374 (2003).
36 Laskin, A. *et al.* A New Approach to Determining Gas-Particle Reaction Probabilities and Application to the Heterogeneous Reaction of Deliquesced Sodium Chloride Particles with Gas-Phase Hydroxyl Radicals. *The Journal of Physical Chemistry A* **110**, 10619-10627, doi:10.1021/jp063263+ (2006).
37 Shapiro, N. & Vigalok, A. Highly Efficient Organic Reactions “on Water”, “in Water”, and Both. *Angew. Chem. Int. Ed.* **47**, 2849-2852, doi:10.1002/anie.200705347 (2008).
38 Wang, J. Molecular dynamics studies of simple model fluids and water confined in carbon nanotube. (2010).
39 Alder, B. J. & Wainwright, T. Studies in molecular dynamics. I. General method. *The Journal of Chemical Physics* **31**, 459-466 (1959).
40 Rapaport, D. C. *The art of molecular dynamics simulation*. (Cambridge university press, 2004).
41 Haile, J. Molecular dynamics simulation: Elementary methods. *Computers in Physics* **7**, 625-625 (1993).
42 Phillips, J. C. *et al.* Scalable molecular dynamics with NAMD. *J. Comput. Chem.* **26**, 1781-1802 (2005).
43 Jones, J. E. in *Proceedings of the Royal Society of London A: Mathematical, Physical and Engineering Sciences.* 463-477 (The Royal Society).
44 Allen, M. P. & Tildesley, D. J. *Computer simulation of liquids*. (Oxford university press, 1989).
45 Scales, M. A. Crystals, Defects and Microstructures. (2000).

46 Jensen, F. *Introduction to computational chemistry*. (John Wiley & Sons, 2013).
47 Frenkel, D. & Smit, B. *Understanding molecular simulation: from algorithms to applications*. Vol. 1 (Academic press, 2001).
48 Hohenberg, P. & Kohn, W. Inhomogeneous electron gas. *Physical review* **136**, B864 (1964).
49 Kohn, W. & Sham, L. J. Self-consistent equations including exchange and correlation effects. *Physical review* **140**, A1133 (1965).
50 Hedin, L. & Lundqvist, B. I. Explicit local exchange-correlation potentials. *Journal of Physics C: Solid state physics* **4**, 2064 (1971).
51 Ceperley, D. M. & Alder, B. Ground state of the electron gas by a stochastic method. *Phys. Rev. Lett.* **45**, 566 (1980).
52 Kohn, W., Vashishta, P., Lundqvist, S. & March, N. (Plenum, New York, 1983).
53 Berendsen, H. J., Postma, J. P., van Gunsteren, W. F. & Hermans, J. in *Intermolecular forces* 331-342 (Springer, 1981).
54 Berendsen, H., Grigera, J. & Straatsma, T. The missing term in effective pair potentials. *J. Phys. Chem.* **91**, 6269-6271 (1987).
55 Jorgensen, W. L., Chandrasekhar, J., Madura, J. D., Impey, R. W. & Klein, M. L. Comparison of simple potential functions for simulating liquid water. *The Journal of chemical physics* **79**, 926-935 (1983).
56 Izadi, S., Anandakrishnan, R. & Onufriev, A. V. Building water models: A different approach. *The journal of physical chemistry letters* **5**, 3863-3871 (2014).
57 Mahoney, M. W. & Jorgensen, W. L. A five-site model for liquid water and the reproduction of the density anomaly by rigid, nonpolarizable potential functions. *The Journal of Chemical Physics* **112**, 8910-8922 (2000).
58 Hribar, B., Southall, N. T., Vlachy, V. & Dill, K. A. How Ions Affect the Structure of Water. *J. Am. Chem. Soc.* **124**, 12302-12311, doi:10.1021/ja026014h (2002).
59 Kunz, W., Henle, J. & Ninham, B. W. 'Zur Lehre von der Wirkung der Salze' (about the science of the effect of salts): Franz Hofmeister's historical papers. *Current Opinion in Colloid & Interface Science* **9**, 19-37, doi:http://dx.doi.org/10.1016/j.cocis.2004.05.005 (2004).
60 Kunz, W., Henle, J. & Ninham, B. W. 'Zur Lehre von der Wirkung der Salze' (about the science of the effect of salts): Franz Hofmeister's historical papers. *Current Opinion in Colloid & Interface Science* **9**, 19-37, doi:10.1016/j.cocis.2004.05.005 (2004).
61 Poynor, A. *et al.* How Water Meets a Hydrophobic Surface. *Phys. Rev. Lett.* **97**, 266101, doi:10.1103/PhysRevLett.97.266101 (2006).
62 Rahaman, A., Grassian, V. H. & Margulis, C. J. Dynamics of Water Adsorption onto a Calcite Surface as a Function of Relative Humidity. *The Journal of Physical Chemistry C* **112**, 2109-2115, doi:10.1021/jp077594d (2008).
63 Ohtaki, H. & Radnai, T. Structure and dynamics of hydrated ions. *Chem. Rev.* **93**, 1157-1204, doi:10.1021/cr00019a014 (1993).
64 Zidi, Z. S. Solvation of Sodium-chloride Ion Pair in Water Cluster at Atmospheric Conditions: Grand Canonical Ensemble Monte Carlo Simulation. *The Journal of Chemical Physics* **123**, doi:10.1063/1.1979476 (2005).
65 Zhao, Z., Rogers, D. M. & Beck, T. L. Polarization and Charge Transfer in the Hydration of Chloride Ions. *The Journal of Chemical Physics* **132**, doi:10.1063/1.3283900 (2010).
66 Tielrooij, K. J., Garcia-Araez, N., Bonn, M. & Bakker, H. J. Cooperativity in Ion Hydration. *Science* **328**, 1006-1009, doi:10.1126/science.1183512 (2010).
67 Ghommem, M. *et al.* Release of Stored Thermochemical Energy from Dehydrated Salts. *Int. J. Heat Mass Transfer* **54**, 4856-4863, doi:10.1016/j.ijheatmasstransfer.2011.06.041 (2011).

68 Hamelberg, D. & McCammon, J. A. Standard Free Energy of Releasing a Localized Water Molecule from the Binding Pockets of Proteins: Double-Decoupling Method. *J. Am. Chem. Soc.* **126**, 7683-7689, doi:10.1021/ja0377908 (2004).
69 Quinn, R. Ion Exchange Resins as Reversible Acid Gas Absorbents. *Sep. Sci. Technol.* **38**, 3385-3407, doi:10.1081/ss-120023405 (2003).
70 Quinn, R., Appleby, J. B. & Pez, G. P. Salt Hydrates: New Reversible Absorbents for Carbon Dioxide. *J. Am. Chem. Soc.* **117**, 329-335, doi:10.1021/ja00106a035 (1995).
71 Stipp, S. L. & Hochella Jr, M. F. Structure and Bonding Environments at the Calcite Surface as Observed with X-ray Photoelectron Spectroscopy (XPS) and Low Energy Electron Diffraction (LEED). *Geochim. Cosmochim. Acta* **55**, 1723-1736, doi:10.1016/0016-7037(91)90142-r (1991).
72 Tian, C. S. & Shen, Y. R. Structure and Charging of Hydrophobic Material/Water Interfaces Studied by Phase-sensitive Sum-frequency Vibrational Spectroscopy. *Proceedings of the National Academy of Sciences* **106**, 15148-15153, doi:10.1073/pnas.0901480106 (2009).
73 Enami, S., Stewart, L. A., Hoffmann, M. R. & Colussi, A. J. Superacid Chemistry on Mildly Acidic Water. *The Journal of Physical Chemistry Letters* **1**, 3488-3493, doi:10.1021/jz101402y (2010).
74 Harmon, K. M., Avci, G. F., Harmon, J. & Thiel, A. C. Hydrogen Bonding: Part 23. Further Studies on Stoichiometry, Stability, and Structure of the Lower Hydrates of Tetramethylammonium Fluoride. *J. Mol. Struct.* **160**, 57-66, doi:10.1016/0022-2860(87)87004-7 (1987).
75 Dai, D. J., Peters, S. J. & Ewing, G. E. Water Adsorption and Dissociation on NaCl Surfaces. *The Journal of Physical Chemistry* **99**, 10299-10304 (1995).
76 Zwanzig, R. W. High‐Temperature Equation of State by a Perturbation Method. I. Nonpolar Gases. *The Journal of Chemical Physics* **22**, 1420-1426, doi:doi:http://dx.doi.org/10.1063/1.1740409 (1954).
77 Bennett, C. H. Efficient estimation of free energy differences from Monte Carlo data. *Journal of Computational Physics* **22**, 245-268, doi:http://dx.doi.org/10.1016/0021-9991(76)90078-4 (1976).
78 Jorgensen, W. L. & Ravimohan, C. Monte Carlo Simulation of Differences in Free Energies of Hydration. *The Journal of Chemical Physics* **83**, 3050-3054, doi:10.1063/1.449208 (1985).
79 Bash, P., Singh, U., Langridge, R. & Kollman, P. Free Energy Calculations by Computer Simulation. *Science* **236**, 564-568 (1987).
80 Lee, M. W. & Meuwly, M. Hydration Free Energies of Cyanide and Hydroxide Ions from Molecular Dynamics Simulations with Accurate Force Fields. *PCCP* **15**, 20303-20312, doi:10.1039/C3CP52713A (2013).
81 Riccardi, E., Wang J.C., and A.I. Liapis. Rational Surface Design for Molecular Dynamics Simulations of Porous Polymer Adsorbent Media. *J. Phys. Chem. B* **112**, 7478-7488 (2008).
82 Leung, K., Rempe, S. B. & von Lilienfeld, O. A. Ab initio Molecular Dynamics Calculations of Ion Hydration Free Energies. *The Journal of Chemical Physics* **130**, doi:10.1063/1.3137054 (2009).
83 Perry Iv, T. D., Cygan, R. T. & Mitchell, R. Molecular Models of a Hydrated Calcite Mineral Surface. *Geochim. Cosmochim. Acta* **71**, 5876-5887, doi:10.1016/j.gca.2007.08.030 (2007).
84 Wang, J., Kalinichev, A. G. & Kirkpatrick, R. J. Effects of Substrate Structure and Composition on the Structure, Dynamics, and Energetics of Water at Mineral Surfaces: A Molecular Dynamics Modeling Study. *Geochim. Cosmochim. Acta* **70**, 562-582, doi:10.1016/j.gca.2005.10.006 (2006).
85 Wang, J., Kalinichev, A. G. & Kirkpatrick, R. J. Asymmetric Hydrogen Bonding and Orientational Ordering of Water at Hydrophobic and Hydrophilic Surfaces: A Comparison of Water/Vapor, Water/Talc, and Water/Mica Interfaces. *Journal of Physical Chemistry C* **113**, 11077-11085, doi:10.1021/jp9018316 (2009).

86 H. de Leeuw, N. & C. Parker, S. Atomistic Simulation of the Effect of Molecular Adsorption of Water on the Surface Structure and Energies of Calcite Surfaces. *J. Chem. Soc., Faraday Trans.* **93**, 467-475, doi:10.1039/a606573b (1997).
87 Kerisit, S., Marmier, A. & Parker, S. C. Ab Initio Surface Phase Diagram of the {10$\bar{1}$4} Calcite Surface. *The Journal of Physical Chemistry B* **109**, 18211-18213, doi:10.1021/jp053489x (2005).
88 Kerisit, S., Parker, S. C. & Harding, J. H. Atomistic Simulation of the Dissociative Adsorption of Water on Calcite Surfaces. *J. Phys. Chem. B* **107**, 7676-7682, doi:10.1021/jp034201b (2003).
89 Lardge, J. S., Duffy, D. M. & Gillan, M. J. Investigation of the Interaction of Water with the Calcite (10.4) Surface Using Ab Initio Simulation. *Journal of Physical Chemistry C* **113**, 7207-7212, doi:10.1021/jp806109y (2009).
90 Lardge, J. S., Duffy, D. M., Gillan, M. J. & Watkins, M. Ab Initio Simulations of the Interaction between Water and Defects on the Calcite (10$\bar{1}$4) Surface. *Journal of Physical Chemistry C* **114**, 2664-2668, doi:10.1021/jp909593p (2010).
91 Carrasco, J., Hodgson, A. & Michaelides, A. A molecular perspective of water at metal interfaces. *Nat Mater* **11**, 667-674 (2012).
92 http://accelrys.com/products/materials-studio/.
93 Delley, B. An all‐electron numerical method for solving the local density functional for polyatomic molecules. *The Journal of Chemical Physics* **92**, 508-517, doi:doi:http://dx.doi.org/10.1063/1.458452 (1990).
94 Perdew, J., Burke, K. & Ernzerhof, M. Generalized Gradient Approximation Made Simple. *Phys. Rev. Lett.* **77**, 3865-3868 (1996).
95 Ewald, P. P. Die Berechnung optischer und elektrostatischer Gitterpotentiale. *Annalen der Physik* **369**, 253-287 (1921).
96 Mezei, M. & Beveridge, D. L. Free Energy Simulations. *Ann. N.Y. Acad. Sci.* **482**, 1-23, doi:10.1111/j.1749-6632.1986.tb20933.x (1986).
97 Straatsma, T. P. & McCammon, J. A. Multiconfiguration thermodynamic integration. *The Journal of Chemical Physics* **95**, 1175-1188, doi:doi:http://dx.doi.org/10.1063/1.461148 (1991).
98 Kirkwood, J. G. Statistical Mechanics of Fluid Mixtures. *The Journal of Chemical Physics* **3**, 300-313, doi:doi:http://dx.doi.org/10.1063/1.1749657 (1935).
99 Miyata, T., Ikuta, Y. & Hirata, F. Free Energy Calculation Using Molecular Dynamics Simulation Combined with the Three Dimensional Reference Interaction Site Model Theory. I. Free Energy Perturbation and Thermodynamic Integration Along a Coupling Parameter. *The Journal of Chemical Physics* **133**, doi:10.1063/1.3462276 (2010).
100 Frary, F. C. & Nietz, A. H. The Hydrolysis of Sodium Carbonate in Solution. *J. Am. Chem. Soc.* **37**, 2268-2273, doi:10.1021/ja02175a003 (1915).
101 Brandell, D., Karo, J., Liivat, A. & Thomas, J. O. Molecular dynamics studies of the Nafion®, Dow® and Aciplex® fuel-cell polymer membrane systems. *J. Mol. Model.* **13**, 1039-1046 (2007).
102 Peng, Z. & Merz, K. M. Theoretical investigation of the CO2 + OH- .fwdarw. HCO3- reaction in the gas and aqueous phases. *J. Am. Chem. Soc.* **115**, 9640-9647, doi:10.1021/ja00074a032 (1993).
103 Sun, H. COMPASS: An ab Initio Force-Field Optimized for Condensed-Phase ApplicationsOverview with Details on Alkane and Benzene Compounds. *The Journal of Physical Chemistry B* **102**, 7338-7364, doi:10.1021/jp980939v (1998).
104 Hamprecht, F. A., Cohen, A. J., Tozer, D. J. & Handy, N. C. Development and assessment of new exchange-correlation functionals. *The Journal of Chemical Physics* **109**, 6264-6271, doi:doi:http://dx.doi.org/10.1063/1.477267 (1998).
105 Nosé, S. A unified formulation of the constant temperature molecular dynamics methods. *The Journal of chemical physics* **81**, 511-519 (1984).

106 Hoover, W. G. Canonical dynamics: equilibrium phase-space distributions. *Physical review A* **31**, 1695 (1985).
107 Kaggwa, G. B., Nalam, P. C., Kilpatrick, J. I., Spencer, N. D. & Jarvis, S. P. Impact of Hydrophilic/Hydrophobic Surface Chemistry on Hydration Forces in the Absence of Confinement. *Langmuir* **28**, 6589-6594, doi:10.1021/la300155c (2012).
108 Brogioli, D., Zhao, R. & Biesheuvel, P. M. A prototype cell for extracting energy from a water salinity difference by means of double layer expansion in nanoporous carbon electrodes. *Energy & Environmental Science* **4**, 772-777, doi:10.1039/C0EE00524J (2011).
109 La Mantia, F., Pasta, M., Deshazer, H. D., Logan, B. E. & Cui, Y. Batteries for Efficient Energy Extraction from a Water Salinity Difference. *Nano Lett.* **11**, 1810-1813, doi:10.1021/nl200500s (2011).
110 Porada, S., Sales, B. B., Hamelers, H. V. M. & Biesheuvel, P. M. Water Desalination with Wires. *The Journal of Physical Chemistry Letters* **3**, 1613-1618, doi:10.1021/jz3005514 (2012).
111 Chan, K. & Eikerling, M. A Pore-Scale Model of Oxygen Reduction in Ionomer-Free Catalyst Layers of PEFCs. *J. Electrochem. Soc.* **158**, B18-B28, doi:10.1149/1.3505042 (2011).
112 Bower, A. F., Guduru, P. R. & Sethuraman, V. A. A finite strain model of stress, diffusion, plastic flow, and electrochemical reactions in a lithium-ion half-cell. *Journal of the Mechanics and Physics of Solids* **59**, 804-828, doi:http://dx.doi.org/10.1016/j.jmps.2011.01.003 (2011).
113 Finlayson-Pitts, B. J. Reactions at surfaces in the atmosphere: integration of experiments and theory as necessary (but not necessarily sufficient) for predicting the physical chemistry of aerosols. *PCCP* **11**, 7760-7779, doi:10.1039/B906540G (2009).
114 Hass, K. C., Schneider, W. F., Curioni, A. & Andreoni, W. The Chemistry of Water on Alumina Surfaces: Reaction Dynamics from First Principles. *Science* **282**, 265-268, doi:10.1126/science.282.5387.265 (1998).
115 Shi, X., Xiao, H., Lackner, K. S. & Chen, X. Capture CO2 from Ambient Air Using Nanoconfined Ion Hydration. *Angew. Chem.* (2016).
116 Doherty, D., Holmes, B., Leung, P. & Ross, R. Polymerization molecular dynamics simulations. I. Cross-linked atomistic models for poly (methacrylate) networks. *Comput. Theor. Polym. Sci.* **8**, 169-178 (1998).
117 Yarovsky, I. & Evans, E. Computer simulation of structure and properties of crosslinked polymers: application to epoxy resins. *Polymer* **43**, 963-969 (2002).
118 Heine, D. R., Grest, G. S., Lorenz, C. D., Tsige, M. & Stevens, M. J. Atomistic simulations of end-linked poly (dimethylsiloxane) networks: structure and relaxation. *Macromolecules* **37**, 3857-3864 (2004).
119 Varshney, V., Patnaik, S. S., Roy, A. K. & Farmer, B. L. A molecular dynamics study of epoxy-based networks: cross-linking procedure and prediction of molecular and material properties. *Macromolecules* **41**, 6837-6842 (2008).
120 Liu, J. *et al.* Understanding flocculation mechanism of graphene oxide for organic dyes from water: Experimental and molecular dynamics simulation. *AIP Advances* **5**, 117151, doi:doi:http://dx.doi.org/10.1063/1.4936846 (2015).
121 Stillinger, F. H. & Rahman, A. Molecular dynamics study of temperature effects on water structure and kinetics. *The Journal of Chemical Physics* **57**, 1281-1292 (1972).
122 Matsumoto, M., Saito, S. & Ohmine, I. Molecular dynamics simulation of the ice nucleation and growth process leading to water freezing. *Nature* **416**, 409-413 (2002).
123 Li, Q. *et al.* Molecular characteristics of H2O in hydrate/ice/liquid water mixture. *Int. J. Mod Phys B* **29**, 1550185 (2015).
124 Bharadwaj, R. K. & Boyd, R. H. Small molecule penetrant diffusion in aromatic polyesters: a molecular dynamics simulation study. *Polymer* **40**, 4229-4236 (1999).

125 Liu, J. W., Mackay, M. E. & Duxbury, P. M. Molecular Dynamics Simulation of Intramolecular Cross-Linking of BCB/Styrene Copolymers. *Macromolecules* **42**, 8534-8542, doi:10.1021/ma901486q (2009).
126 Lu, C., Ni, S., Chen, W., Liao, J. & Zhang, C. A molecular modeling study on small molecule gas transportation in poly (chloro-p-xylylene). *Computational Materials Science* **49**, S65-S69 (2010).
127 Tsuzuki, S., Uchimaru, T., Mikami, M. & Urata, S. Magnitude and orientation dependence of intermolecular interaction of perfluoropropane dimer studied by high-level ab initio calculations: Comparison with propane dimer. *The Journal of chemical physics* **121**, 9917-9924 (2004).
128 Pavel, D. & Shanks, R. Molecular dynamics simulation of diffusion of O 2 and CO 2 in blends of amorphous poly (ethylene terephthalate) and related polyesters. *Polymer* **46**, 6135-6147 (2005).
129 Lin, Y. & Chen, X. Investigation of moisture diffusion in epoxy system: experiments and molecular dynamics simulations. *Chem. Phys. Lett.* **412**, 322-326 (2005).
130 Wu, C. & Xu, W. Atomistic simulation study of absorbed water influence on structure and properties of crosslinked epoxy resin. *Polymer* **48**, 5440-5448 (2007).
131 Chang, S.-H. & Kim, H.-S. Investigation of hygroscopic properties in electronic packages using molecular dynamics simulation. *Polymer* **52**, 3437-3442 (2011).
132 Lee, S. G., Jang, S. S., Kim, J. & Kim, G. Distribution and diffusion of water in model epoxy molding compound: molecular dynamics simulation approach. *Advanced Packaging, IEEE Transactions on* **33**, 333-339 (2010).
133 Humbert, H., Gallard, H., Suty, H. & Croué, J.-P. Performance of selected anion exchange resins for the treatment of a high DOC content surface water. *Water Res.* **39**, 1699-1708 (2005).
134 Johnson, C. J. & Singer, P. C. Impact of a magnetic ion exchange resin on ozone demand and bromate formation during drinking water treatment. *Water Res.* **38**, 3738-3750 (2004).
135 Feng, D., Aldrich, C. & Tan, H. Treatment of acid mine water by use of heavy metal precipitation and ion exchange. *Miner. Eng.* **13**, 623-642 (2000).
136 Wang, T. *et al.* Characterization of kinetic limitations to atmospheric CO2 capture by solid sorbent. *Greenhouse Gases: Science and Technology* (2015).
137 Einstein, A. *Investigations on the Theory of the Brownian Movement*. (Courier Corporation, 1956).
138 Lu, Y. *et al.* Continuous formation of supported cubic and hexagonal mesoporous films by sol–gel dip-coating. *Nature* **389**, 364-368 (1997).
139 Vyas, P. V. *et al.* Characterization of heterogeneous anion-exchange membrane. *Journal of Membrane Science* **187**, 39-46 (2001).
140 Drese, J. H. *et al.* Synthesis–structure–property relationships for hyperbranched aminosilica CO2 adsorbents. *Adv. Funct. Mater.* **19**, 3821-3832 (2009).
141 Choi, S., Gray, M. L. & Jones, C. W. Amine‐Tethered Solid Adsorbents Coupling High Adsorption Capacity and Regenerability for CO2 Capture From Ambient Air. *ChemSusChem* **4**, 628-635 (2011).
142 Yuh-Shan, H. Citation review of Lagergren kinetic rate equation on adsorption reactions. *Scientometrics* **59**, 171-177 (2004).
143 Springer, G. S. Environmental effects on composite materials. Volume 3. (1988).